Area Hosting Capacity Assessment

Final Report

Donald and Tarnagulla Microgrid Feasibility Study

RMIT University

May 2021

Researchers

Lead Researcher: Dr Arash Vahidnia

Research Team: Dr Inam Nutkani, Dr Manoj Datta, A/Prof. Lasantha Meegahapola, Prof. Brendan McGrath, A/Prof. Mahdi Jalili, Dr Kazi Hasan, Dr Moudud Ahmed, Dr Hui Song, Prof Liuping Wang, Dr Nuwantha Fernando, Dr Richardt Wilkinson, Dr Carlos Teixeira, Prof. Pierluigi Mancarella, Dr. Maria Vrakopoulou, Dr. Reza Razzaghi, Dr Behrooz Bahrani, Mr Yasin Zabihinia Gerdroodbari

Organisation: RMIT University

Partners: Monash University; University of Melbourne

Table of Contents

1. Executive Summary 4
2. Project Background and Objectives 5
3. Project Methodology 5
4. Project Outcomes 7
   4.1. Donald and Tarnagulla Microgrid Models 7
   4.2. Data Analytics 15
   4.3 Hosting Capacity Assessment 21
      4.3.1. Methodology 22
      4.3.2. Donald Town Microgrid Hosting Capacity Assessment 24
      4.3.3. Tarnagulla Town Microgrid Hosting Capacity Assessment 29
      4.3.4. Summary and Conclusions 34
   4.4. Microgrid Reliability Analysis 35
      4.1.1. Microgrid Reliability Model 35
      4.4.2. Summary and Conclusions 40
   4.5. Microgrid Operation Analysis 40
      4.5.1. Analysis of Donald Network 44
      4.5.2. Analysis of Tarnagulla Network 61
      4.5.3. Summary and Conclusions 77
   4.6. Hosting Capacity Improvement 77
      4.6.1. Methodology: 77
      4.6.2. Tarnagulla Network 78
      4.6.3. Donald Network: 92
      4.6.4. Conclusions 99
5. Summary and Conclusions 100

1. Executive Summary

This project addresses parts of a feasibility study for microgrids in two regional Victorian towns under the Federal Government's Regional and Remote Communities Reliability Program Fund – Microgrids Fund 2019-20 Grant. The project is awarded to Centre for New Energy Technologies (C4NET) and RMIT University in collaboration with C4NET, Monash University, University of Melbourne and Powercor have conducted the detailed hosting capacity assessment study for the proposed microgrid facilities at "Donald" and "Tarnagulla". These two regional Victorian towns have been experiencing supply vulnerabilities. The project aimed to explore various hosting scenarios to assess the hosting capacity and feasibility of partial or full microgrids in these two towns. The outcomes of this project will be utilized in the other parts (projects) of this feasibility study to provide the communities with potential alternative solutions for their energy supply.

This projected have been divided into four tasks and the detailed results and outcomes of these tasks are provided in this report. In the first task, the detailed models of the networks of Donald and Tarnagulla with associated distributed energy resources (DERs) have been developed in the simulation platform. This was followed by identifying customer types and behaviour by applying state-of-the-art machine learning and data analysis techniques on the de-identified smart meter and network data provided by C4NET and Powercor. The hosting capacity has been assessed for various operation modes of the microgrids such as grid-connected, stand-alone and VPP modes considering both the economic and reliability aspects of the network. This was followed by simulating various load and generation hosting scenarios to assess the capacity of the MV and LV networks of these towns as well as their supply network. Furthermore, the load and generation profiles identified through the data analytics phase of the project are used to perform quasi-dynamic simulation in order to quantify the network impact associated with the observed customer behaviours. Additionally, the study explored the feasibility and effects of advanced and innovative technologies in increasing the hosting capacity of the proposed microgrids. Each task's key findings and conclusions are provided at the end of each section of this report and summarized in Section 5.

2. Project Background and Objectives

This project is part of a larger project to assess partial or full microgrid feasibility in two regional Victorian towns with supply vulnerabilities. The two load centres of Donald and Tarnagulla have 1034 and 144 predominately residential customers respectively and are supplied through long rural lines with high-reliability risks for these communities. The network operators and the community groups in these two towns have been interested in improving the reliability of their power supply by enabling cost-effective fully or partially self-sustaining microgrids through alternative energy resources such as solar and battery storage.

This project aims at providing a detailed hosting capacity assessment study for the proposed microgrid facilities at Donald and Tarnagulla where various hosting scenarios for self-generation are considered, modelled and analysed. This project explores different mixes of generation technologies, such as solar, wind, diesel, and storage and demand response, to perform the hosting capacity analysis. The project also considers the consumers' behaviour by applying state-of-the-art machine learning techniques on the available smart meter and network data. This is then used to build reliable models for load profiling, which is critical for the hosting capacity assessment. Furthermore, the study explores the feasibility and effects of advanced and innovative control technologies in increasing the hosting capacity of the proposed microgrids.

3. Project Methodology

This Study assesses partial or full microgrid feasibility in two regional Victorian towns (Donald and Tarnagulla) with supply vulnerabilities. The two load centres have 1034 and 144 predominately residential customers and are supplied through long rural lines with high reliability risks for these communities. The project objectives are achieved through the following tasks:

Task 1: Developing Representative Microgrid Models and Data Analysis

The representative power system models for Donald and Tarnagulla microgrids are developed with associated local generation, storage and load scenarios. The developed model is studied in Task 2 and 3 for area hosting capacity assessment.

A. ***Microgrid power system modelling:*** Microgrid network model is developed with system loads, load profiles, local generation (including e.g. PV and diesel), storage, and feeder models.
B. ***Microgrid data analytics:*** Local generation profiles, smart meter data and net import-export within the microgrid consumers and with the external grid are analysed based on the state-of-the-art machine learning techniques. The clustered and estimated data will be used to develop the various operational scenarios for hosting capacity analysis.

Task 2: Assessing the Area Hosting Capacity

This task specifically looks at analysing the different hosting scenarios for self-generation including solar, wind, diesel/gas gen-sets, storage and demand response as well as grid-connected operation of the microgrids.

C. ***Hosting capacity for reliable operation:*** Microgrid hosting capacity is analysed from resource availability, and power system operation perspectives to ensure system stability and reliability.
D. ***Hosting capacity for economic operation:*** Microgrid hosting capacity is analysed from economic perspectives by considering the market price of electricity, and existing asset utilization.

Task 3: Analysing the Autonomous and Semi-autonomous Microgrid Operation

As the two regional towns are concerned with supply vulnerabilities, the focus of the study is to various grid-connected and self-sustaining microgrid operation conditions.

E. ***Steady state performance of the microgrid:*** For different hosting scenarios, as considered in Task 2, a comparative analysis is performed to represent autonomous and semi-autonomous operations by analysing the voltage profiles of the microgrids.

F. ***Dynamic performance of the microgrid:*** For different hosting scenarios, as considered in Task 2, a comparative analysis is performed to represent autonomous and semi-autonomous operation by analysing the dynamic performance of the microgrids.

Task 4: Hosting Capacity Improvement Scenarios

This task investigates possible approaches for improving the hosting capacity of the microgrids of these two towns through innovative control technologies. In this task, the effectiveness of additional control and improvement methods on enhancing the performance and hosting capacity of the microgrids are investigated.

The timeline of the project is provided below:

Task Number	Task Name
1	*Developing Representative Microgrid Models and Data Analysis*
2	*Assessing the Area Hosting Capacity*
3	*Analysing the Autonomous and Semi-autonomous Microgrid Operation*
4	*Analysing Hosting Capacity Improvement Scenarios*

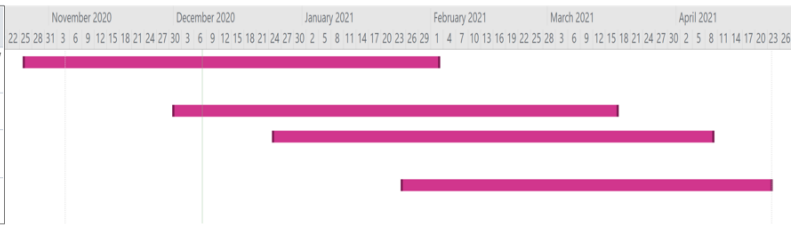

4. Project Outcomes

4.1. Donald and Tarnagulla Microgrid Models

This task aimed to develop the Donald and Tarnagulla microgrid models for hosting capacity assessment and reliability analysis in Task #2, #3, and #4.

The microgrid models developed in this task comprise actual MV network, distribution substations with typical LV feeders, and associated distributed energy resources (DERs) such as solar PV, storage, synchronous generators, and load. The microgrids are modelled using various combination of data sources as elaborated in Fig. 4.1.1. The MV network and distribution substations locations are adopted from the SINCAL model provided by the Powercore while the distribution transformers kVA ratings are estimated based on the substations statistical load data. Each distribution substation is modelled to have lumped load, solar PV, storage, and synchronous generators, which can be easily connected/disconnected to create different scenarios of DERs integration in Task #2 and 3. In addition, a few selected substations are modelled with typical LV feeders to account for the voltage drop in the LV network. The LV feeder's types are assumed after taking into consideration the given load data and Ausnet Standards.

Moreover, it was observed that the incoming supply feeders (zone-substation to these towns) significantly impact the network and user voltage and play a key role in determining the load and generation hosting capacity during the grid-connected mode. To capture the dynamics of incomings feeders, both Donald and Tarnagulla microgrid models are combined with their respective incoming supply feeders, as shown in Fig. 4.1.1.

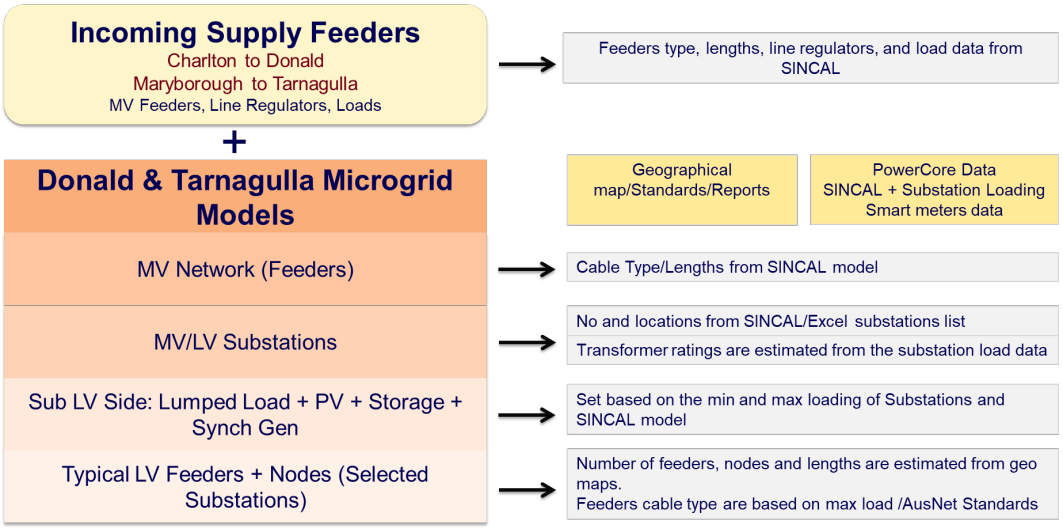

Fig. 4.1.1. Modelling approach

Donald Microgrid Model

Geographical and single-line diagrams of the Donald microgrid are shown in Fig. 4.1.2, 4.1.3, and Fig. 4.1.4, and the key information is summarised below.

Charlton to Donald Supply Feeder:

- ~ 41.7km with an ampacity of 140A.

- Includes two auto-tap line-voltage regulators with 2 × ±10% = ±20% voltage regulation capability.

Donald Microgrid Model

- Donald MV feeders are up to 3.83km with ampacity in the range from 105A to 140A. The MV feeders' cable type, impedance, and lengths are adopted from the SINCAL model.
- Donald town (excluding Donald South and Litchfield) comprises 45 distribution substations as follows:
  - 06 × 25 kVA
  - 01 × 50 kVA (1ph)
  - 16 × 63 kVA
  - 05 × 100 kVA
  - 13 × 200 kVA
  - 04 × 315 kVA
- Each distribution substation is modelled with 22 kV/433 V transformer and lumped load, solar PV, storage, and synchronous generator on the LV side. The transformer kVA ratings are assumed based on the maximum load demand of each substation.
- One substation (T09) is modelled in detail to account for the voltage drop in the distribution transformer and LV feeders. The detailed LV substation comprises 3 × 350m LV feeders with ten (10) nodes/feeder, as shown in Fig. 4.1.4.
- The Donald South and Litchfield areas are also included in the model due to their dependency on the Donald network. Both feeders can be disconnected if they are required to be excluded from the Study.

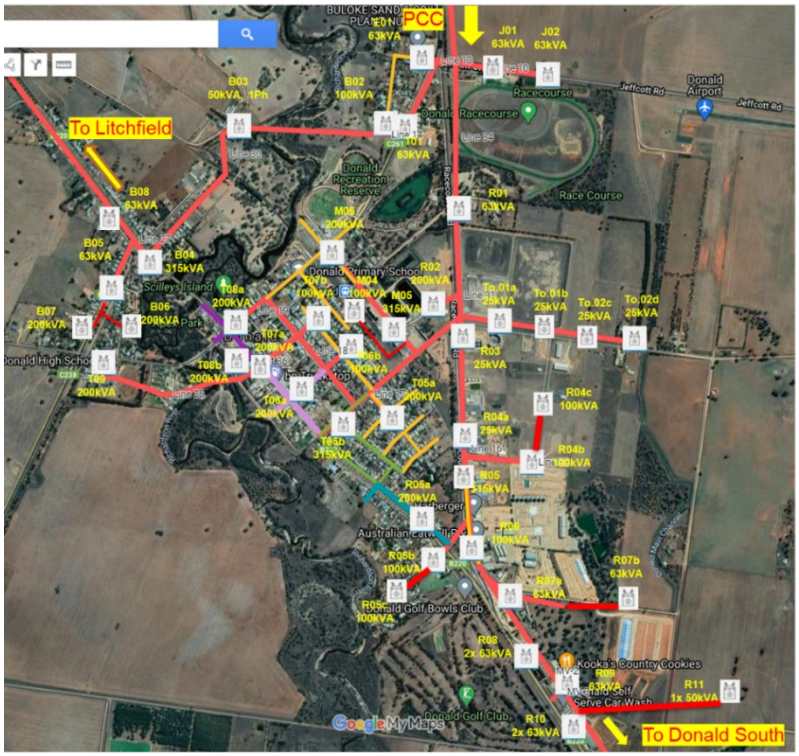

Fig. 4.1.2. Geographical diagram showing Donald distribution substations

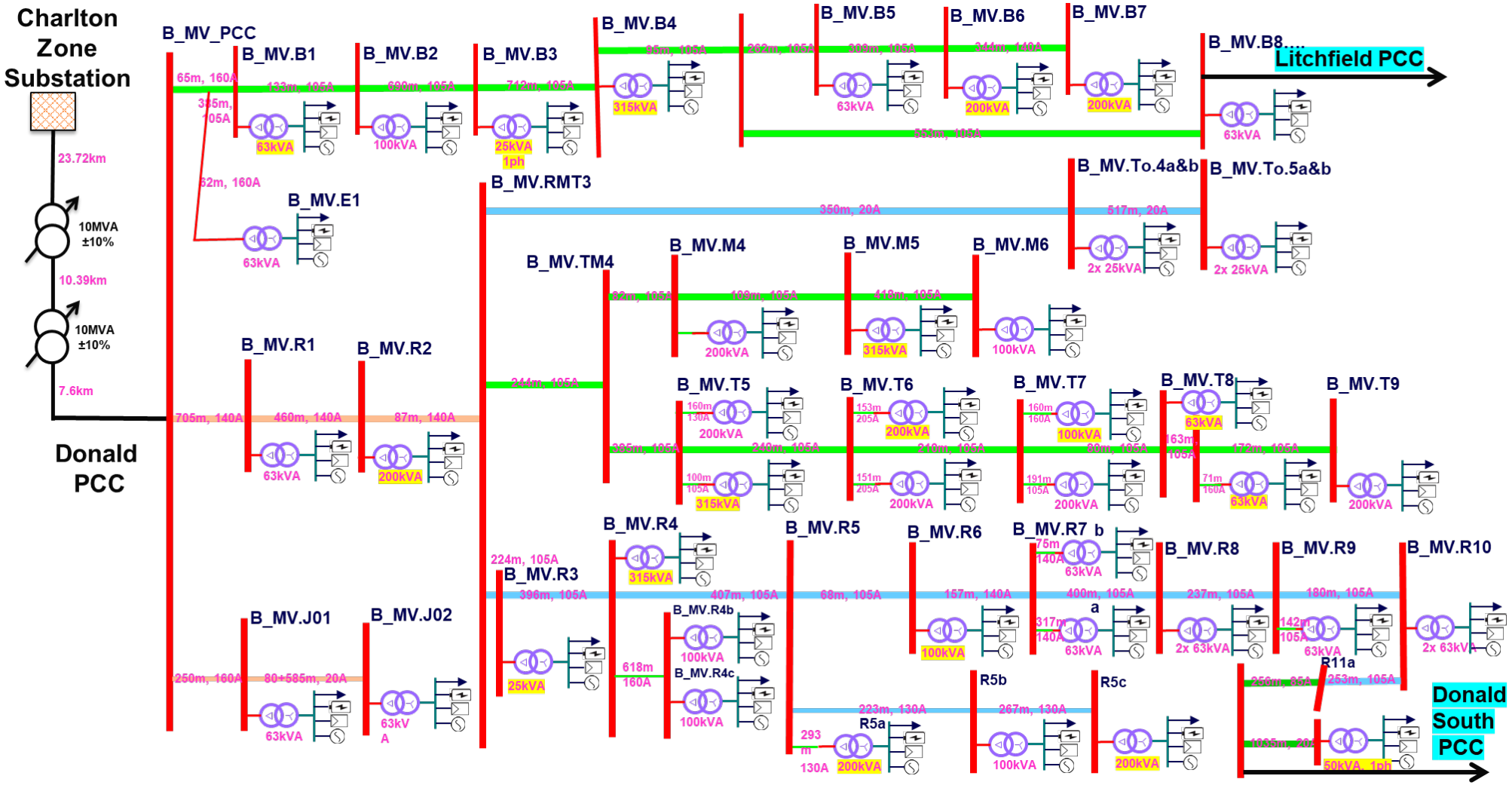

Fig. 4.1.3. Single line diagram of Donald microgrid with supply incoming feeder

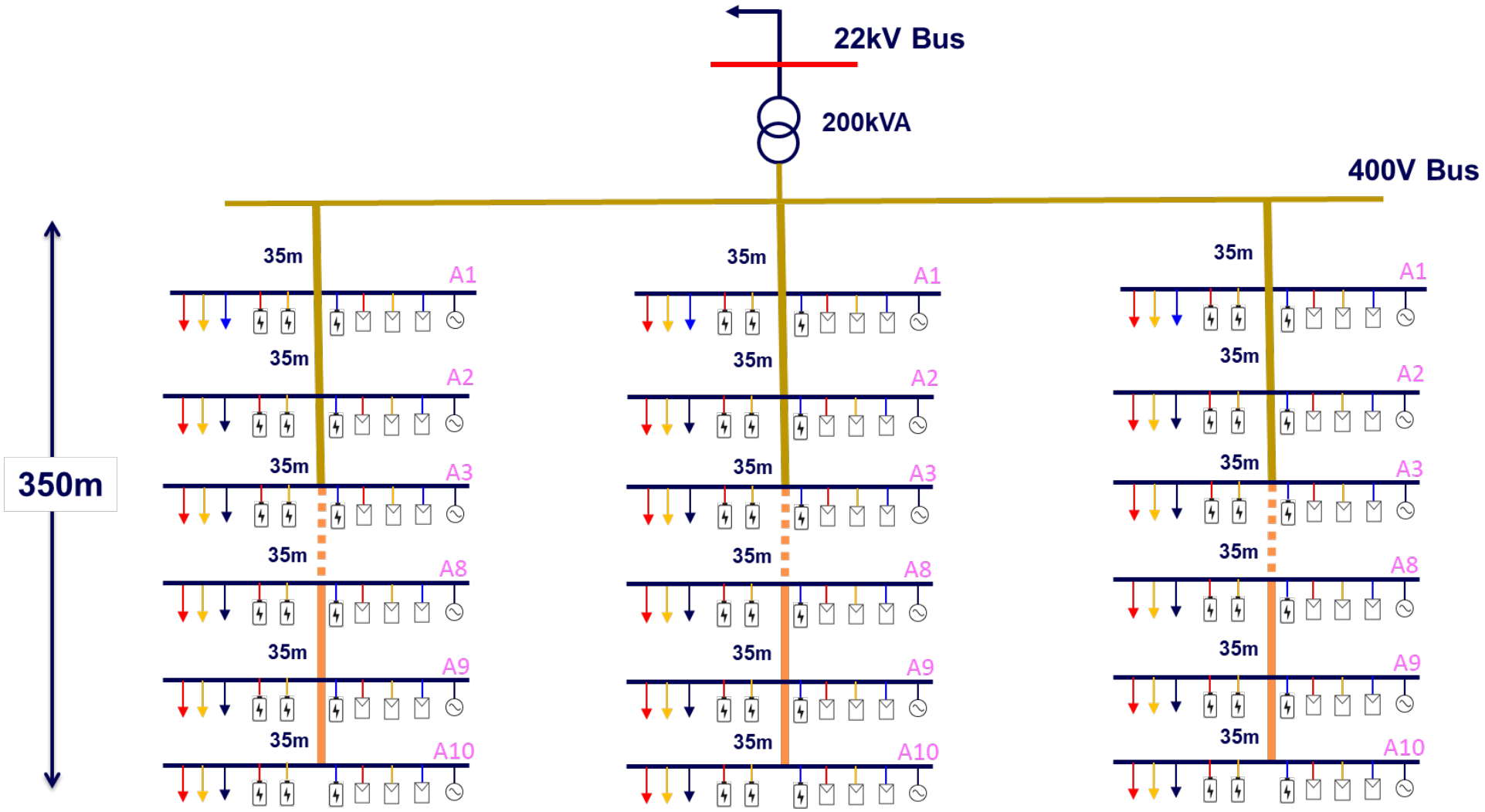

Fig. 4.1.4. Single line diagram showing Donald typical LV substation

Tarnagulla Microgrid Model

Single-line diagrams of the Tarnagulla microgrid MV network, LV network and geographical placement of substations/nodes are shown in Fig. 4.1.5 and 4.1.6, and 4.1.7, respectively. The model key information is summarised below.

Maryborough to Tarnagulla Supply Feeder:

- ~ 53.95 km with an immediate connecting feeder's ampacity of 20 A.
- Includes two auto-tap line-voltage regulators with 2 × ±10% = ±20% voltage regulation capability.

Tarnagulla Microgrid Model

- Tarnagulla MV feeders are up to 1.48km with ampacity in the range from 20 A to 160 A. The MV feeders' cable type, impedance, and lengths are adopted from the SINCAL model.
- Tarnagulla town comprises nine (9) distribution substations, as follows:
  - 03 × 25kVA
  - 04 × 63kVA
  - 02 × 100kVA
- Each distribution substation is modelled with 22kV/433V transformer and lumped load, solar PV, storage, and synchronous generator on the LV side. The transformer kVA ratings are assumed based on the maximum load demand for each substation.
- Four residential substations (TF-G, TF-V, TF-C, TF-W) are modelled in detail to account for the voltage drop in the distribution transformers and LV feeders. The feeders' length and the number of nodes are estimated based on the public domain information (e.g., Google street images), as follows:

Substation		**Length (m)**	**Number of Nodes**
TF-W	Feeder 1	225	335
	Feeder 2	4	5
TF-C	Feeder 1	240	300
	Feeder 2	4	5
TF-G	Feeder 1	400	500
	Feeder 2	4	5
TF-W	Feeder 1	440	440
	Feeder 2	4	3

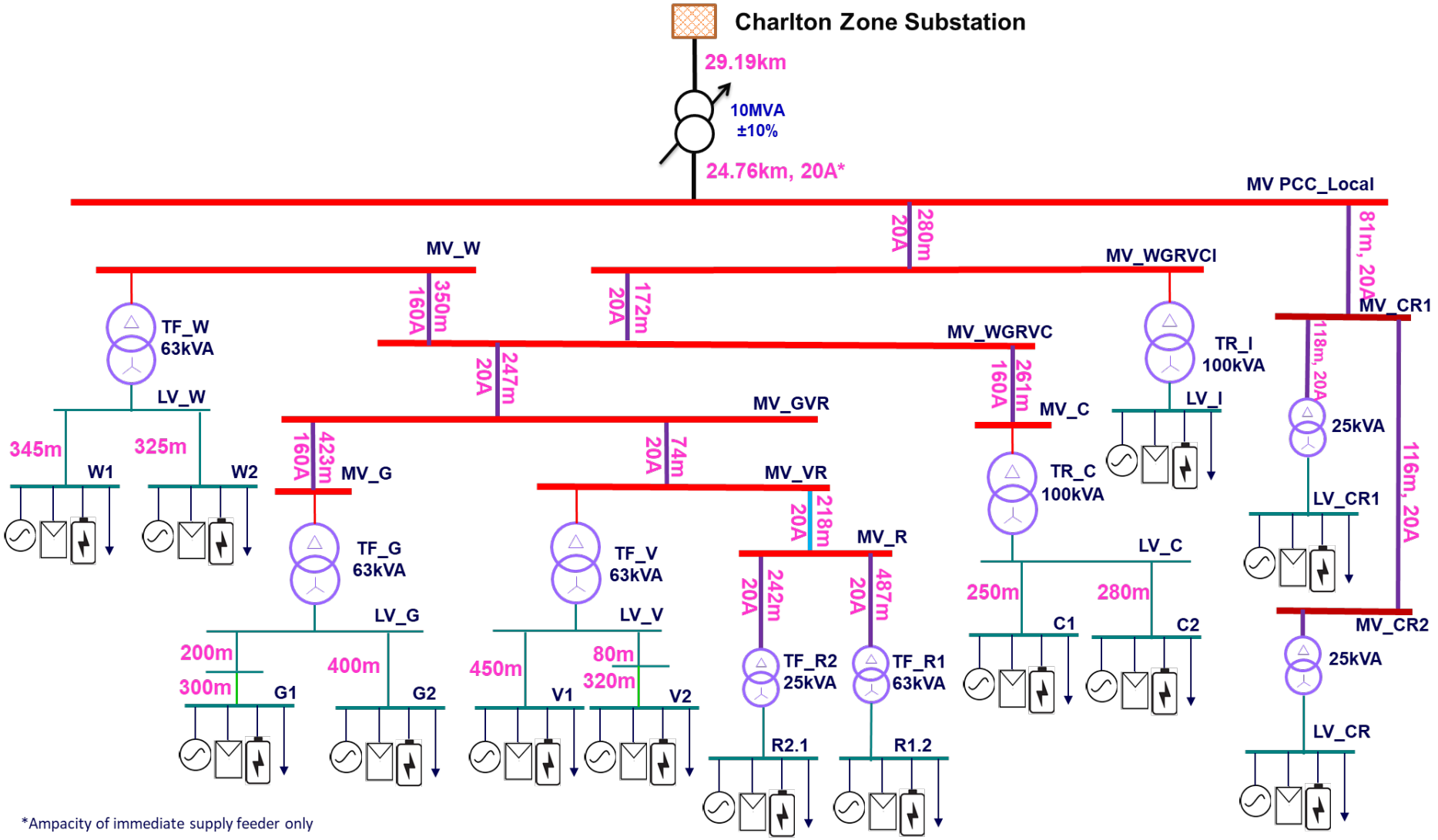

Fig. 4.1.5. Single line diagram of Tarnagulla microgrid with supply incoming feeder

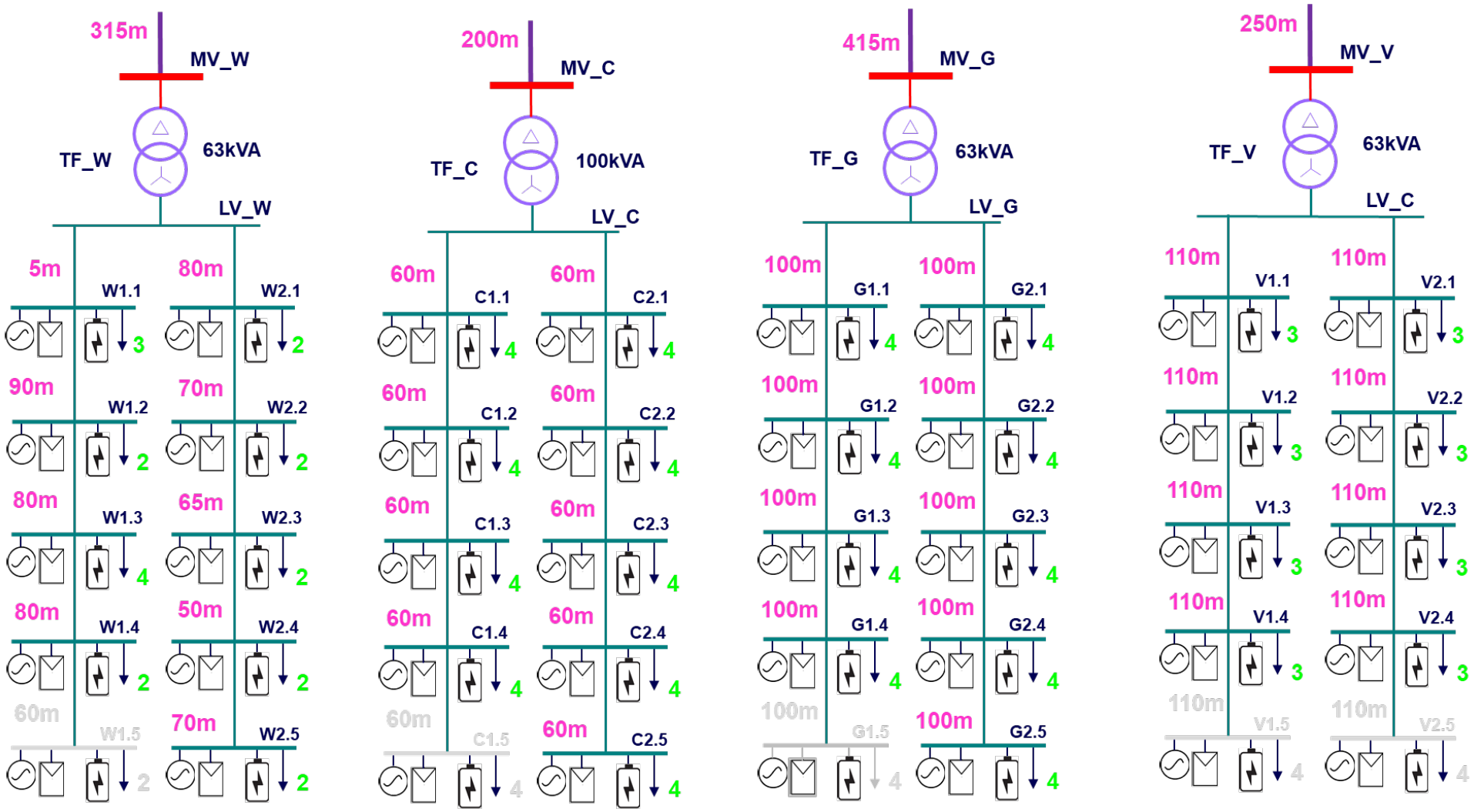

Fig. 4. 1.6. Single line diagram of Tarnagulla LV substations

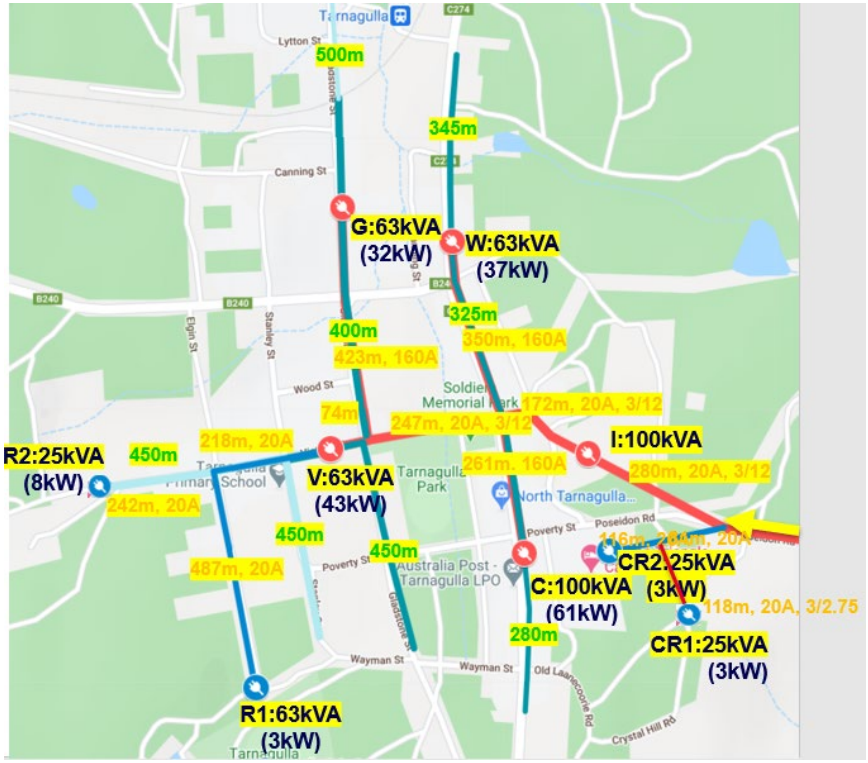

Fig. 4.1.7. Geographical diagram showing Tarnagulla distribution substations

The microgrid models developed during this task are suitable for steady-state and dynamic simulation studies such as load flow, sweep/quasi dynamic analysis, and reliability analysis and are used in project Task #2, #3, and #4 for network hosting capacity assessment and improvement

4.2. Data Analytics

The data analysis is performed using the provided smart-meter (consumption and generation) data for Donald and Tarnagulla. The maximal daily temperature in 2020 is taken into consideration and clustered into different groups, i.e., (7.9, 15.0], (15.0, 20.0], (20.0, 30.0], (30.0, 43.8]. To find the energy categories, e.g., commercial, industrial, agricultural, and residential, kmeans is applied to cluster the energy profile over postcode 3551 and 3480 into different groups.

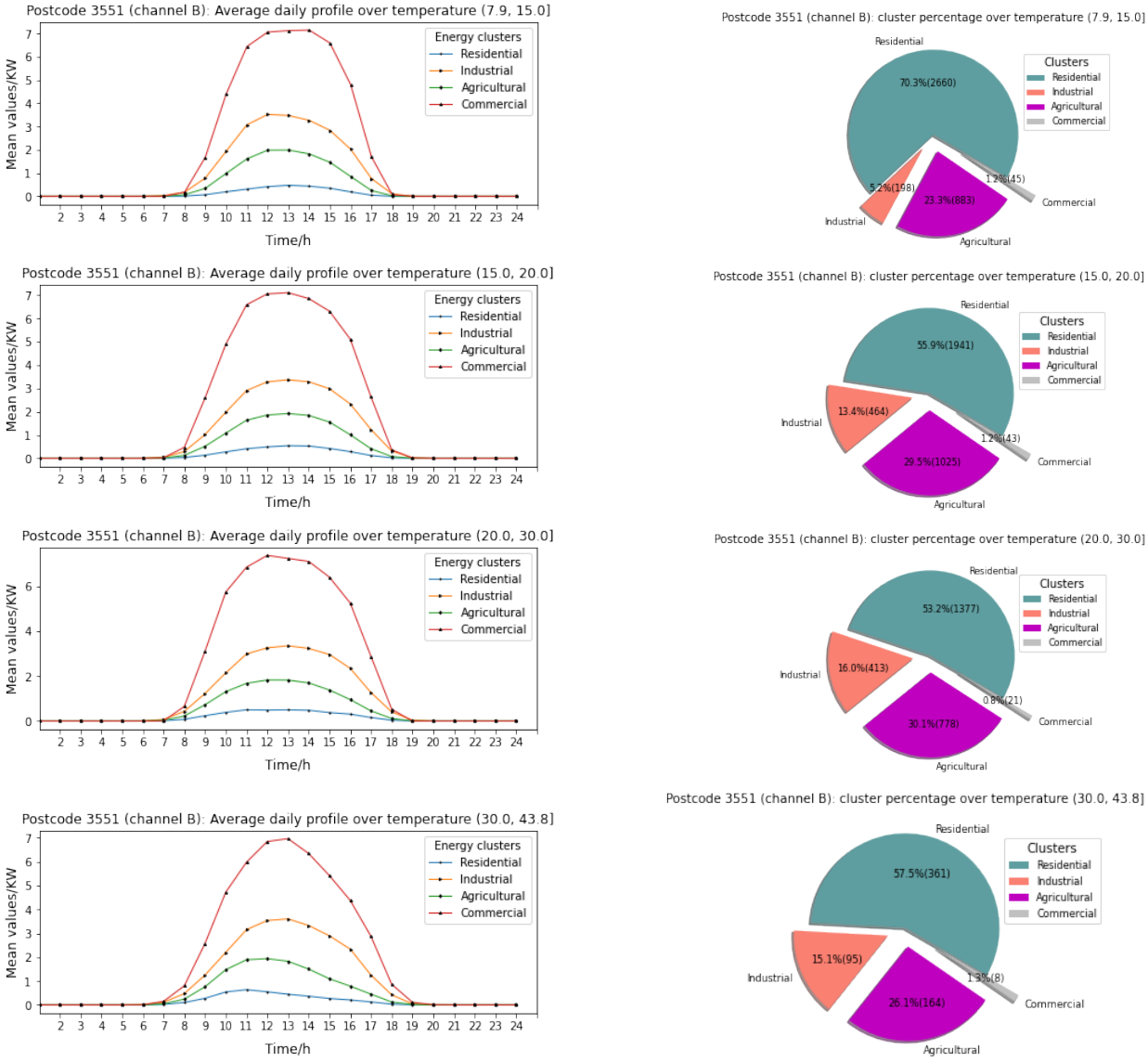

Fig. 4.2.1: The average daily load profile (postcode 3551, channel B) over different energy clusters under temperature clusters. The pie charts represent the proportion (counts) for each energy cluster in the left figure.

Fig. 4.2.2: The average daily load profile (postcode 3551, channel E) over different energy clusters under temperature clusters. The pie charts represent the proportion (counts) for each energy cluster in the left figure.

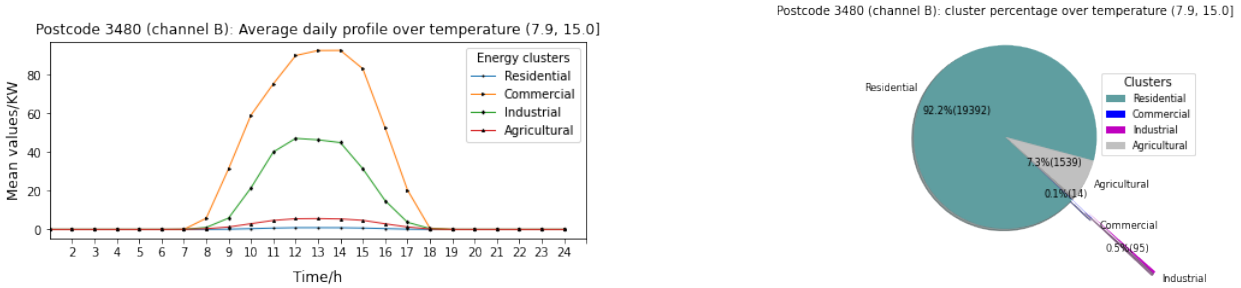

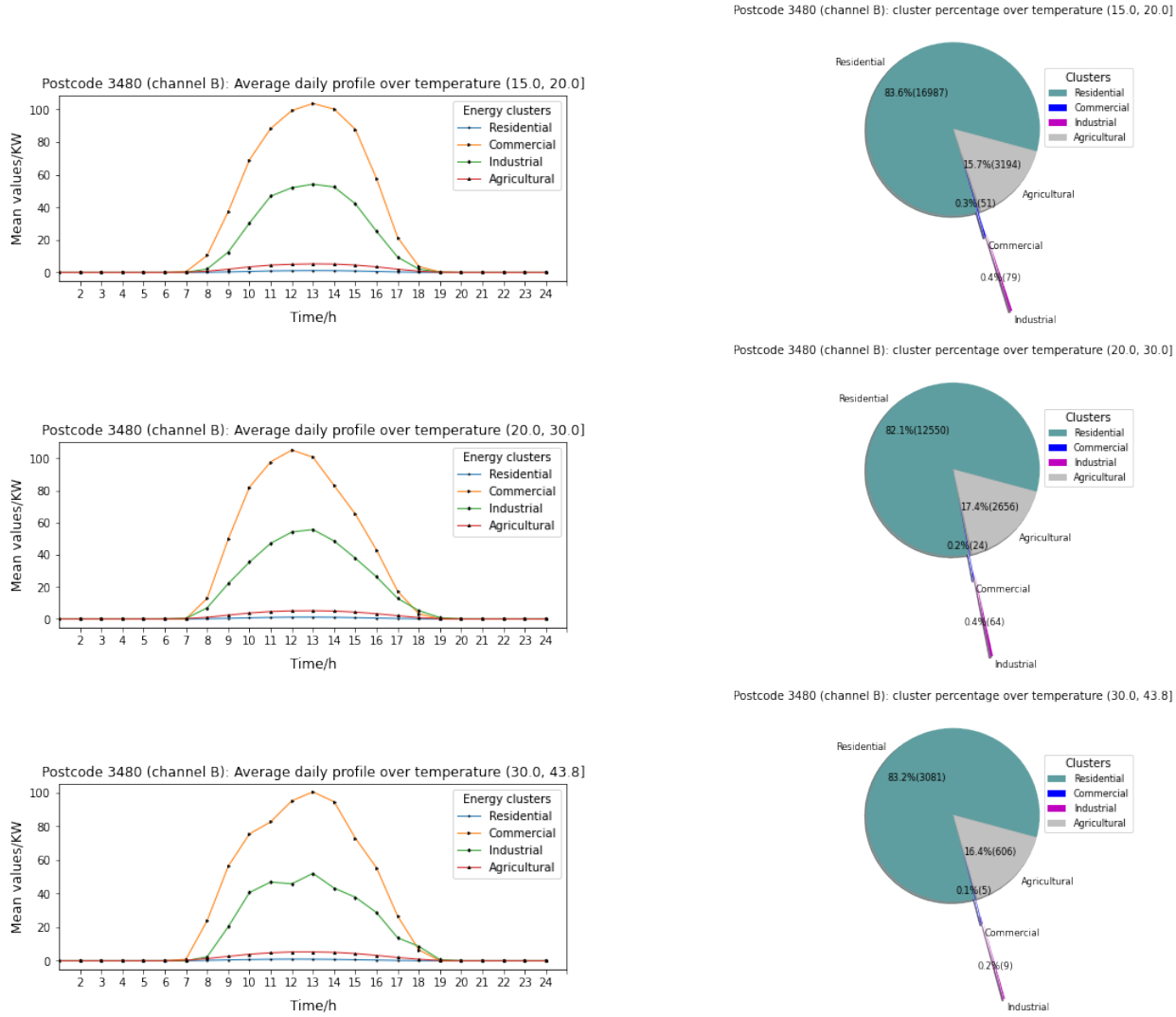

Fig. 4.2.3: The average daily load profile (postcode 3480, channel B) over different energy clusters under temperature clusters. The pie charts represent the proportion (counts) for each energy cluster in the left figure.

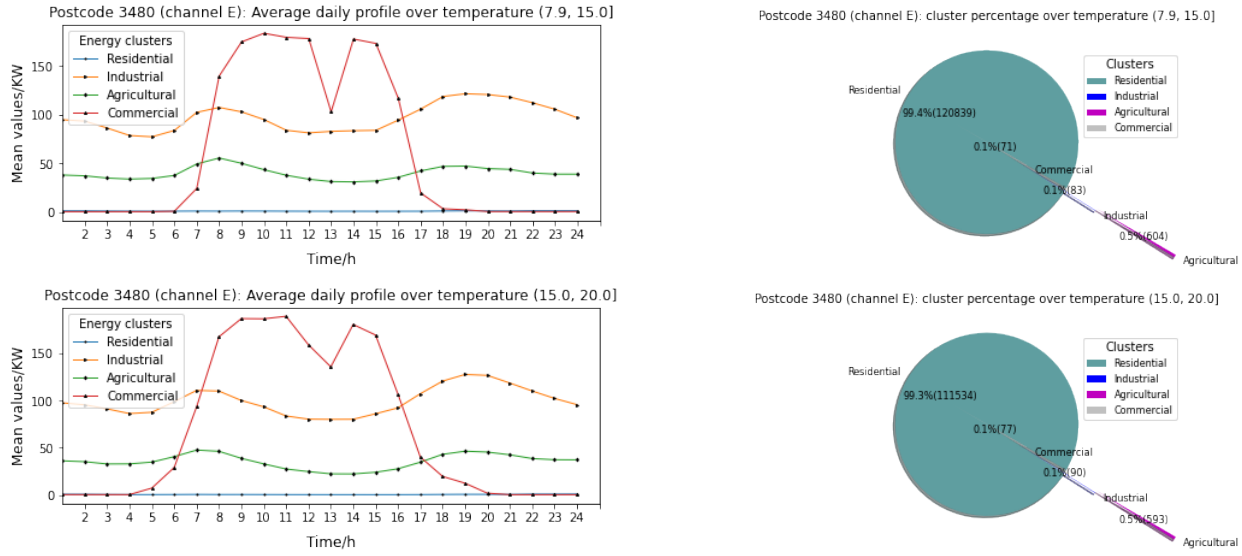

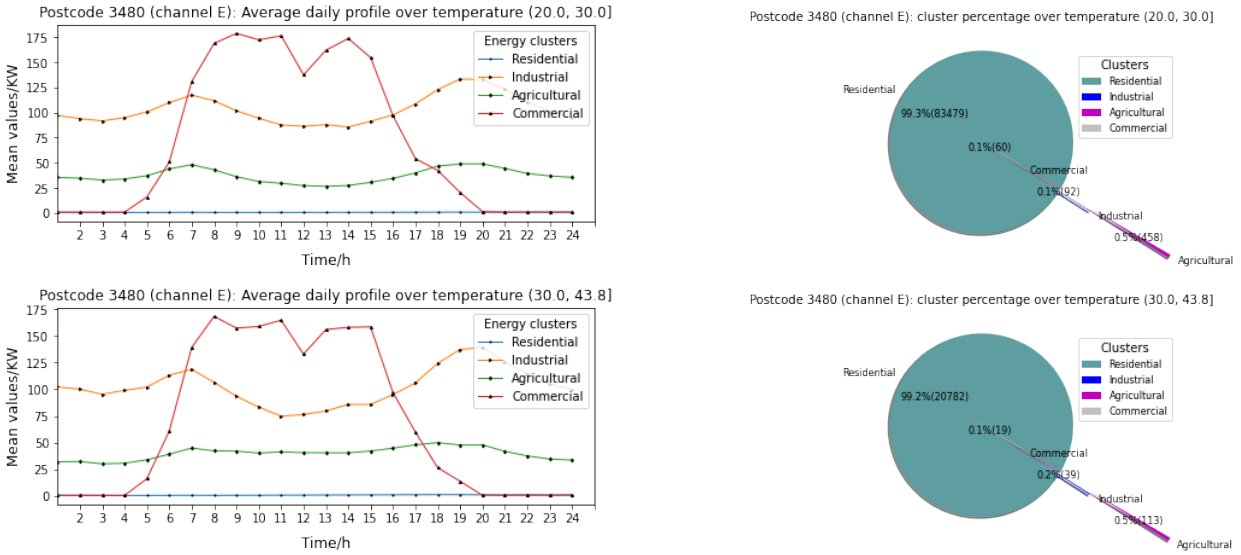

Fig. 4.2.4: The average daily load profile (postcode 3480, channel E) over different energy clusters under temperature clusters. The pie charts represent the proportion (counts) for each energy cluster in the left figure.

From the visualizations from Fig. 4.2.1 to Fig. 4.2.4, it is obvious that it seems reasonable to clustering all customers into four groups, i.e., residential, industrial, commercial, agricultural, is reasonable for the data in both postcodes (i.e., 3551 and 3480) across channel B and E. The influence of temperature is not so significant for postcode 3551 in comparison to postcode 3480 from the maximal mean energy value over each category. Further analysis is essential to be performed if we want to explore the impact of temperature.

In addition to the above analysis, we have performed data analysis over the residential data in each postcode. The residential data is clustered into two and three groups using kmeans for postcode 3551 and 3480, respectively.

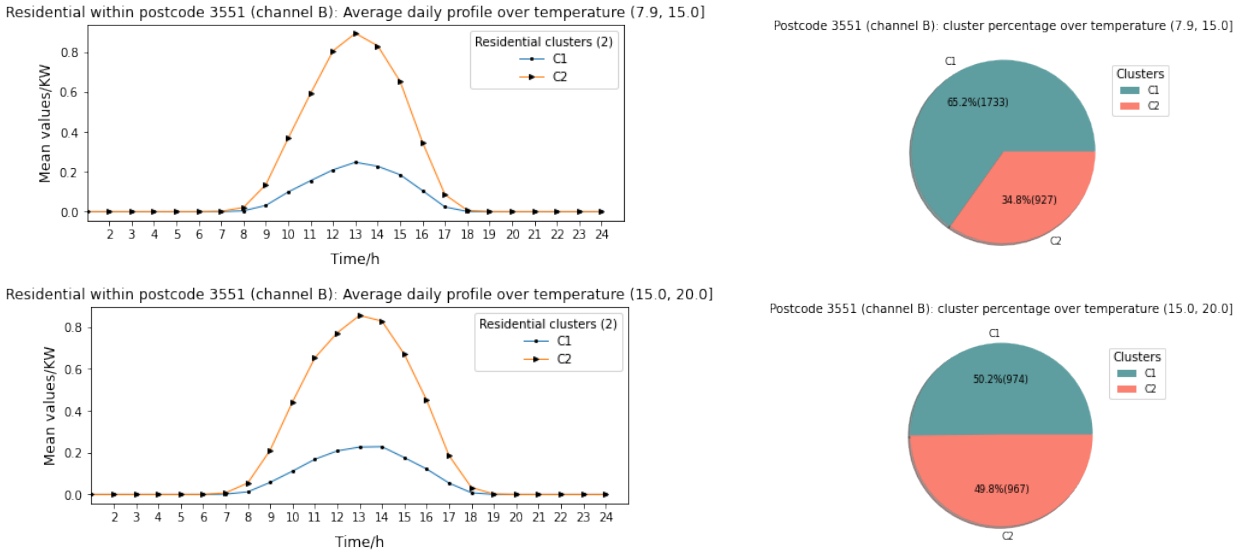

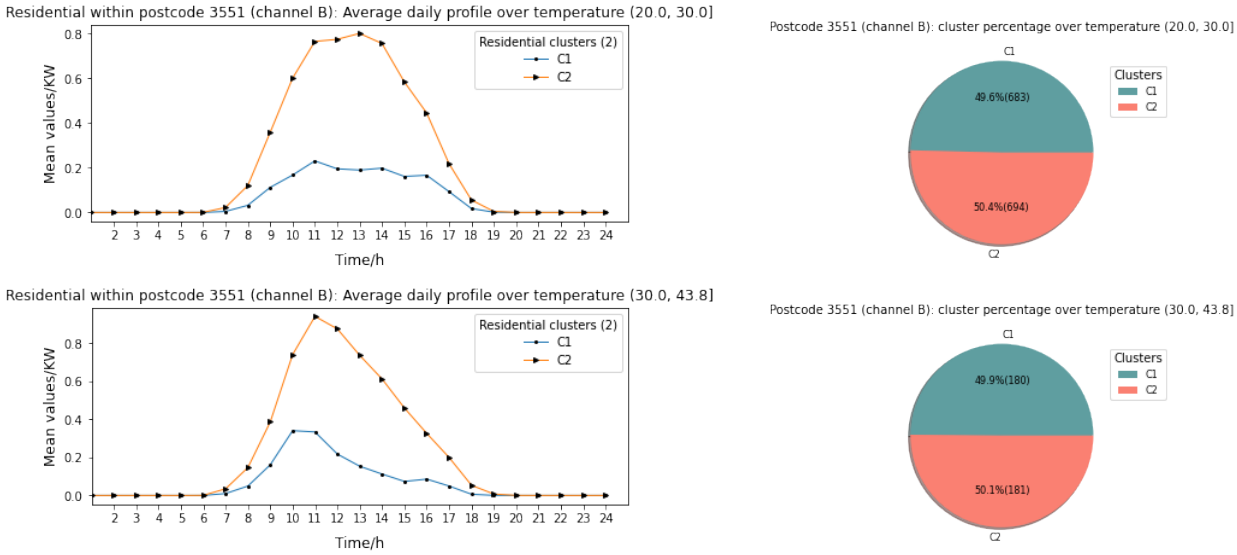

Fig. 4.2.5: The average daily profile (postcode 3551, channel B) for residential over two clusters (C1, C2) under temperature clusters. The pie charts represent the proportion (counts) for each energy cluster in the left figure.

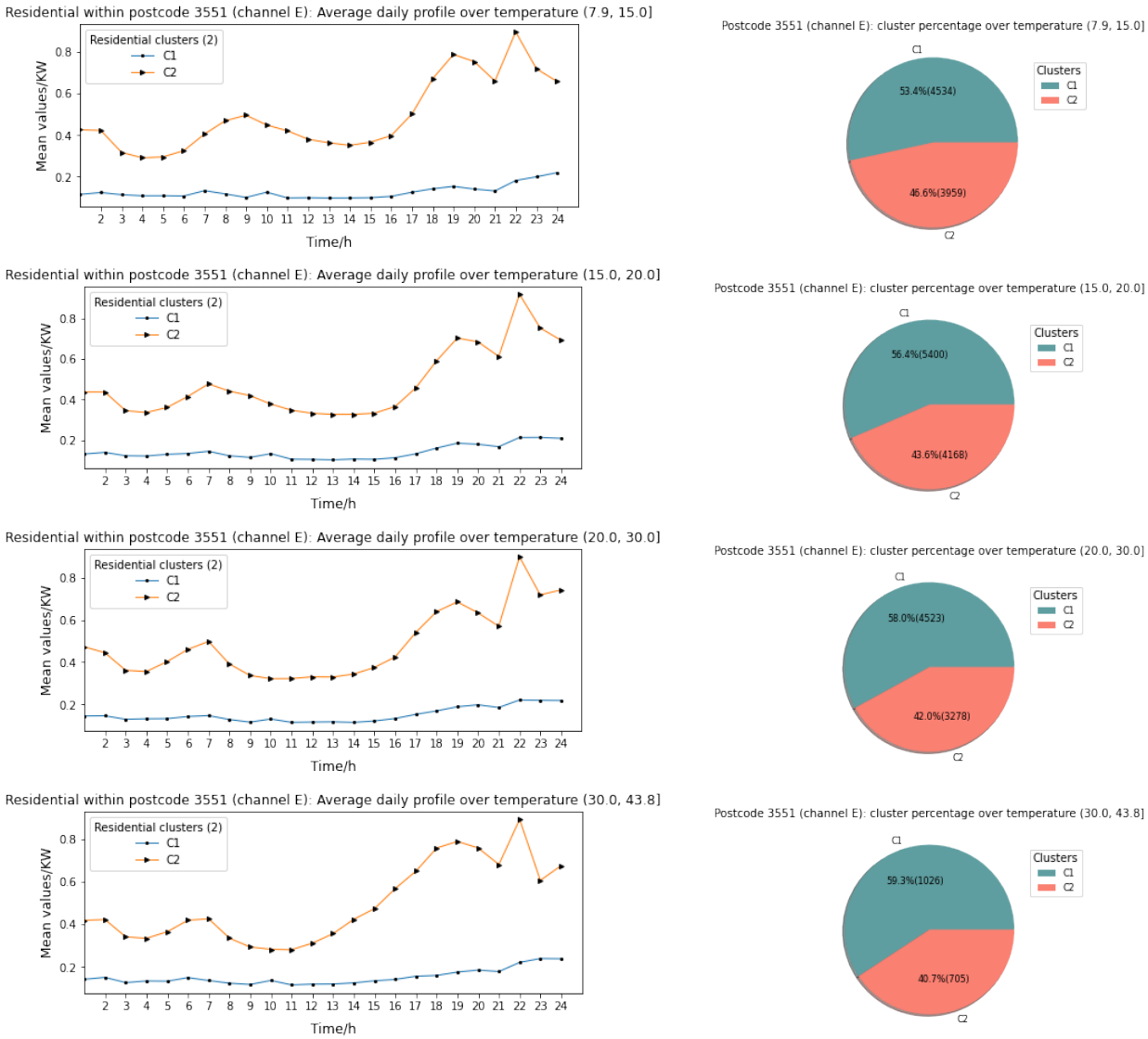

Fig. 4.2.6: The average daily profile (postcode 3551, channel E) for residential over two clusters (C1, C2) under temperature clusters. The pie charts represent the proportion (counts) for each energy cluster in the left figure.

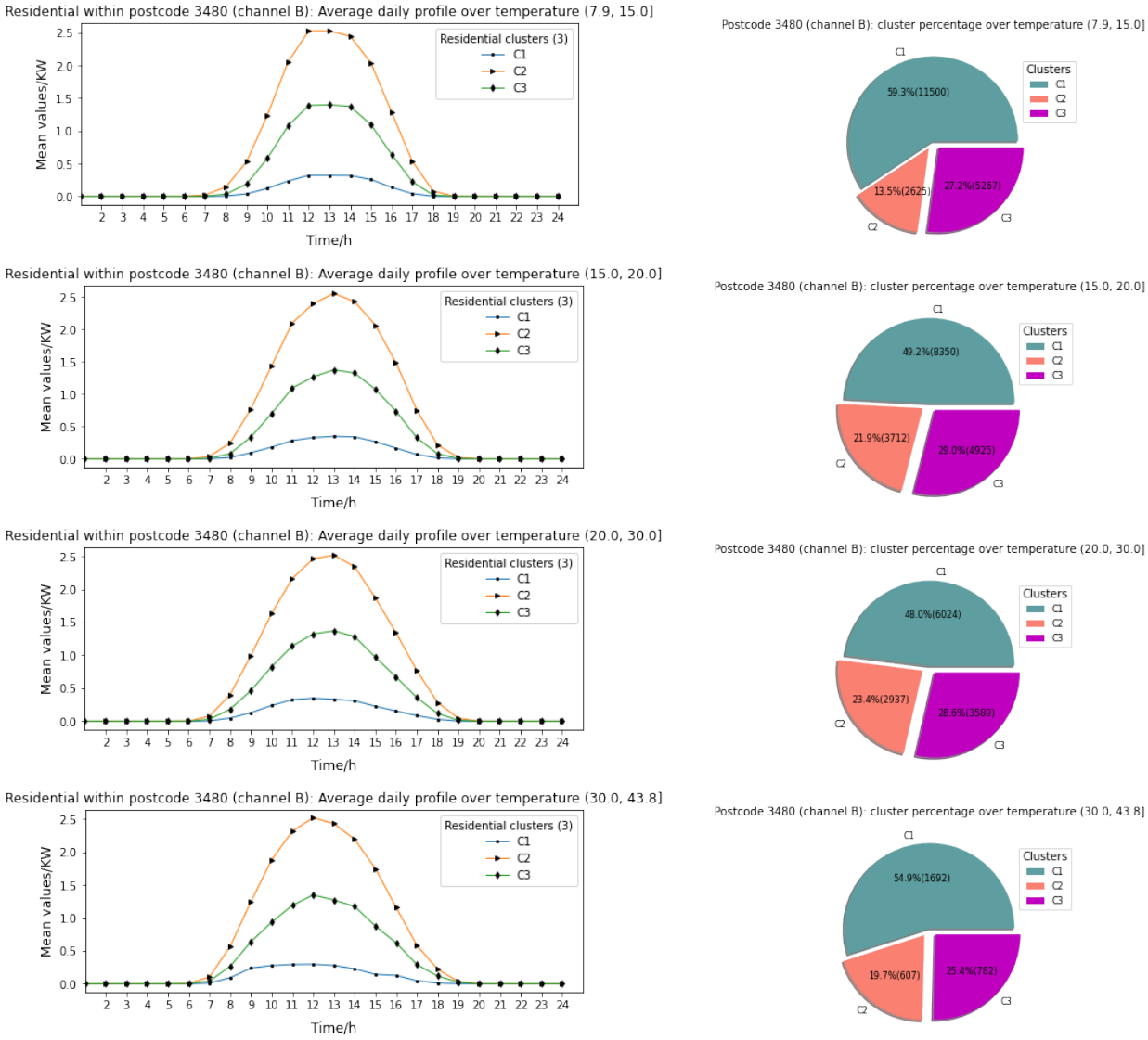

Fig. 4.2.7: The average daily profile (postcode 3480, channel B) for residential over three clusters (C1, C2, C3) under temperature clusters. The pie charts represent the proportion (counts) for each energy cluster in the left figure.

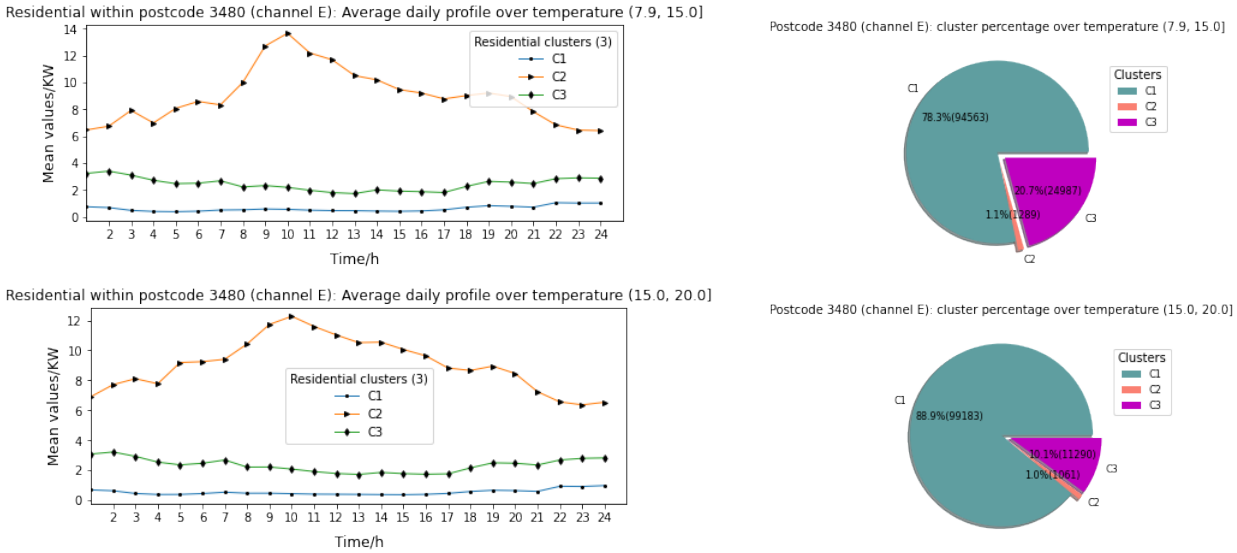

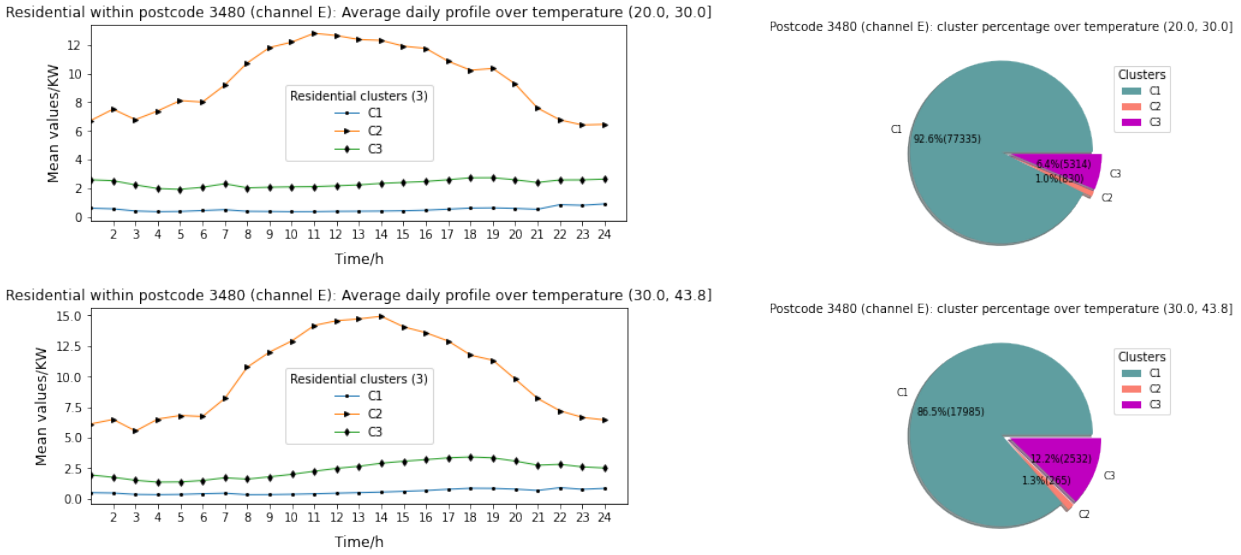

Fig. 4.2.8: The average daily profile (postcode 3480, channel E) for residential over three clusters (C1, C2, C3) under temperature clusters. The pie charts represent the proportion (counts) for each energy cluster in the left figure.

Fig. 4.2.5 to Fig. 4.2.8 illustrate the clusters of the residential category within postcodes 3551 and 3480 for channel B and E. It is clear that clustering the residential data into two groups for postcode 3551 and three groups for 3480 is reasonable. Similarly, the impacts of temperature on energy usage and generation need to be further explored if necessary.

Following the network modelling, steady state and dynamic simulations are being performed on the models to examine the important network characteristics for base (current) case as well as different hosting scenarios. In order to show the effect of various network elements on the system performance, load-flow studies have been performed on Tarnagulla Network where voltage drops in different points in the MV and LV networks are analysed as shown in Fig. 4.1.5-4.1.6.

4.3 Hosting Capacity Assessment

Along with the microgrid network modelling of Section 4.1 and data analytics of Section 4.2, it is crucial to study the optimal control, optimal microgrid component sizing, and the operation of microgrids with different renewable energy technologies and storages to find the best design choices if the microgrid is installed at a given location. For example, the energy dispatch and economic operation of a microgrid can be analysed from the perspective of integrating photovoltaic (PV) generators, energy storage systems (ESS), different distributed energy resources (DER) and backup generators by using professional power system tools or customised optimisation algorithms considering simple economics, reliability, and renewable generation uncertainty issues.

HOMER Pro is a professional microgrid design and optimisation tool which is first developed by the National Renewable Energy Laboratory (NREL) and Department of Energy (DOE), the USA, in 1993. Although various professional tools and customised mathematical algorithms have been proposed for microgrid planning and hosting capacity assessment in the coming years, HOMER

Pro remains the most widely used tool for microgrid design and optimal sizing due to its adequate mathematical modelling and optimisation algorithms. In this project, the HOMER Pro is used to find optimal component sizing and hosting capacity assessment of Donald and Tarnagulla microgrids to ensure economical operation and control and system reliability.

4.3.1. Methodology

Figure 4.3.1 shows the HOMER Pro working principle with simple input and output blocks and their functionalities. For optimal hosting capacity assessment and optimal sizing of microgrid component by HOMER pro, the following are the required input data: electrical load demand; renewable resources and availability; microgrid component (renewable and non-renewable generators, inverter/converter, energy storages, grid electricity prices and grid reliability) details; microgrid system constraints; microgrid system energy dispatch and control; emission data.

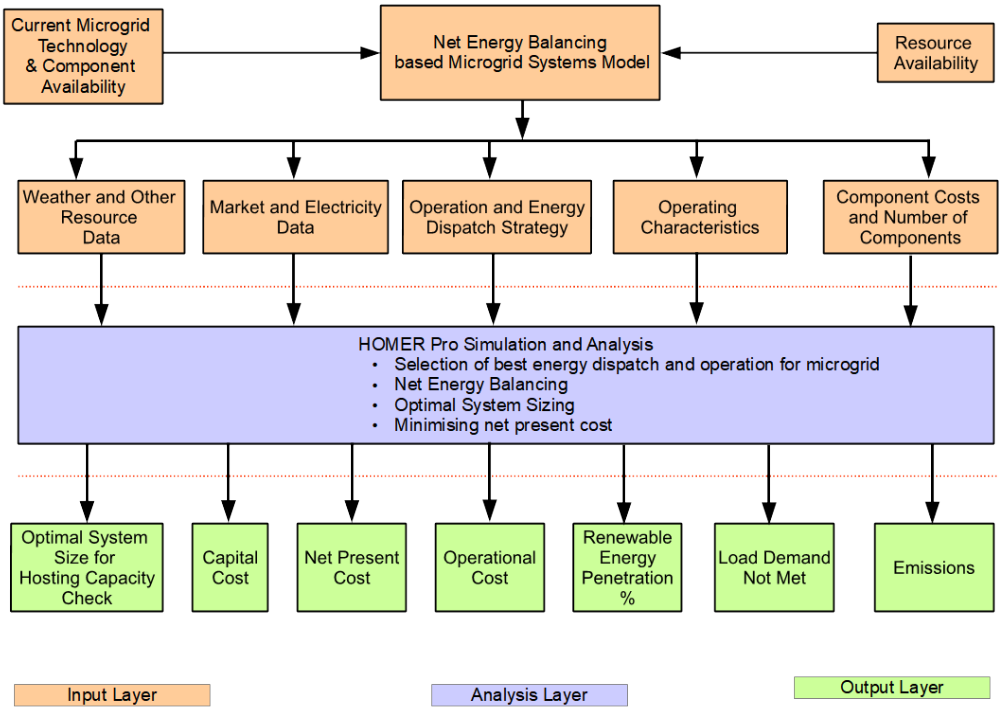

Figure 4.3.1: Simple block diagram of HOMER Pro analysis for microgrid hosting capacity calculations.

Once these input data are provided to HOMER Pro, according to the available constraints, it outputs a set of results, including optimal component sizes, net present cost (NPC), cost of energy (COE), levelised cost of energy (LCOE), capital cost, capacity shortage, excess energy generation, and renewable energy fraction. The main focus of this analysis will be the optimal component sizing which will then be used in the detailed microgrid reliability analysis (described in Section 4.4) and in the microgrid operation (described in Section 4.5) and hosting capacity improvement (described Section 4.6) to ensure that the power system reliability, voltage, and frequency requirements have been met. Figure 4.3.2 shows the overall project methodology highlighting the optimal hosting section.

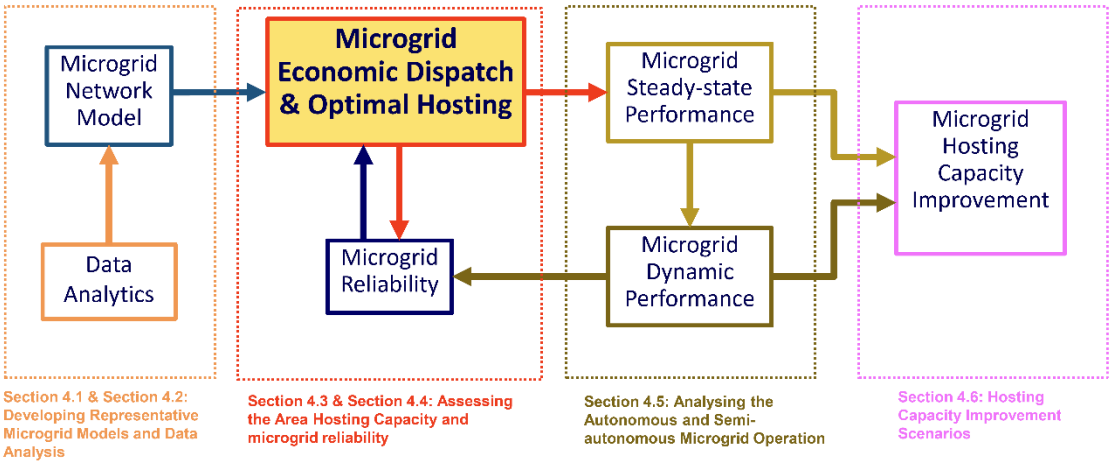

Figure 4.3.2: Overall project methodology highlighting the connection of optimal hosting capacity calculation to microgrid network modelling, reliability and operation.

Microgrid Control and Generator Dispatch Scenarios

When finding optimal hosting capacity of a microgrid, it is important to consider different controls and energy dispatch scenarios for a particular microgrid. A microgrid controller is the intelligent brain of a microgrid that will make the best energy management decision considering weather, resource availability, renewable power production, battery capacity, and grid power availability. It decides how the daily electrical load demand is met, how and when the battery energy storage is used in the charging/discharging modes, and if the back-up generator needs to be turned on to meet any energy deficiency. In this project, three modes (grid-connected, islanded, and virtual power plant) of microgrid operation are examined under the following energy dispatch strategies to find optimal hosting capacity of a microgrid.

Load Following (LF) - Whenever a generator operates, it produces only enough power to meet the primary electrical load demand. Lower-priority objectives such as charging the battery bank or serving any deferrable electrical load are left to the renewable power sources. The backup generator can still ramp up and sell power to the utility grid if it is economically feasible.

Cycle Charging (CC) - Whenever a generator needs to serve the primary electrical load, it operates at full output power. Surplus electrical power production goes toward the lower-priority objectives such as, in order of decreasing priority: serving the deferrable electrical load or charging the battery storage.

Combined Dispatch (CD) - In every timestep, the CD decides which is the cheapest dispatch strategy between LF and CC to meet the energy demand.

Generator Order (GO) - Under the GO, energy dispatch follows a defined order of generator combinations, and uses the first combination in the order that meets the operating capacity of the microgrid. The GO only supports systems with generators, PVs, wind turbines, converter/inverters, and storage systems. It does not work in the grid-connected mode.

Predictive Dispatch (PD) – Under PD, the dispatch algorithm knows the incoming electrical load demand, as well as the PV and wind resource availability. It sometimes produces results with lower system operating costs compared to the other dispatch strategies. This dispatch strategy has 48-hour foresight and uses this knowledge to operate the batteries in an economical way. It uses forecasting to improve energy dispatch performance.

Figure 4.3.3 show the three microgrid operation modes under different dispatch strategies to find optimal hosting capacities.

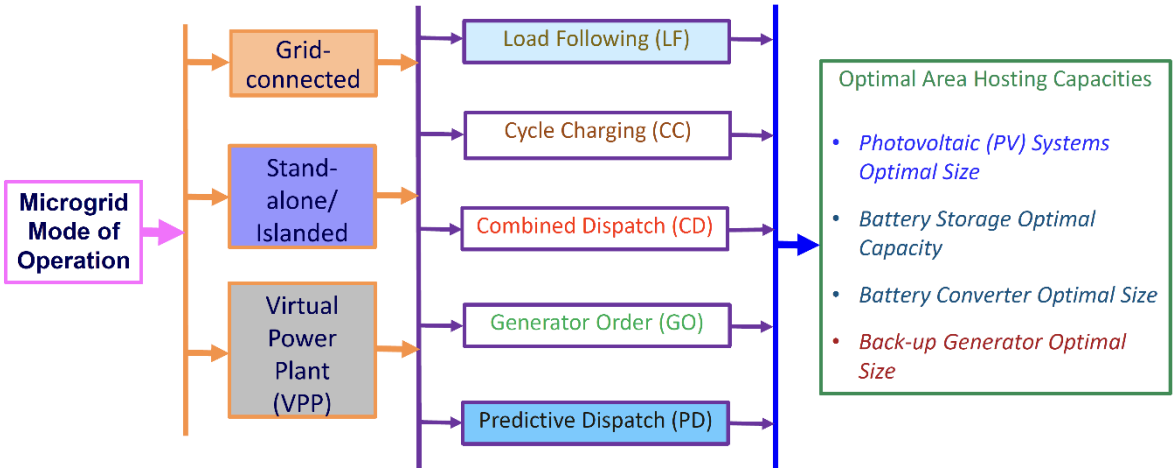

Figure 4.3.3: Microgrid operation under different dispatch strategy to find optimal area hosting capacities.

4.3.2. Donald Town Microgrid Hosting Capacity Assessment

Areas to be Considered

Figure 4.3.4 shows the areas which will be covered by Donald Town microgrid along with respective postcodes.

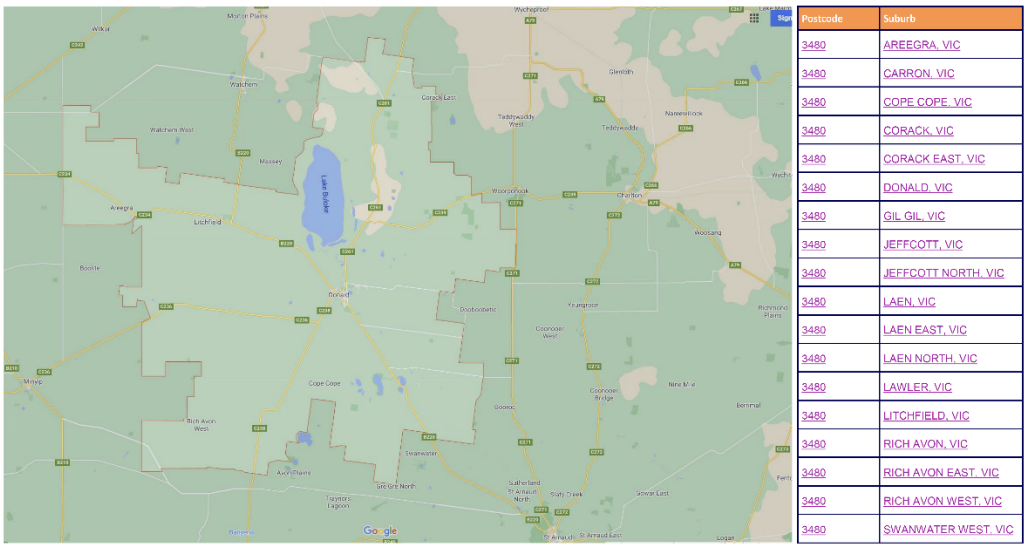

Postcode	Suburb
3480	AREEGRA, VIC
3480	CARRON, VIC
3480	COPE COPE, VIC
3480	CORACK, VIC
3480	CORACK EAST, VIC
3480	DONALD, VIC
3480	GIL GIL, VIC
3480	JEFFCOTT, VIC
3480	JEFFCOTT NORTH, VIC
3480	LAEN, VIC
3480	LAEN EAST, VIC
3480	LAEN NORTH, VIC
3480	LAWLER, VIC
3480	LITCHFIELD, VIC
3480	RICH AVON, VIC
3480	RICH AVON EAST, VIC
3480	RICH AVON WEST, VIC
3480	SWANWATER WEST, VIC

Figure 4.3.4: Donald Town (3480) microgrid- areas to be considered.

Smart meter load data analysis for HOMER Pro input

Powercor Australia has supplied smart meter load data for the year 2020 at all the available power system load nodes in the Donald town area. These data files are provided in 30 minutes resolution starting on January 1 at 0.00 hours and ending at 23:30 hours on the same day for 366 days. Some of the days' data were missing. These missing data are filled by using the HOMER Pro load data analysis module. Figure 4.3.5 shows the aggregated smart meter load data analysis.

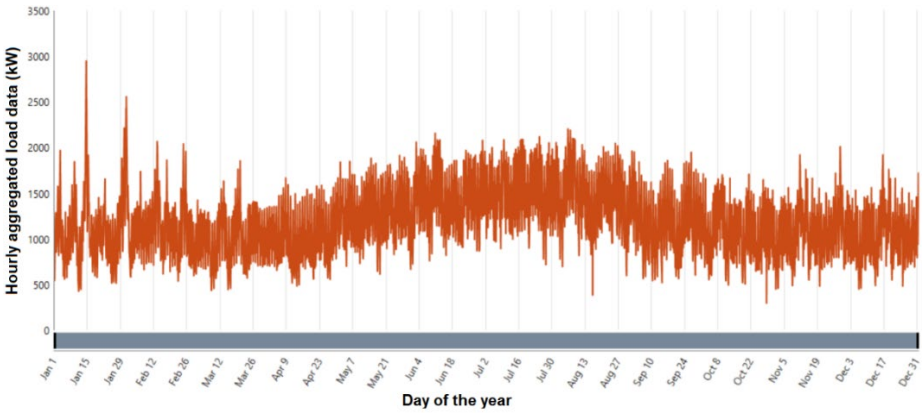

(a)

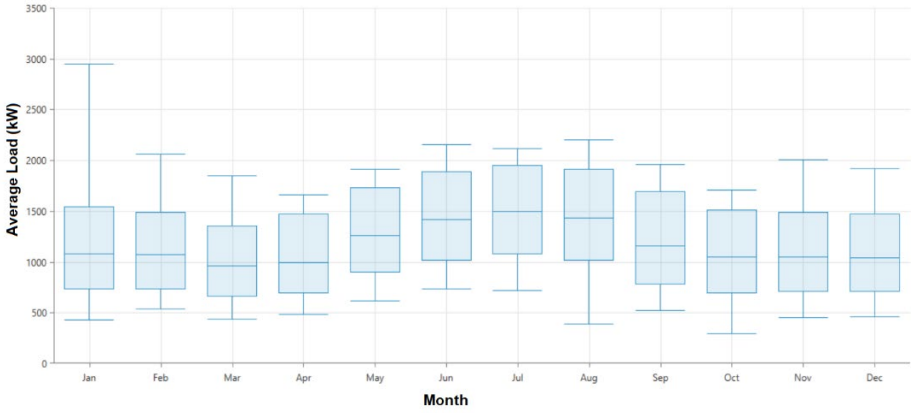

(b)

Figure 4.3.5: Aggregated total load of Donald Town (3480) for the year 2020. (a) Hourly data. (b) Monthly average load

Table 4.3.1 shows the aggregated load data analysis results. Peak load and number of customers match with the total transformer loading capacity and customer nodes found in Donald microgrid network modelling of Section 4.1.

Table 4.3.1: Donald Town aggregated load data for the year 2020.

Metric	**Baseline**
Total Customer/Smart Meter Data Nodes	**1092 (approximate)**
Peak Load Month	**July**
Average (kWh/day)	**28,128**
Average (kW)	**1,172**

Peak (kW)	**2,949.6**
Load Factor	**0.4**

Smart meter generation data analysis for HOMER Pro input

Powercor Australia has also supplied smart meter generation data for the year 2020 at all the available local generation nodes in the Donald town area. Same as the load data, these data files are provided in 30 minutes resolution starting on January 1 at 0.00 hours and ending at 23:30 hours on the same day for 366 days. Some of the days' data were missing. These missing data are filled by using the HOMER Pro PV generation analysis. Figure 4.3.6 shows the aggregated smart meter current generation data analysis.

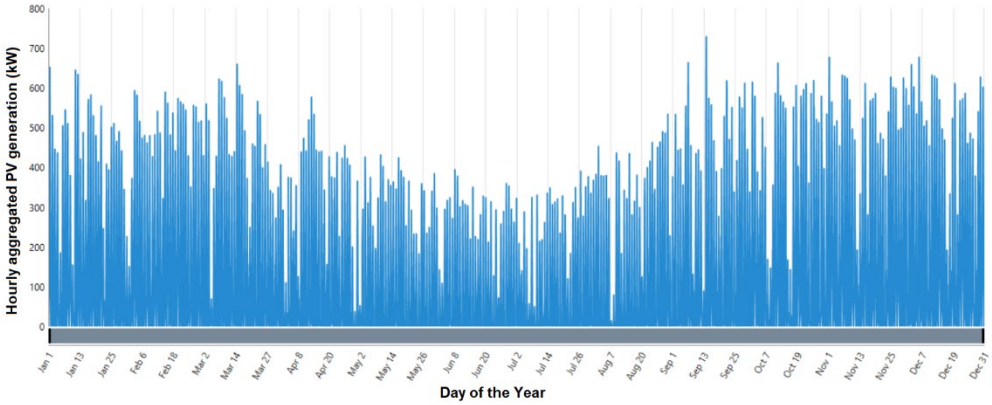

(a)

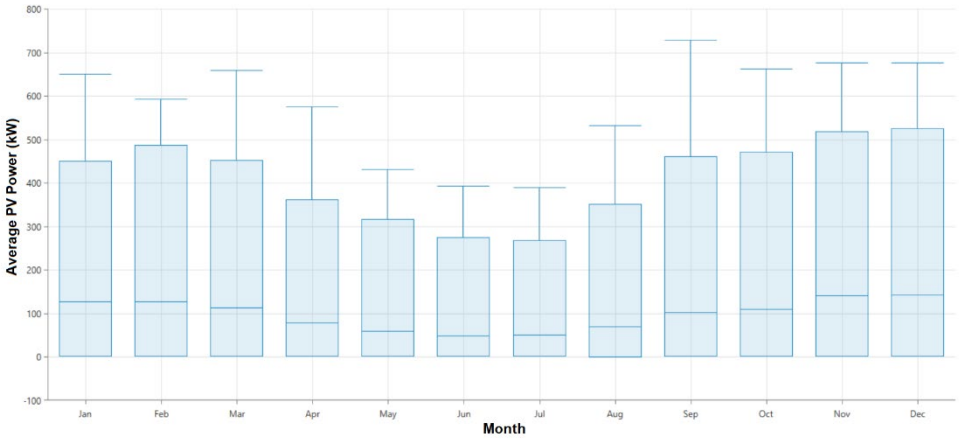

(b)

Figure 4.3.6: Aggregated total PV generation of Donald Town (3480) for the year 2020. (a) Hourly PV generation data. (b) Monthly average PV generation

Table 4.3.2 shows the aggregated PV generation data analysis results. Peak generation and number of PV customers match with information provided in the Powercor Presentation slides.

Table 4.3.2: Donald Town aggregated PV generation data for the year 2020.

Metric	**Baseline**
Total Customers with PV	**201(approximate)**
Peak PV generation Month	**December**

Average PV generation (kWh/day)	**2,333.8**
Average PV (kW)	**97.2**
Peak PV (kW)	**728.66**

Weather data for HOMER Pro input

Solar irradiance (kWh/m^2/day) and temperature (°C) data of the Donald town have been collected from the NASA surface metrology. These data can also be collected from Bureau of Metrology, Australia. Figure 4.3.6 shows the solar irradiance and temperature data of Donald town for the year 2020.

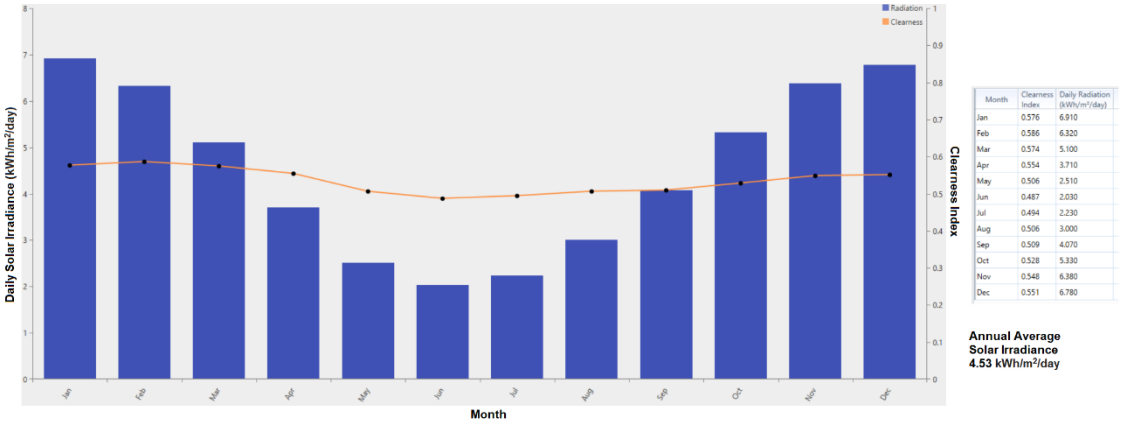

(a)

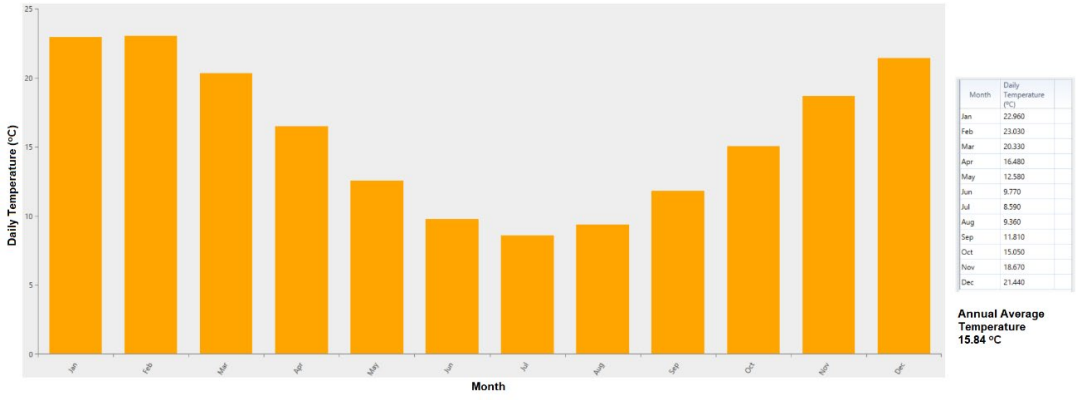

(b)

Figure 4.3.7: Weather Data of Donald Town. (a) Daily average solar irradiance. (b) Daily Temperature.

Donald Town Microgrid-Optimal Hosting Capacities

Table 4.3.3 shows the optimal hosting capacities under the most appropriate energy dispatch strategy for three operation modes of the microgrid. It is expected that the microgrid will mostly operate in grid-connected mode, and only when a major outage/fault occurred in the main grid, the microgrid will operate in the stand-alone mode. Hosting capacities for VPP mode result in higher battery storage capacity requirement. Table 4.3.3 also shows the actual microgrid components suggested for this design. These hosting capacities have been tested in Section 4.5 for microgrid operation to ensure that the power system operation does not violate the upper and lower voltage limits.

Table 4.3.3: Grid-connected, VPP, and Stand-alone operation of Donald Town Microgrid and Area Hosting Capacities

Operation Mode	Energy Dispatch Strategy	PV Hosting Capacity (kW)	Storage Hosting Capacity (kWh)	Storage Converter Size (kW)	Back-up Generator Size (kW)
Grid-connected	**Load Following** • *Time of Use Tariff* • *Dispatch Algorithm has no advance knowledge of grid outages*	**3078**	**1015**	**641**	1000 (Small)
VPP (grid-connected)	**Predictive + Load Following** • *Forecasted load + Forecasted generation* • *Time of Use Tariff* • *Dispatch Algorithm has no advance knowledge of grid outages*	**3507**	**7049**	**1716**	2800 (Large) 1800 (Medium) 1000 (Small)
Stand-Alone/Islanded	Load Following	**3216**	**4627**	**1639**	2800 (Large)
Data Input: • 30 minutes resolution load data of 2020 supplied by Powercor • 30 minutes resolution PV generation data of 2020 supplied by Powercor • Actual Solar Irradiance data collected from NASA surface metrology • Actual Temperature (NASA surface metrology) • GloBird Energy Time of Use electricity pricing for postcode 3480 • Incoming feeder reliability data supplied by Powercor	Suggested Microgrid Component: ➢ **PV Unit:** Generic Flat Plate PV; Rated Capacity:1 kW; NOCT-47^{0}C; Efficiency: 13%; Temperature Co-efficient: -0.5 ➢ **Storage (Battery Unit):** Generic 1 kWh Li-Ion; Nominal Voltage: 6V; Nominal Ah: 167; Max. Charge Current: 167 A; Max. Discharge Current: 500 A; Roundtrip Efficiency: 90% ➢ **Converter Unit for Battery:** 1 kW Generic bi-directional converter; Inverter/rectifier efficiency: 95% ➢ **Alternative Storage (Hydrogen Unit):** UNSW LAVO, 40 kWh hydrogen storage, Nominal Voltage: 48V; Nominal Ah: 833; Max. Charge Current: 833 A; Max. Discharge Current: 833 A; Roundtrip Efficiency: 95% ➢ **Converter Unit for Hydrogen: 5** kW Generic bi-directional converter; Inverter/rectifier efficiency: 95% ➢ **Back-up Generator Unit (Diesel)**: Caterpillar CAT-3500 kVA (2800 kW)/ 50 HZ/1500 RPM Prime Power; Caterpillar CAT-C3516B Prime (1825 kW)/ 50 HZ Prime Power; Caterpillar CAT-C32 Prime (910 kW)/ 50 HZ Prime Power ➢ **Alternative Back-up Generator Unit (Biodiesel B20):** GFC SG550A-550 kVA (440 kW)/500 kVA (400 kW), 50 Hz; GFC HSW-305 T5 330 KVA (264 kW)/300 kVA (240 kW), 50 Hz; GFC HFW-160 T5 175 kVA (140 kW)/ 160 kVA(128 kW), 50 Hz				

Donald Town Microgrid- Comparison of Grid-connected and VPP operation modes

Time-domain simulation for net energy balancing is performed for the year 2020 considering the load and weather data under grid-connected and VPP operation modes. Figure 4.3.8 shows the various energy generation and consumption from June 10 to June 16 of the year 2020.

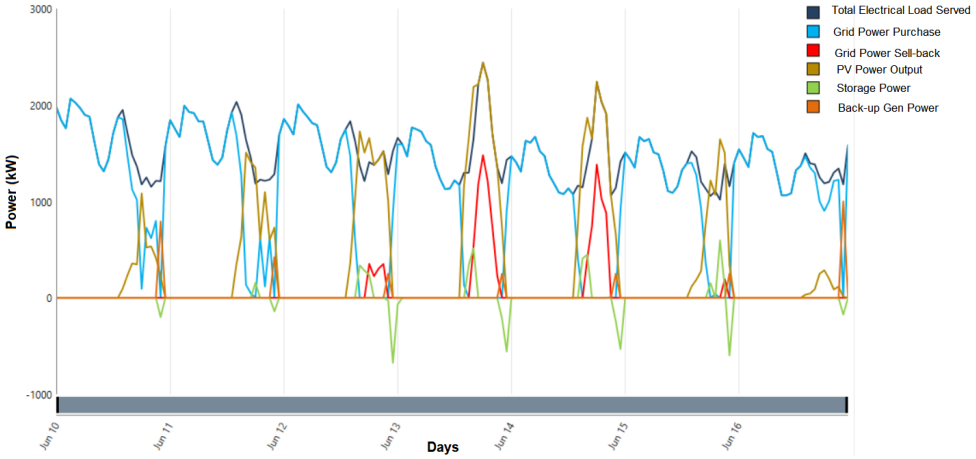

Figure 4.3.8: Time-domain simulation of energy balancing under grid connected mode (Donald Town Microgrid)

Table 4.3.4 shows the comparison of grid-connected and VPP mode operations with the smallest back-up generator considering various main grid reliability parameters.

Table 4.3.4 : Comparison of Grid-connected and VPP mode operations of Donald Town Microgrid

Operation Mode	PV Hosting Capacity (kW)	Storage Hosting Capacity (kWh)	Storage Converter Size (kW)	Back-up Generator Size (kW)	Cost of Energy (COE)	Initial Capital cost	Renewable Energy Fraction	Main Grid Reliability Mean outage frequency/year = 7 Mean Repair Time = 0.5 hour	Main Grid Reliability Mean outage frequency/year = 14 Mean Repair Time = 1 hour	Main Grid Reliability Mean outage frequency/year = 14 Mean Repair Time = 2 hour
Grid-connected	**3078**	**1015**	**641**	1000 (Small)	$0.164	$ 8.75 millions	36.9%	Can manage	**Cannot manage. Small % of load unmet**	**Cannot manage. Small % of load unmet**
VPP (grid-connected)	**3507**	**7049**	**1716**	1000 (Small)	$0.206	$13.2 millions	42.2%	Can manage	Can manage	Can manage

4.3.3. Tarnagulla Town Microgrid Hosting Capacity Assessment

Areas to be Considered

Figure 4.3.9 shows the areas which will be covered by Tarnagulla Town microgrid along with respective postcodes.

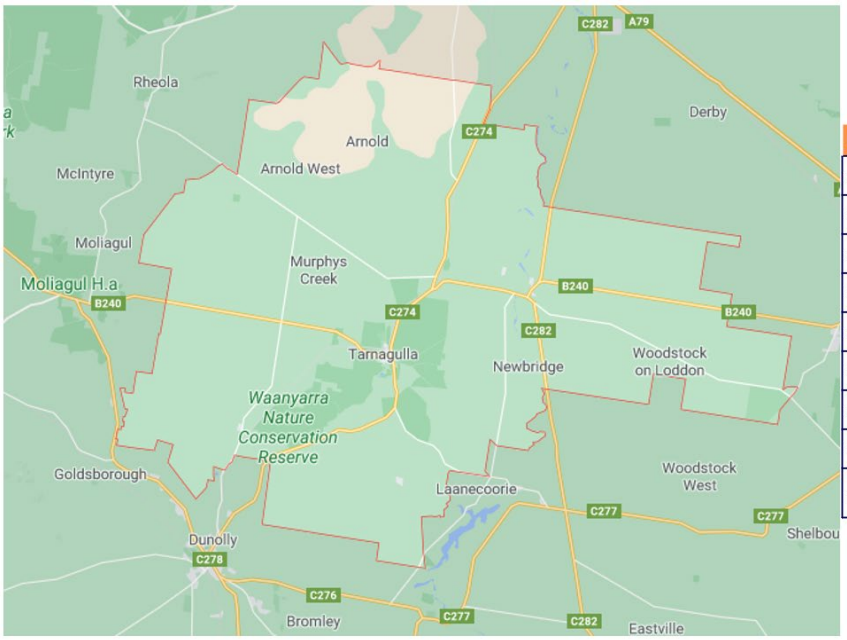

Postcode	Suburb
3551	ARNOLD, VIC
3551	ARNOLD WEST, VIC
3551	LLANELLY, VIC
3551	MURPHYS CREEK, VIC
3551	NEWBRIDGE, VIC
3551	PAINSWICK, VIC
3551	TARNAGULLA, VIC
3551	WAANYRRA, VIC
3551	WOODSTOCK ON LODDON, VIC

Figure 4.3.9: Tarnagulla Town (3551) microgrid- areas to be considered.

Smart meter load data analysis for HOMER Pro input

Powercor Australia has supplied smart meter load data for the year 2020 at all the available power system load nodes in the Tarnagulla town area. These data files are provided in 30 minutes resolution starting on January 1 at 0.00 hours and ending at 23:30 hours on the same day for 366 days. Same as the Donald town load data, some of the days' data were missing. These missing data

are filled by using the HOMER Pro load data analysis module. Figure 4.3.10 shows the aggregated smart meter load data.

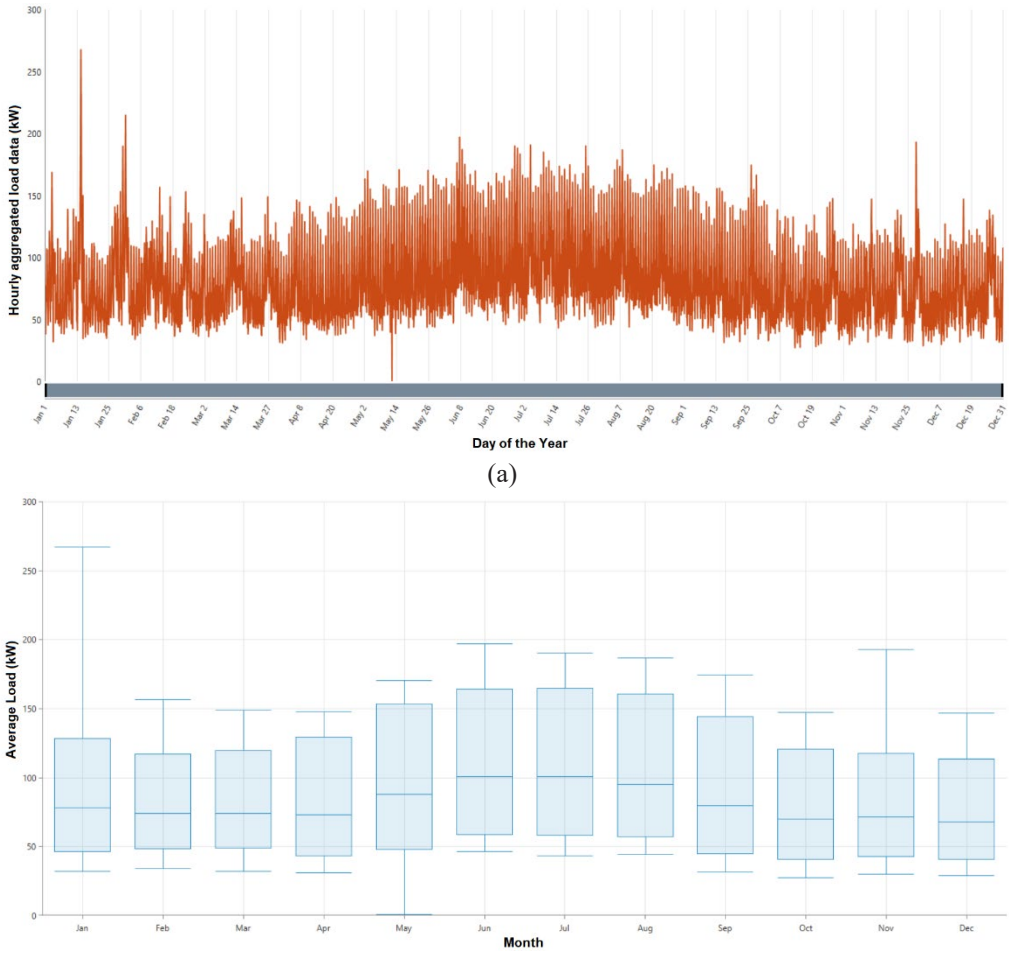

Figure 4.3.10: An aggregated total load of Tarnagulla Town (3551) for the year 2020. (a) Hourly data. (b) Monthly average load

Table 4.3.5 shows the aggregated load data analysis results. Peak load and the number of customers match with the total transformer loading capacity and customer nodes found in Tarnagulla microgrid network modelling of Section 4.1.

Table 4.3.5: Tarnagulla Town aggregated load data for the year 2020.

Metric	**Baseline**
Total Customer/Smart Meter Data Nodes	**151 (approximate)**
Peak Load Month	**July**
Average (kWh/day)	**1,947.5**
Average (kW)	**81.15**
Peak (kW)	**267.48**
Load Factor	**0.3**

Smart meter generation data analysis for HOMER Pro input

Same as Donald town, Powercor Australia has also supplied smart meter generation data for the year 2020 at all the available local generation nodes in the Tarnagulla town area. Same as the load data, these data files are provided in 30 minutes resolution starting on January 1 at 0.00 hours and ending at 23:30 hours on the same day for 366 days. Some of the days' data were missing. These missing data are filled by using the HOMER Pro PV generation analysis. Figure 4.3.11 shows the aggregated smart meter current generation data analysis.

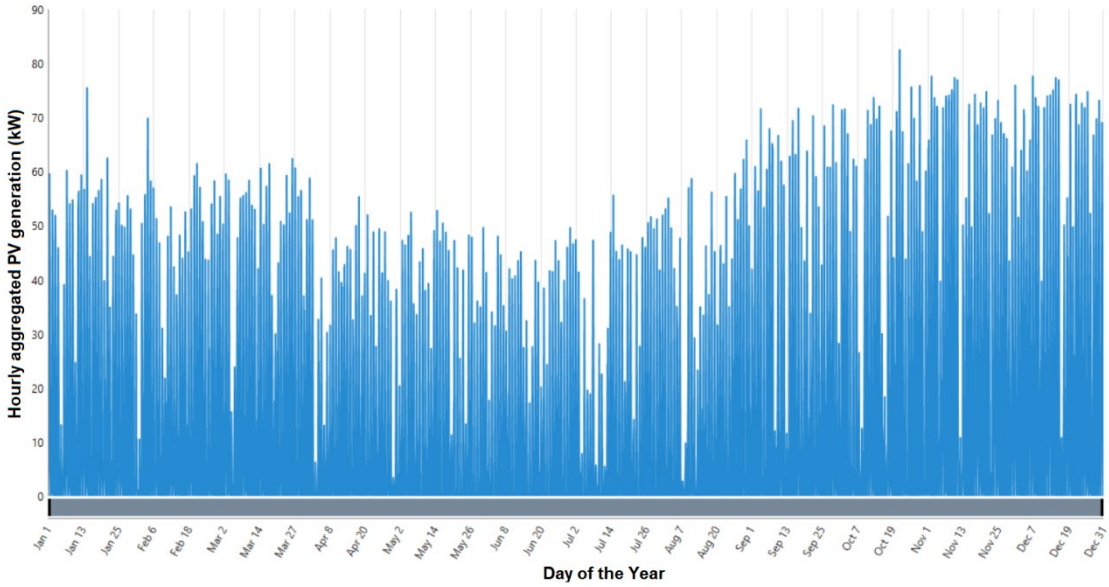

(a)

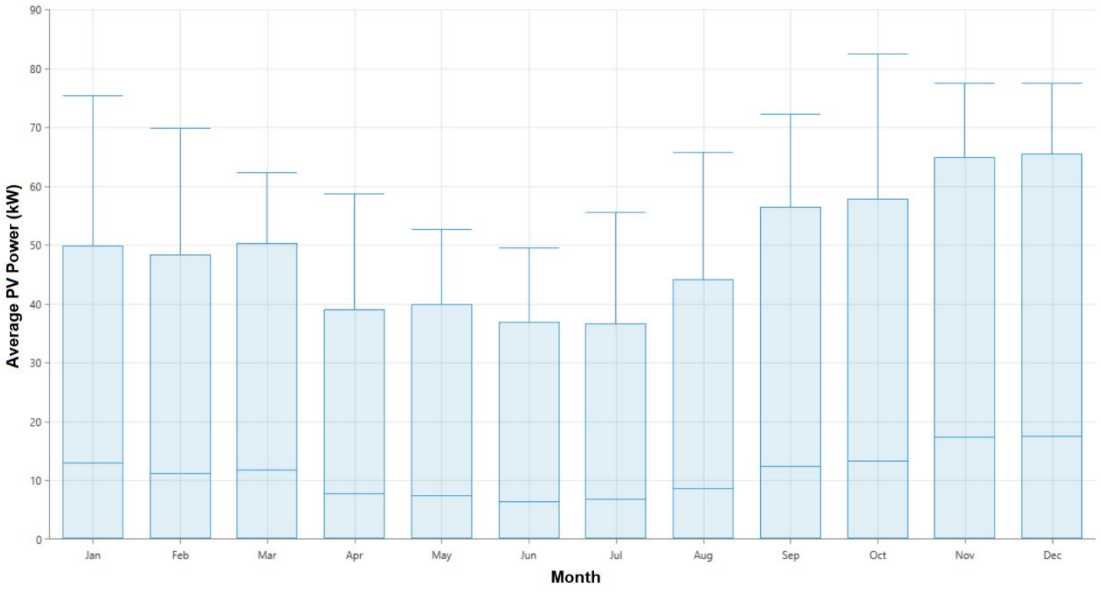

(b)

Figure 4.3.11: Aggregated total PV generation of Tarnagulla Town (3551) for the year 2020. (a) Hourly PV generation data. (b) Monthly average PV generation

Table 4.3.6 shows the aggregated PV generation data analysis results. Peak generation and number of PV customers match with information provided in the Powercor Presentation slides.

Table 4.3.6: Tarnagulla Town aggregated PV generation data for the year 2020.

Metric	Baseline
Total Customers with PV	**34 (approximate)**
Peak PV generation Month	**December**
Average PV generation (kWh/day)	**266.26**
Average PV (kW)	**11.09**
Peak PV (kW)	**82.5**

Weather data for HOMER Pro input

Same as Donald town, solar irradiance (kWh/m^2/day) and temperature (^{o}C) data of the Tarnagulla town have been collected from the NASA surface metrology. These data can also be collected from Bureau of Metrology, Australia. Figure 4.3.12 shows the solar irradiance and temperature data of Tarnagulla town for the year 2020.

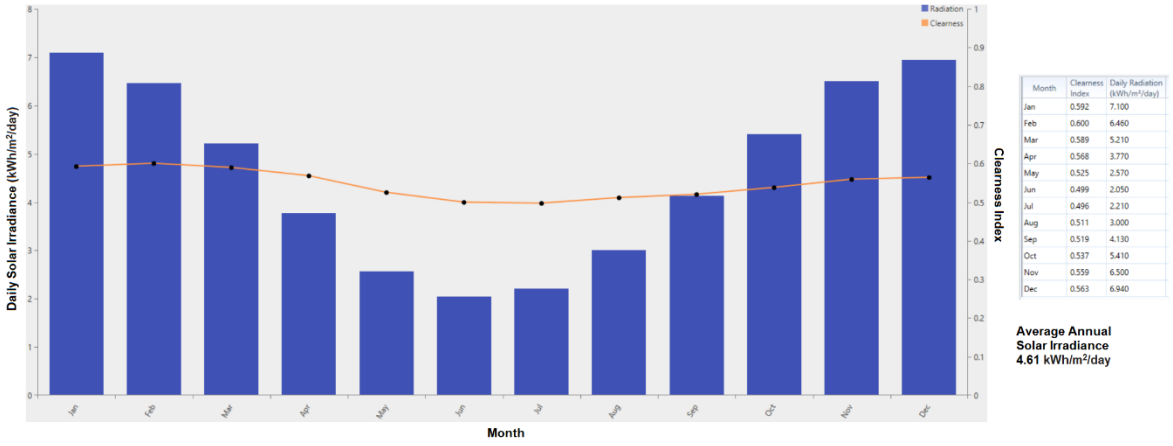

(a)

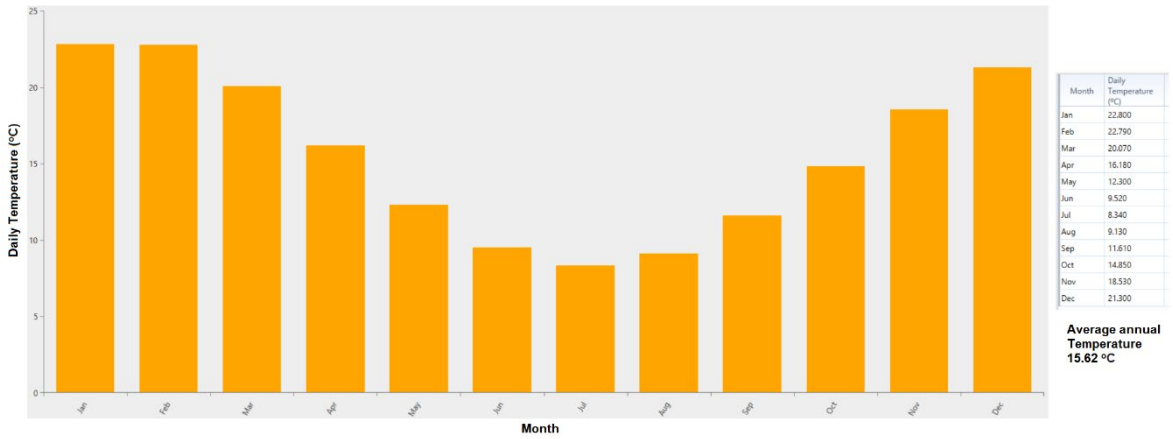

(b)

Figure 4.3.12: Weather Data of Tarnagulla Town. (a) Daily average solar irradiance. (b) Daily Temperature.

Tarnagulla Town Microgrid-Optimal Hosting Capacities

Table 4.3.7 shows the optimal hosting capacities under the most appropriate energy dispatch strategy for three operation modes of the Tarnagulla microgrid. It is expected that the Tarnagulla microgrid will mostly operate in grid-connected mode and only when a major outage/fault occurred in the main grid, the microgrid will operate in the stand-alone mode. Hosting capacities for VPP mode result in higher battery storage capacity requirement. Table 4.3.7 also shows the actual microgrid components suggested for this design. These hosting capacities have been tested in Section 4.5 for microgrid operation to ensure that the power system operation does not violate the upper and lower voltage limits.

Table 4.3.7: Grid-connected, VPP, and Stand-alone operation of Tarnagulla Town Microgrid and Area Hosting Capacities

Operation Mode	Energy Dispatch Strategy	PV Hosting Capacity (kW)	Storage Hosting Capacity (kWh)	Storage Converter Size (kW)	Back-up Generator Size (kW)
Grid-connected	**Load Following** • *Time of Use Tariff* • *Dispatch Algorithm has no advance knowledge of grid outages*	**115**	**75**	**23**	120 (Small)
VPP (grid-connected)	**Predictive + Load Following** • *Forecasted load + Forecasted generation* • *Time of Use Tariff* • *Dispatch Algorithm has no advance knowledge of grid outages*	**155**	**192**	**111**	320 (Large) 240 (Medium) 120 (Small)
Stand-Alone/Islanded	Load Following	**131**	**148**	**101**	320 (Large)
Data Input: • 30 minutes resolution load data of 2020 supplied by Powercor • 30 minutes resolution PV generation data of 2020 supplied by Powercor • Actual Solar Irradiance data collected from NASA surface metrology • Actual Temperature (NASA surface metrology) • GloBird Energy Time of Use electricity pricing for postcode 3551 • Incoming feeder reliability data supplied by Powercor	Suggested Microgrid Component: ➢ **PV Unit:** Generic Flat Plate PV; Rated Capacity:1 kW; NOCT-47^{0}C; Efficiency: 13%; Temperature Co-efficient: -0.5 ➢ **Storage (Battery Unit):** Generic 1 kWh Li-Ion; Nominal Voltage: 6V; Nominal Ah: 167; Max. Charge Current: 167 A; Max. Discharge Current: 500 A; Roundtrip Efficiency: 90% ➢ **Converter Unit for Battery:** 1 kW Generic bi-directional converter; Inverter/rectifier efficiency: 95% ➢ **Alternative Storage (Hydrogen Unit):** UNSW LAVO, 40 kWh hydrogen storage, Nominal Voltage: 48V; Nominal Ah: 833; Max. Charge Current: 833 A; Max. Discharge Current: 833 A; Roundtrip Efficiency: 95% ➢ **Converter Unit for Hydrogen: 5** kW Generic bi-directional converter; Inverter/rectifier efficiency: 95% ➢ **Back-up Generator Unit (Diesel)**: Caterpillar CAT-C13 Prime (365 kW)/ 50 HZ Prime Power, Caterpillar CAT-C9 Prime (275 kW)/ 50 HZ Prime Power, Caterpillar CAT-150kVA (120 kW)/50 Hz prime power ➢ **Alternative Back-up Generator Unit (Biodiesel B20):** GFC SG550A-550 kVA (440 kW)/500 kVA (400 kW), 50 Hz; GFC HSW-305 T5 330 KVA (264 kW)/300 kVA (240 kW), 50 Hz; GFC HFW-160 T5 175 kVA (140 kW)/ 160 kVA(128 kW), 50 Hz				

Tarnagulla Town Microgrid- Comparison of Grid-connected and VPP operation modes

Same as Donald microgrid, time-domain simulation for net energy balancing is performed for the year 2020 considering the load and weather data under grid-connected and VPP operation modes. Figure 4.3.13 shows the various energy generation and consumption from May 25 to May 31 of the year 2020.

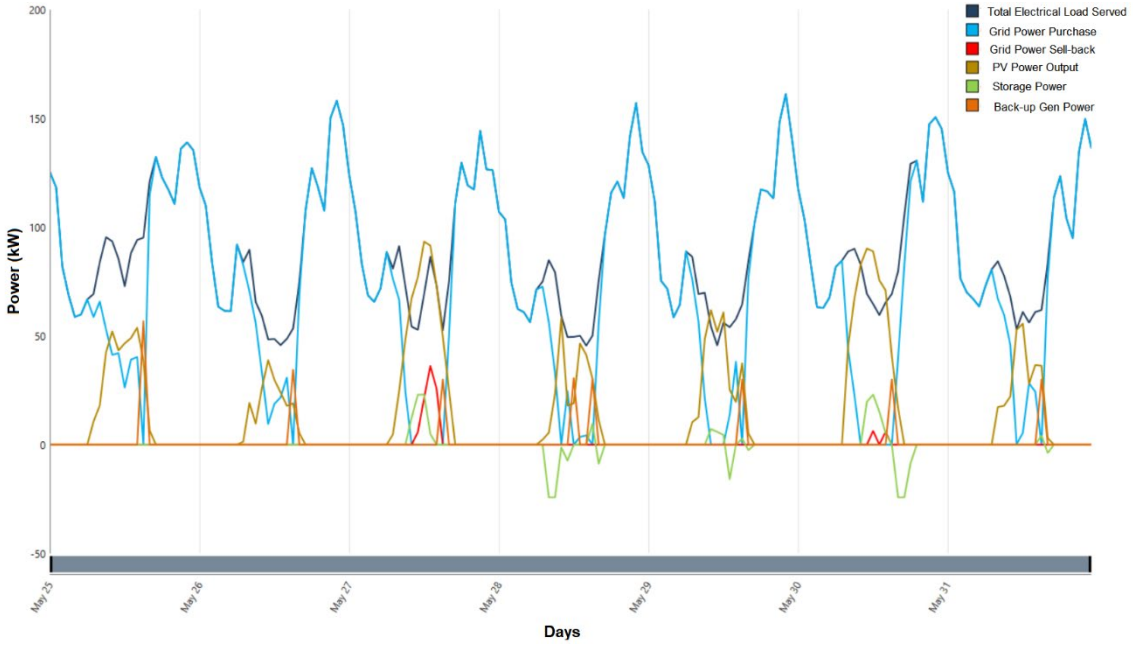

Figure 4.3.13: Time-domain simulation of energy balancing under grid connected mode (Tarnagulla Town Microgrid)

Table 4.3.8 shows the comparison of grid-connected and VPP mode operations with the smallest back-up generator considering various main grid reliability parameters.

Table 4.3.8 : Comparison of Grid-connected and VPP mode operations of Tarnagulla Town Microgrid

Operation Mode	**PV Hosting Capacity (kW)**	**Storage Hosting Capacity (kWh)**	**Storage Converter Size (kW)**	**Back-up Generator Size (kW)**	**Cost of Energy (COE)**	**Initial Capital cost**	**Renewable Energy Fraction**	**Main Grid Reliability** Mean outage frequency/year = 11 Mean Repair Time = 1 hour	**Main Grid Reliability** Mean outage frequency/year = 22 Mean Repair Time = 2 hours	**Main Grid Reliability** Mean outage frequency/year = 22 Mean Repair Time = 4 hours
Grid-connected	**115**	**75**	**23**	120 (Small)	$0.171	$ 335.65 thousands	23.0%	Can manage	**Cannot manage. Small % of load unmet**	**Cannot manage. Small % of load unmet**
VPP (grid-connected)	**155**	**192**	**111**	120 (Small)	$0.178	$ 526.40 thousands	30.2%	Can manage	Can manage	Can manage

4.3.4. Summary and Conclusions

- From the time series results of net energy balancing, it has been found that the optimally sized microgrid can meet the electric load demand reliably and continuously under different operation scenarios.
- Grid-connected operation of microgrid under load following dispatch strategy provides the most cost-effective design of microgrid. However, if the incoming utility feeder's reliability (Charlton aka CTN and Maryborough aka MRO) is somewhat less than the standard requirements, the energy security will be compromised unless a large backup generator or large-capacity storage system is present.

- Grid connected operation of microgrid under virtual power plant (VPP) and load following dispatch strategy provides the most ideal design. However, the initial capital cost will be significant and can be recovered within a couple of years.
- VPP operation provides the best energy security. However, if significant forecasting errors are present in the load and generation forecasting, an intelligent energy management solution will be necessary.
- These optimal hosting capacities of the Donald and Taranagulla microgrid are used as the base-case scenario for the microgrid's steady-state and quasi-dynamic operation simulations and are found to be acceptable as they do not violate the distribution voltage limits.

4.4. Microgrid Reliability Analysis

The reliability analysis of a microgrid mostly represents the service availability to the microgrid community. The reliability is influenced mainly by the (un)availability of the supply feeder and various equipment outage. Microgrid network model has been designed with all relevant protection devices for reliability analysis. Three selected reliability indices have been presented here, which are SAIDI (System Average Interruption Duration Index), SAIFI (System Average Frequency Duration Index), and ENS (Energy Not Supplied). Reliability calculation has been performed considering one-year timeframe. The reliability analysis has been performed in grid-connected and islanded mode with respect to different solar PV hosting capacity levels.

4.1.1. Microgrid Reliability Model

Details of the microgrid model (for power flow simulation) has been presented in Section 4.1. In addition to that, the reliability model is equipped with additional protection devices (such as circuit breakers) and reliability model of the individual devices. Figure 4.4.1 and Fig. 4.4.2 presents the reliability model of the Donald and Tarnagulla microgrid respectively. The reliability models of the feeder, transformer, solar PV and battery storage devices are presented in Table 4.4.1.

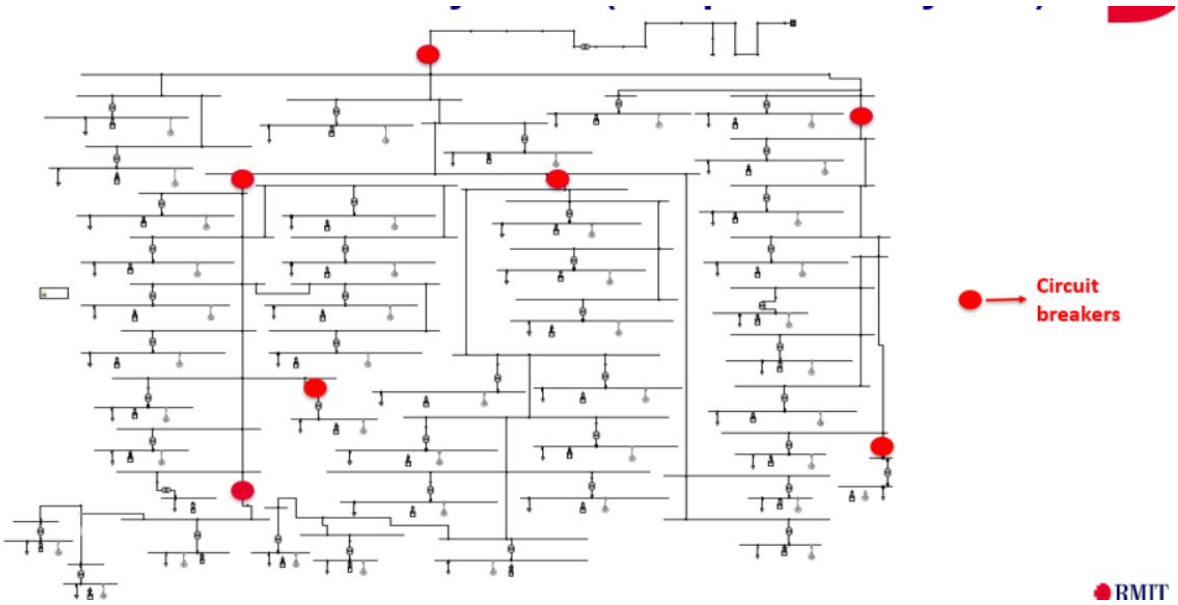

Fig. 4.4.1: The reliability model of the Donald microgrid.

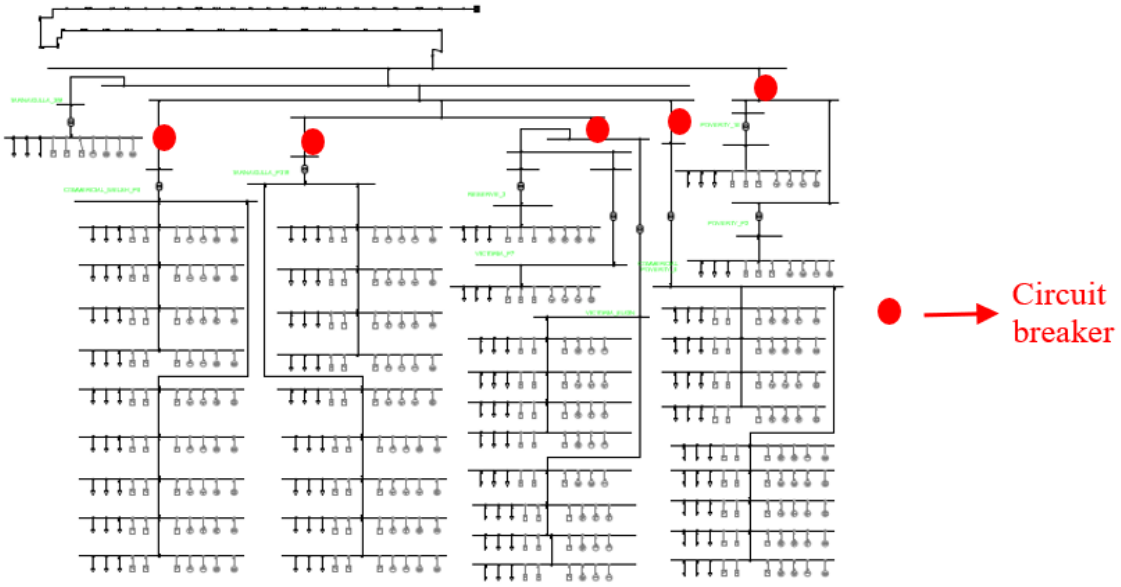

Fig. 4.4.2: The reliability model of the Tarnagulla microgrid.

Table 4.4.1: Input reliability parameters.

Input Reliability data		
CB at 22 kV feeder	Time to actuate switch	30 min
	CB fails to open	5%
CB at secondary side of transformer	Time to actuate switch	1 min
Terminal 22 kV	Forced Outage rate	0.0104 1/a
	Forced Outage Expectancy	0.208 h/a
	Forced Outage Duration	20 h
	Failure frequency	1.99094
Terminal 0.4 kV	Repair duration	1.914055
22 kV overhead lines	Failure frequency	0.177 1/(_a*km)
	Repair duration	10 h
	Transient fault frequency	12.5053
Solar-PV	Failure rate	0.2487
	Repair duration	40 h
Battery	Failure rate	0.2487
	Repair duration	40 h

Reliability Indices

Three reliability indices have been calculated for both microgrids, which are described below:

SAIDI (System Average Interruption Duration Index, in units of [h/C/a]) indicates the total duration of interruption for the average customer during the period in the calculation. It is commonly measured in customer minutes or customer hours of interruption (per year).

$$SAIDI = \frac{\sum ACIT_i * C_i}{\sum C_i} \text{ h/C/a}$$

Here, $ACIT$ is average customer interruption time, C_i is the number of customers supplied by load point i, and C is the number of customers.

SAIFI (System Average Interruption Frequency Index, in units of [1 /C/a]), indicates how often the average customer experiences a sustained interruption during the period specified in the calculation.

$$SAIFI = \frac{\sum ACIF_i * C_i}{\sum C_i} \text{ 1/C/a}$$

Here, $ACIF$ is average customer interruption frequency, C_i is the number of customers supplied by load point i, and C is the number of customers.

ENS (Energy Not Supplied, in units of [MWh/a]), is the total amount of energy on average not delivered to the system loads.

Microgrid Reliability

The reliability results (SAIDI, SAIFI, and ENS) have been presented below in grid-connected mode and islanded mode with respect to different levels of hosting capacity.

Grid-connected vs. islanded mode reliability

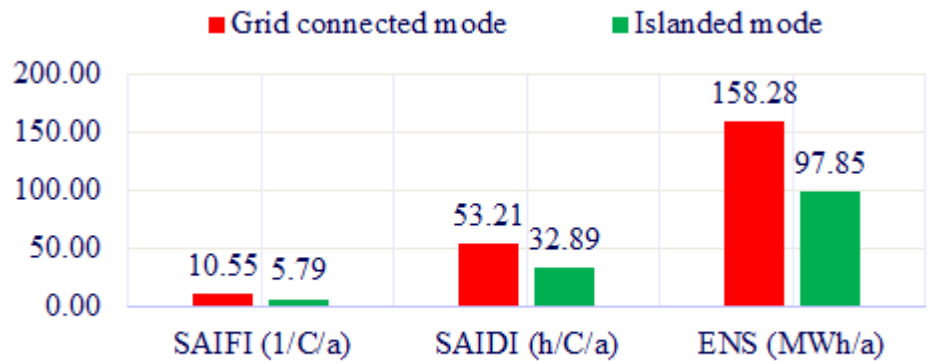

Fig. 4.4.3: The reliability indices of the Donald microgrid in grid-connected and islanded mode.

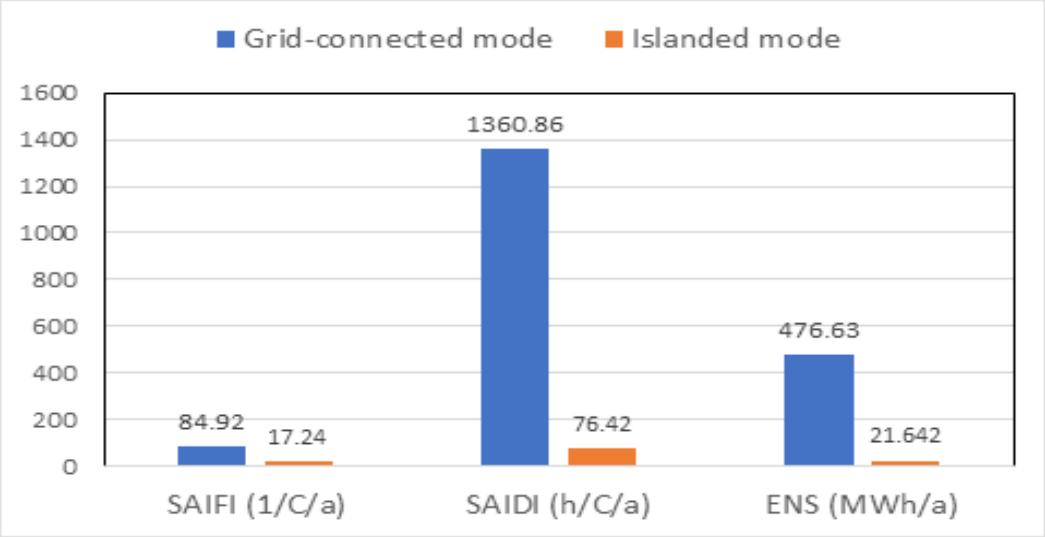

Fig. 4.4.4: The reliability indices of the Tarnagulla microgrid in grid-connected and islanded mode.

Figure 4.4.3 presents the SAIDI, SAIFI, and ENS values for grid-connected and islanded mode. It can be seen from the figure that all reliability parameters have been decreased significantly. A decline in the reliability parameters (SAIDI, SAIFI, and ENS) in the islanded mode indicate higher reliability of the microgrid. The SAIDI, SAIFI, and ENS have been decreased by 45%, 38%, and 38%, respectively, in the islanded mode. The Donald microgrid is supplied by a long feeder, which experiences low reliability. It is common for long rural feeder to suffer from low reliability. Due to the low reliability of the incoming supply feeder, the system reliability has been improved in the islanded mode.

Figure 4.4.4 presents the SAIDI, SAIFI, and ENS values of the Tarnagulla microgrid for grid-connected and islanded mode. It can be seen from the figure that all reliability parameters have been decreased significantly. A decline in the reliability parameters (SAIDI, SAIFI, and ENS) in the islanded mode indicate higher reliability of the microgrid. The SAIDI, SAIFI, and ENS have been decreased by 79.66%, 94.38%, and 95.45%, respectively, in the islanded mode. The Tarnagulla microgrid is supplied by a 53 km long feeder, which experiences low reliability. It is common for long rural feeder to suffer from low reliability. Due to the low reliability of the incoming supply feeder, the system reliability has been improved in the islanded mode.

Grid-connected mode: reliability w.r.t. PV hosting capacity

Figure 4.4.5 presents the SAIDI, SAIFI, and ENS values with respect to different levels of PV hosting capacity for grid connected mode. It can be seen from the figure that all reliability parameters have been decreased, with increased PV hosting capacity. A decline in the reliability parameters (SAIDI, SAIFI, and ENS) with increased hosting capacity indicate higher reliability of the microgrid. The change in the system reliability with respect to the increased hosting capacity is measured by a sensitivity index, as presented below:

$$Reliability\ change\ factor = \frac{Change\ in\ Reliability}{Change\ in\ PV\ hosting\ capacity}$$

The reliability change factor for SAIDI, SAIFI, and ENS have been calculated -1.8, -7.5, and -22.4 respectively, for average 1 unit of PV scaling factor. The negative sign in the reliability change factor indicates that SAIDI, SAIFI and ENS will decrease (resulting higher reliability) with increased PV hosting capacity. Also, 1 unit (100%) increase of PV hosting capacity will decrease SAIDI, SAIFI and ENS by 1.8, 7.5 and 22.4 unit, respectively.

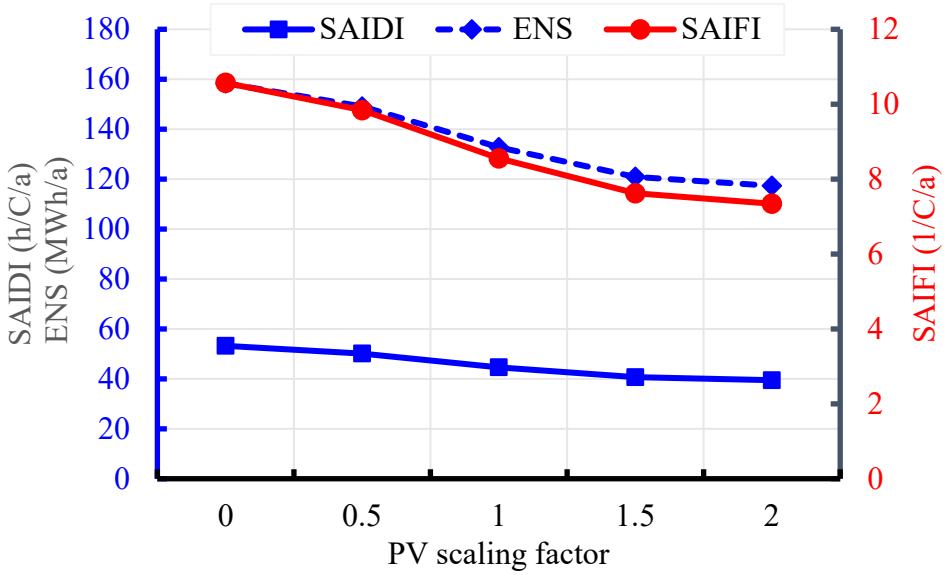

Fig. 4.4.5: The reliability indices of the Donald microgrid in grid-connected mode with different hosting capacity.

Islanded mode: reliability w.r.t. PV hosting capacity

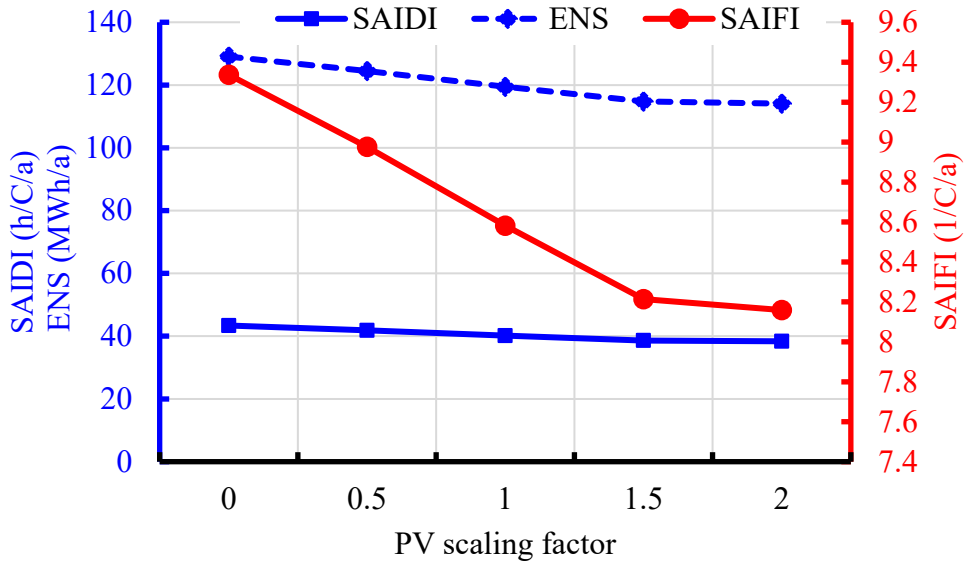

Fig. 4.4.6: The reliability indices of the Donald microgrid in islanded mode with different hosting capacity.

Figure 4.4.6 presents the SAIDI, SAIFI, and ENS values with respect to different levels of PV hosting capacity for islanded mode. It can be seen from the figure that all reliability parameters have been decreased, with increased PV hosting capacity. A decline in the reliability parameters (SAIDI, SAIFI, and ENS) with increased hosting capacity indicate higher reliability of the microgrid. The change in the system reliability with respect to the increased hosting capacity is measured by a sensitivity index, as presented below:

$$Reliability\ change\ factor = \frac{Change\ in\ Reliability}{Change\ in\ PV\ hosting\ capacity}$$

The reliability change factor for SAIDI, SAIFI, and ENS have been calculated -0.72, -3.0, and -8.95 respectively, for average 1 unit of PV scaling factor. The negative sign in the reliability change factor indicates that SAIDI, SAIFI and ENS will decrease (resulting higher reliability) with increased PV hosting capacity. Also, 1 unit (100%) increase of PV hosting capacity will decrease SAIDI, SAIFI and ENS by 0.72, 3.0 and 8.95 unit, respectively.

4.4.2. Summary and Conclusions

Reliability analysis is identifying the availability and quality of services to the community. This sub-task has developed microgrid reliability model with all relevant protection devices for reliability analysis. Three most widely used reliability indices, SAIDI, SAIFI, and ENS, have been calculated. The reliability analysis has been performed in grid-connected and islanded mode with respect to different levels of PV hosting capacity.

In this study, standard reliability indices (SAIDI, SAIFI and ENS) have been calculated for multiple outage duration and multiple load interruption percentages. System reliability is deteriorated (with higher values of SAIDI, SAIFI and ENS) with increased outage duration and with higher percentages of load interruption. System reliability is increased in islanded mode compared to grid-connected mode. SAIDI, SAIFI, and ENS are decreased (i.e. system reliability is increased) with respect to the higher percentages of PV hosting capacity.

4.5. Microgrid Operation Analysis

Following the network modelling, steady-state and dynamic simulations are performed on the models to examine the important network characteristics for the base (current) case as well as different hosting scenarios. In order to show the effect of various network elements on the system performance, load-flow studies have been performed on Tarnagulla Network where voltage drops in different points in the MV and LV networks are analysed as shown in Figs. 4.5.1 and 4.5.2.

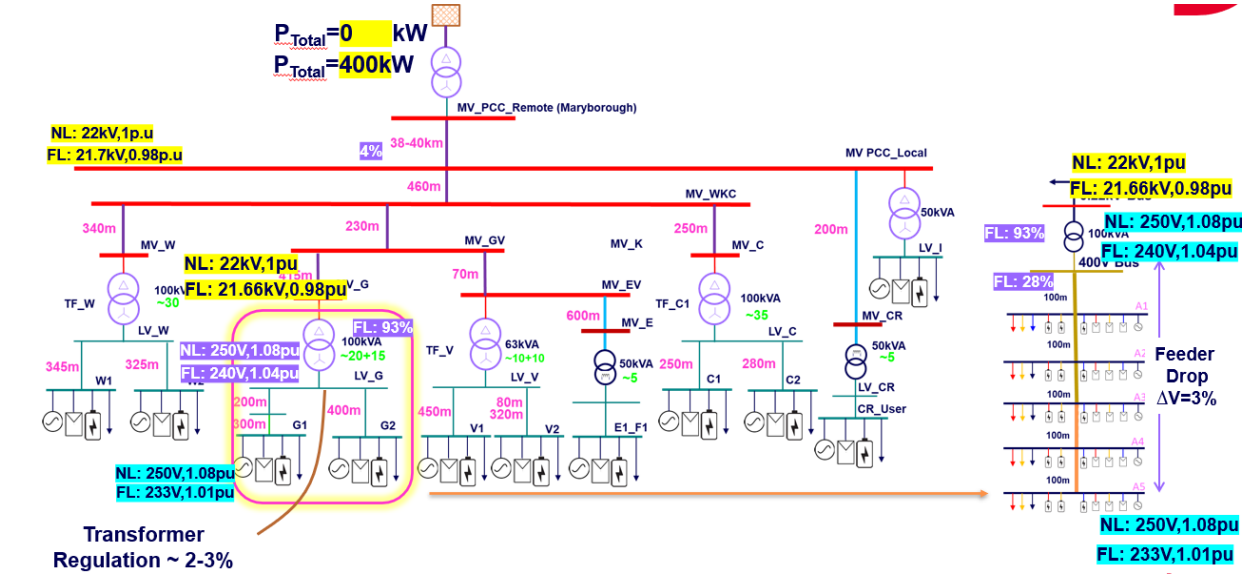

Fig. 4.5.1 Tarnagulla Network in different loading conditions

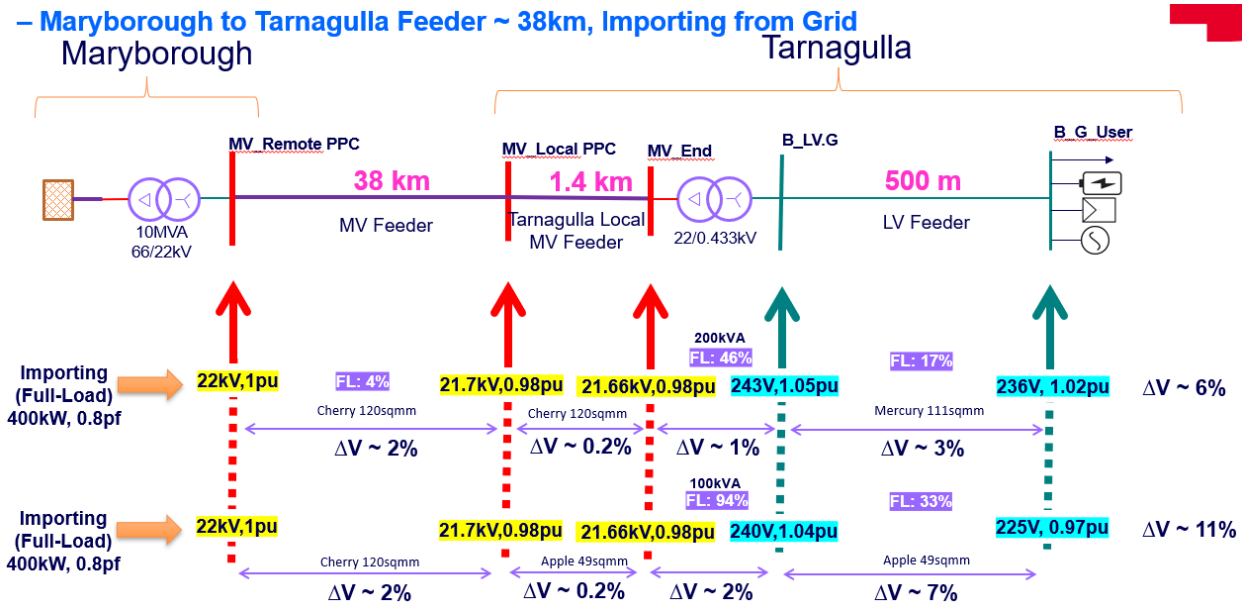

Fig. 4.5.2 Tarnagulla Network with different feeder characteristics

The analysis showed the importance of accurate modelling and network characteristics on system voltage and currents which can significantly affect the network hosting assessment. In this model, the following assumptions were considered:

- Transformers rating are estimated based on the maximum demand and the provided SINCAL model load data.
- Maximum Load Scenario: max value is decided based on the provided SINCAL and substation load data.
- As some substations load data were not available, the load is considered to be 50% of the transformer rating.
- Detailed LV Substation/Feeders is a typical network.

In order to establish the framework for further studies on both Donald and Tarnagulla networks, initial assessments have been performed on the Tarnagulla network to determine the effects of load and generation variations on system voltage levels. In these scenarios, the network load and generation (PV) are changed in the time sweep simulations, and the results are summarized in Figs. 4.5.3 to 4.5.6.

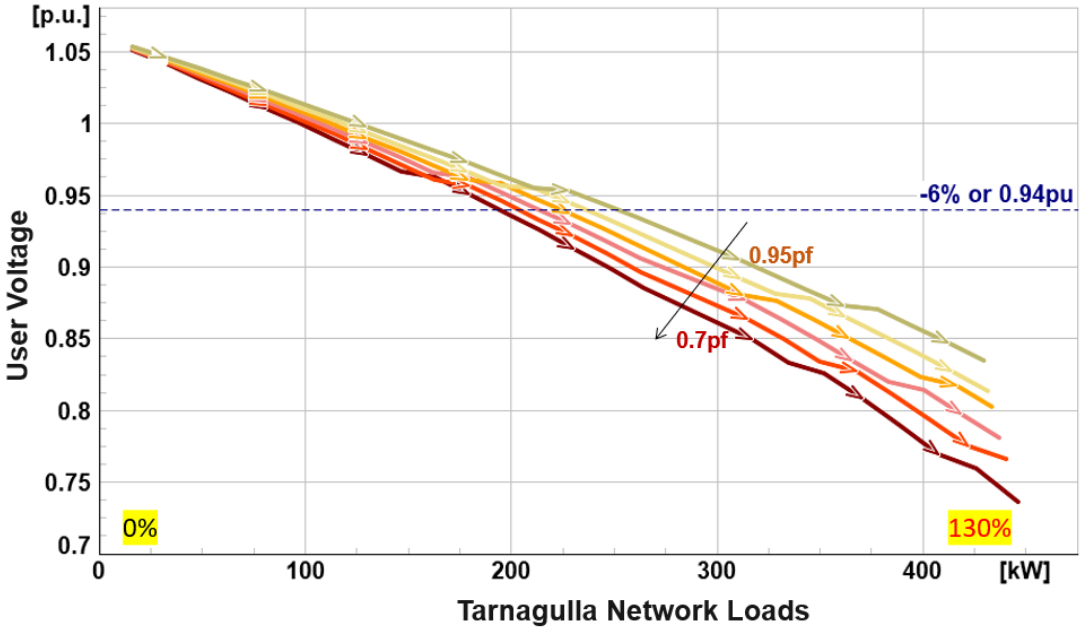

Fig. 4.5.3 Tarnagulla LV Network with different loading conditions

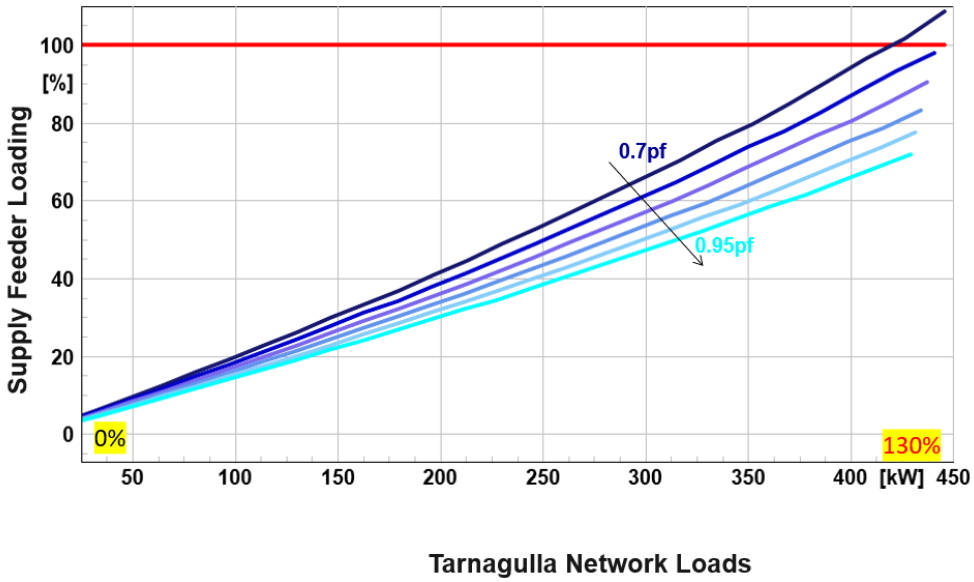

Fig. 4.5.4 Tarnagulla MV Network with different loading conditions

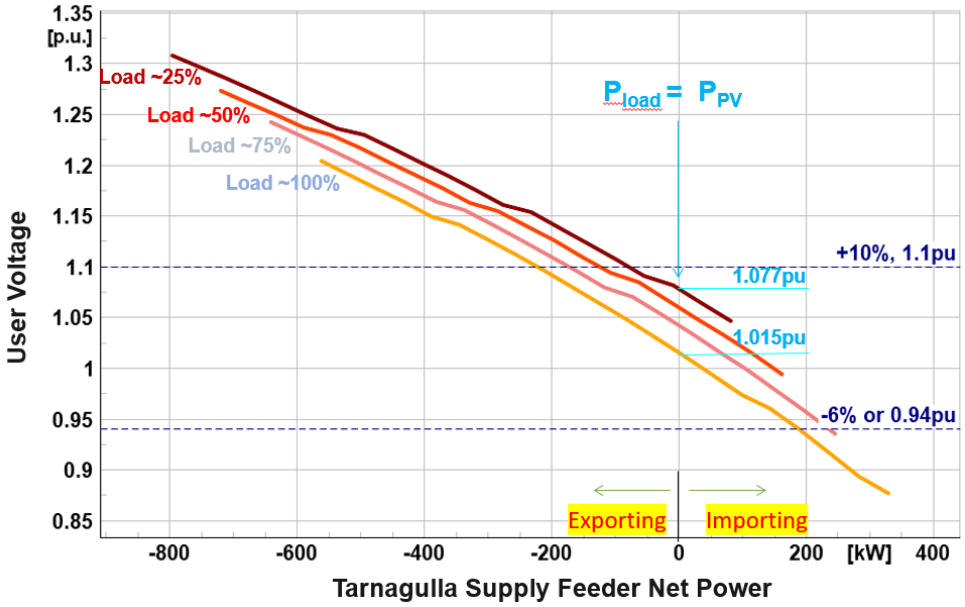

Fig. 4.5.5 Tarnagulla LV Network with different import-export scenarios

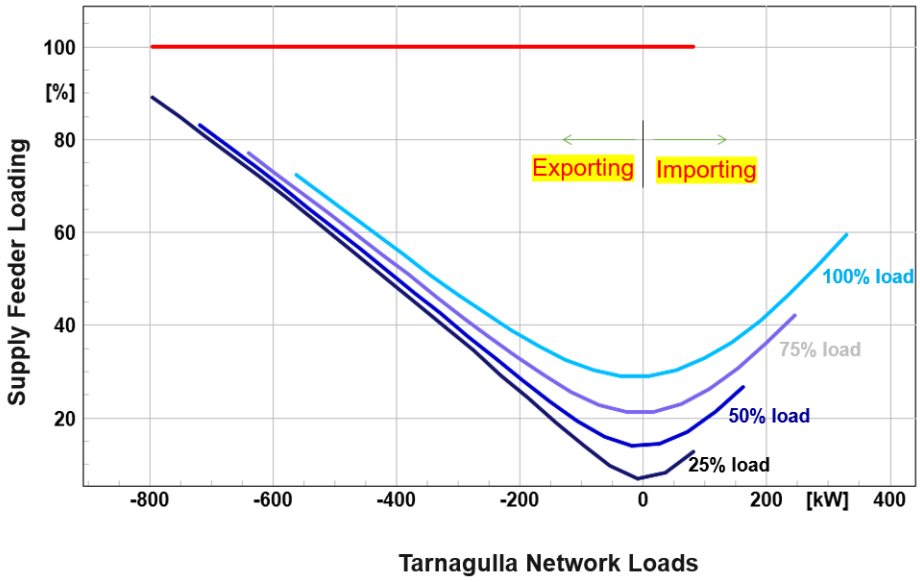

Fig. 4.5.6 Tarnagulla MV Network with different import-export scenarios

These results show that the thermal rating of the existing MV network and supply feeder is adequate with more than 400kW import 800kW export capacity. However, the load hosting and import capacity of the Tarnagulla is constrained at around 200 MW (for various pf scenarios) due to low ampacity and high impedance of the supply feeder. Furthermore, the network operating voltage remains within the permissible range (1.015pu – 1.077pu) when the load demand is met by the local generation (distributed PV) while the power export capability of the network is constrained at around 80 MW during light load condition. The export of power beyond this limit will raise the network voltage above 1.1pu, causing PV inverters to malfunction.

Following the studies explained above and based on the hosting capacity assessment studies, various scenarios have been developed and studied for the networks of Donald and Tarnagulla. Fig. 4.5.7 summarizes the methodology for microgrid operational analysis in which are presented in detail in the following sub-sections.

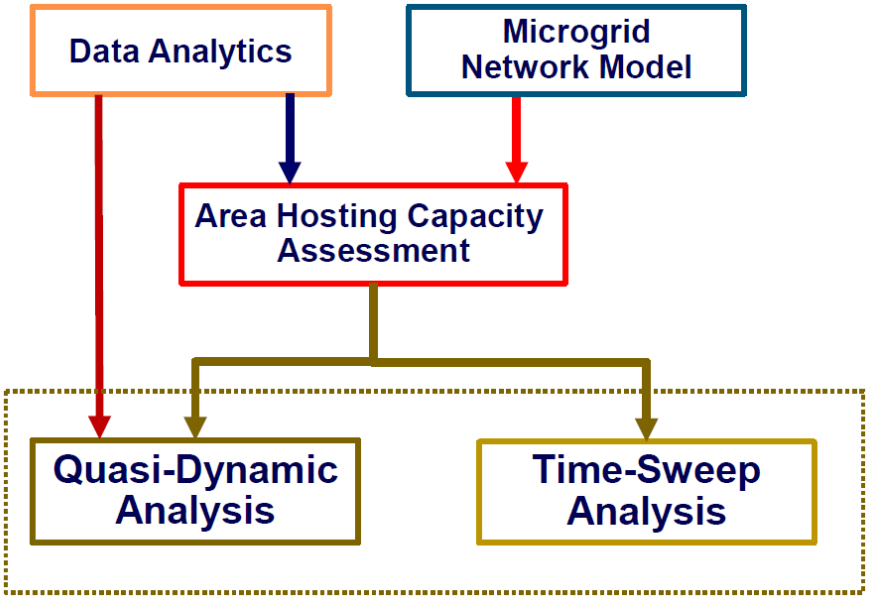

Fig. 4.5.7 Analysing the Microgrid Operation

4.5.1. Analysis of Donald Network

By analysing Donald's yearly smart meter and consumption data, the peak and average load of the network are obtained and used for hosting capacity assessment through HOMER Pro Microgrid Analysis Tool. The outcome of the hosting capacity assessment is used to create various grid-connected and stand-alone microgrid operation scenarios which are summarized in Table 4.5.1.

TABLE 4.5.1 - INTEGRATION AND OPERATIONAL SCENARIOS FOR Time-Sweep Studies of Donald

Integration Scenario	Total Load (KW)	Load Variation	Total PV (KW)	PV Variation	Total Battery Inveter (KW)	Battery Variation	Backup Generator
1	2949.6	0-130%	0		0		
2	2949.6		3216	0-130%	0		
3	2949.6		0		1639 (c)	0-130%	
4	2949.6		0		1639 (d)	0-130%	
5	1172		3216	0-130%	0		
6	1172		3216	0-130%	1639 (c)		
7	1172		3216	0-130%	1639 (d)		
8	2949.6		3216	0-130%	1639 (c)		
9	2949.6		3216	0-130%	1639 (d)		
10	2949.6		3507	0-130%	1716 (c)		

11	2949.6		3507	0-130%	1716 (d)		
12	1172		3507	0-130%	1716 (c)		
13	1172		3507	0-130%	1716 (d)		
14	2949.6		3507	0-130%	4516 (d)		
15	2949.6	0-130%	0		0		2800 kW
16	2949.6		3216	0-130%	0		2800 kW
17	2949.6		3216	0-130%	1639 (c)		2800 kW
18	2949.6		3216	0-130%	1639 (d)		2800 kW

In the developed scenarios, the loads, PV generation and Battery have changed between 0 and 130% of the nominal capacity of each scenario as shown in Table 4.5.1 through time-weep analysis. The batteries were considered in both charging (c) and discharging (d) modes. The backup generators were also used in some scenarios to investigate the stand-alone operation of the microgrid. In the stand-alone mode, the microgrid was isolated from the supply feeder at the PCC and the back-up generator was placed to support the network. In the simulated cases, voltages across different parts of the MV and LV network were analysed and the 3 phase voltage variations at 2 MV buses (**B_MV.RMT03** and **B_MV.R07**) and 2 LV buses (**B_LV.T08b** and **B_LV.T09_400V**) with respect to the total net load of the system (as seen from the PCC supply point) are illustrated in Figs. 4.5.8 – 4.5.25 to demonstrate the system operational capacities in various scenarios.

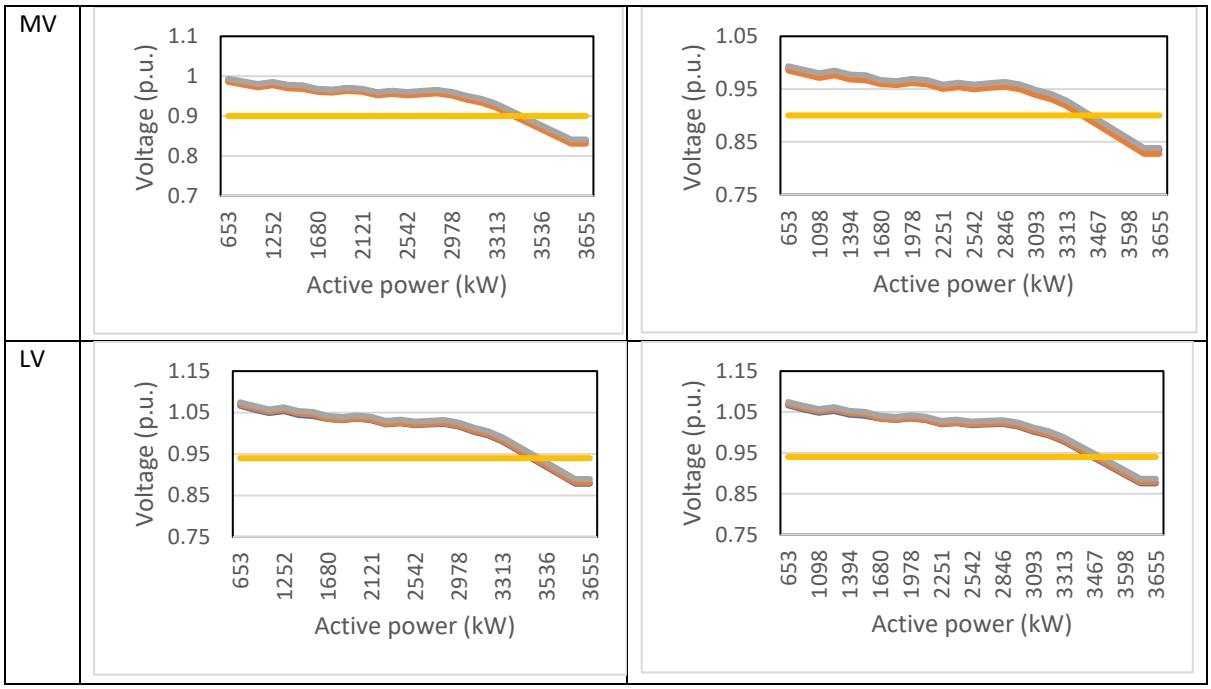

Fig. 4.5.8 Donald time-sweep integration scenario 1

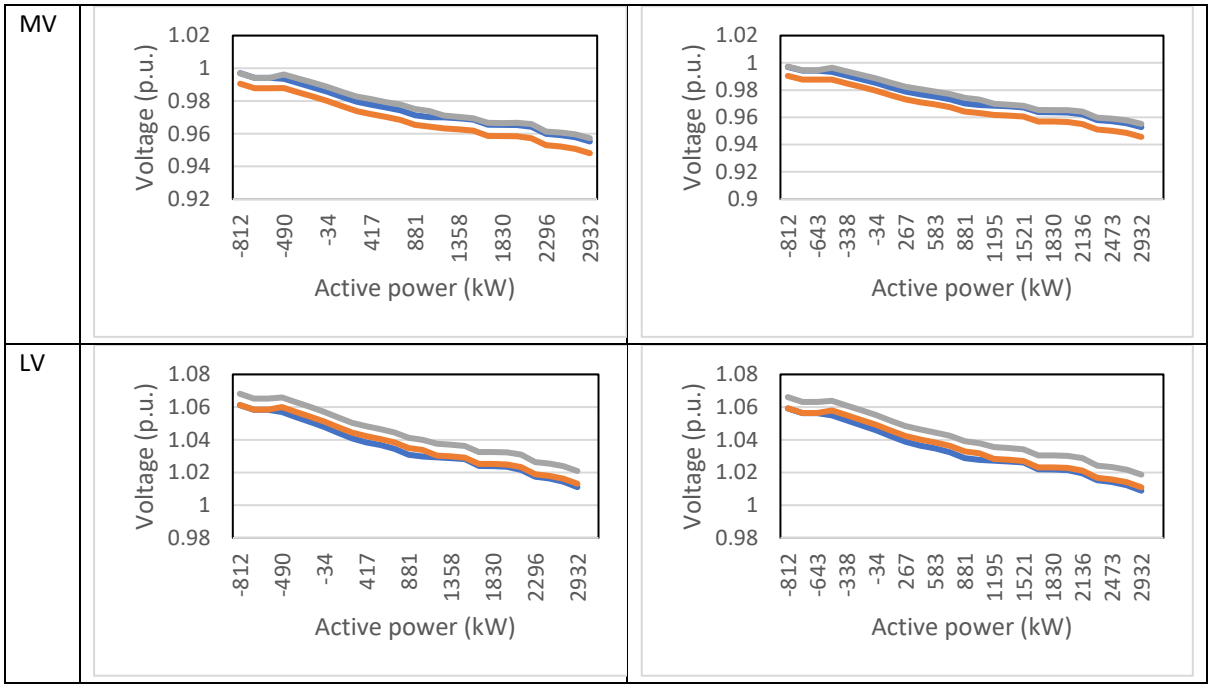

Fig. 4.5.9 Donald time-sweep integration scenario 2

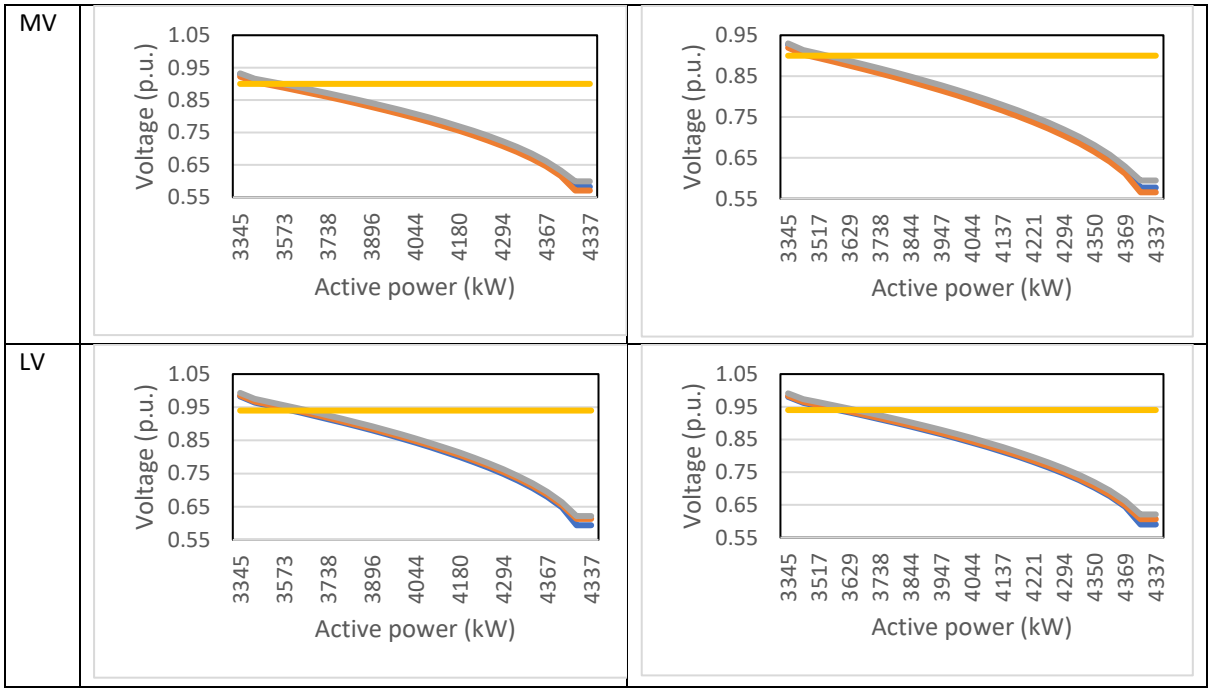

Fig. 4.5.10 Donald time-sweep integration scenario 3

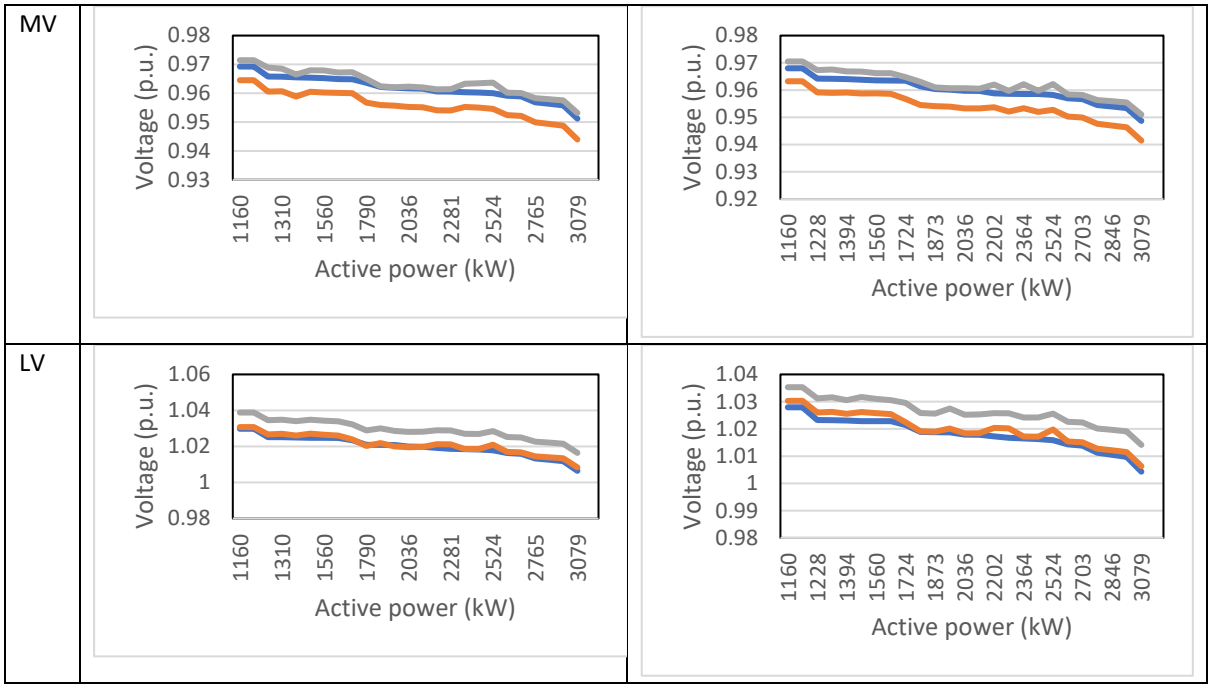

Fig. 4.5.11 Donald time-sweep integration scenario 4

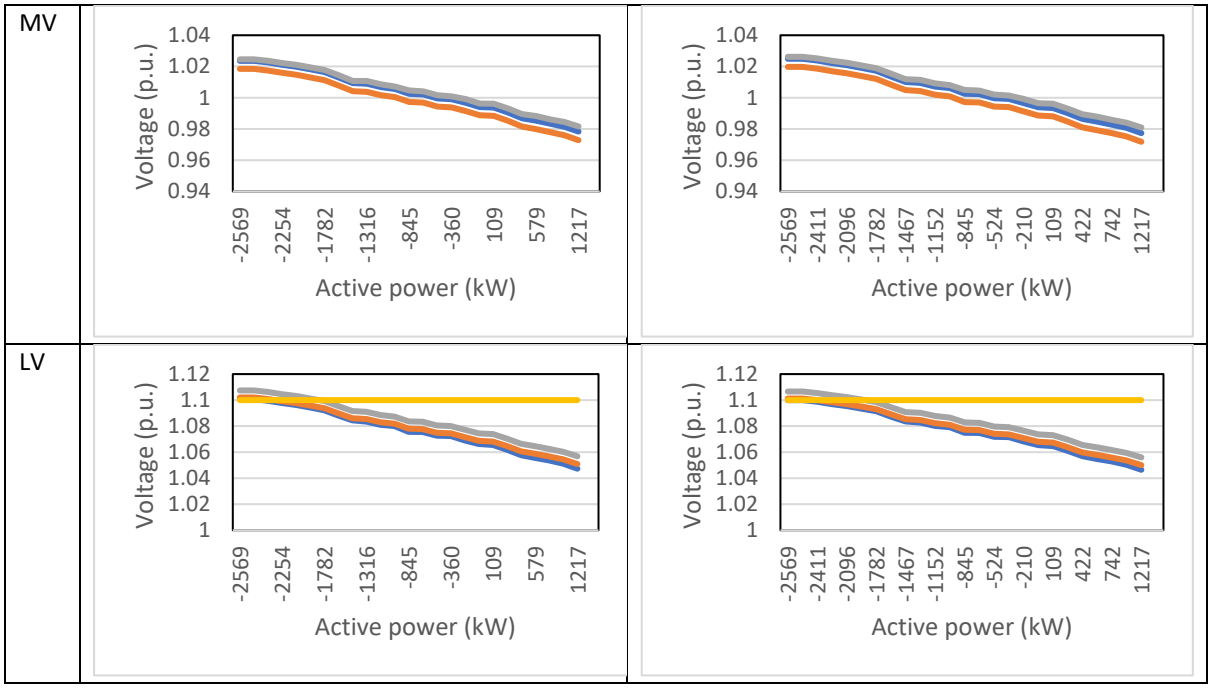

Fig. 4.5.12 Donald time-sweep integration scenario 5

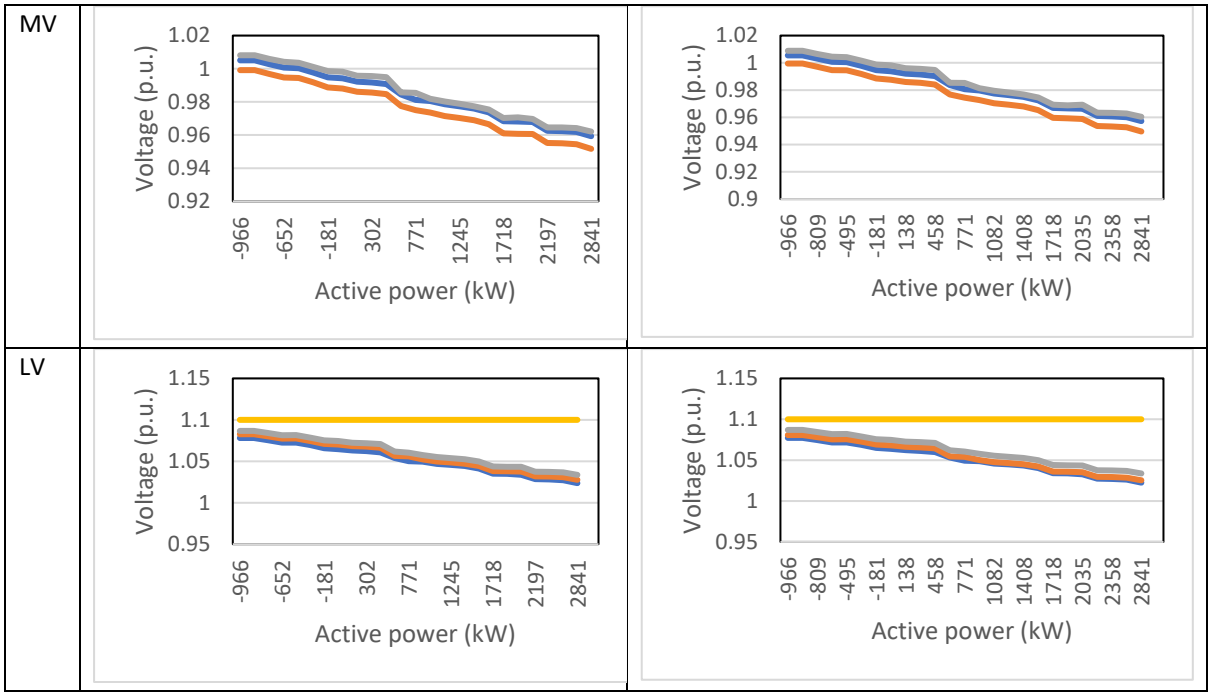

Fig. 4.5.13 Donald time-sweep integration scenario 6

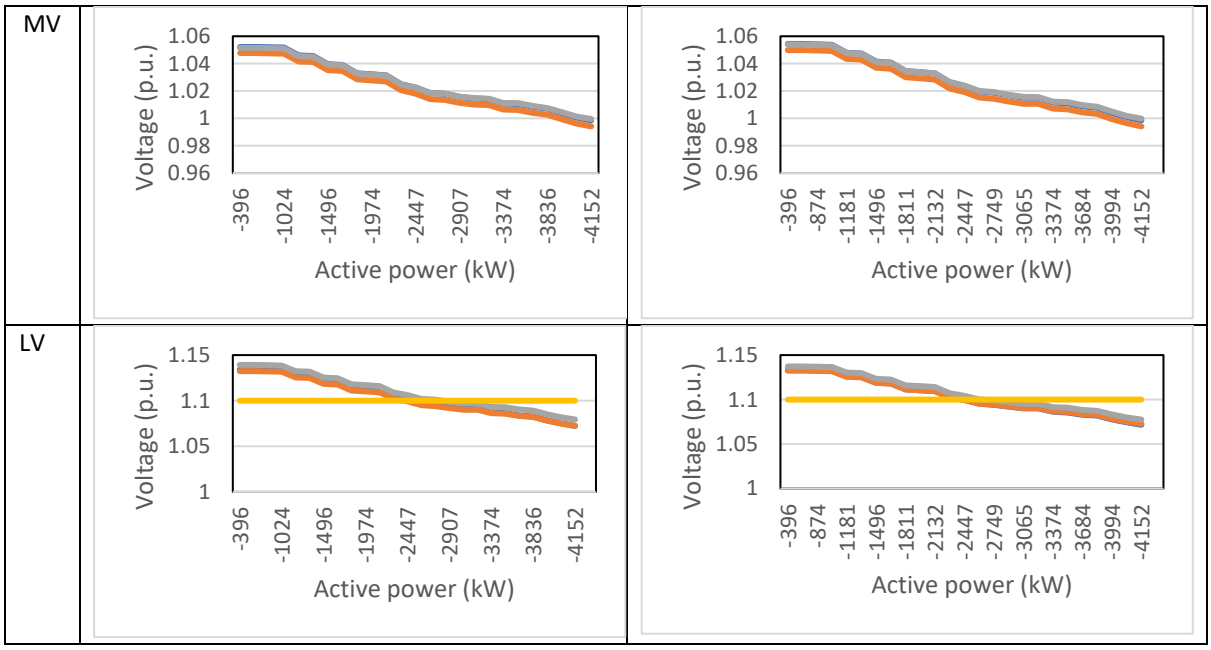

Fig. 4.5.14 Donald time-sweep integration scenario 7

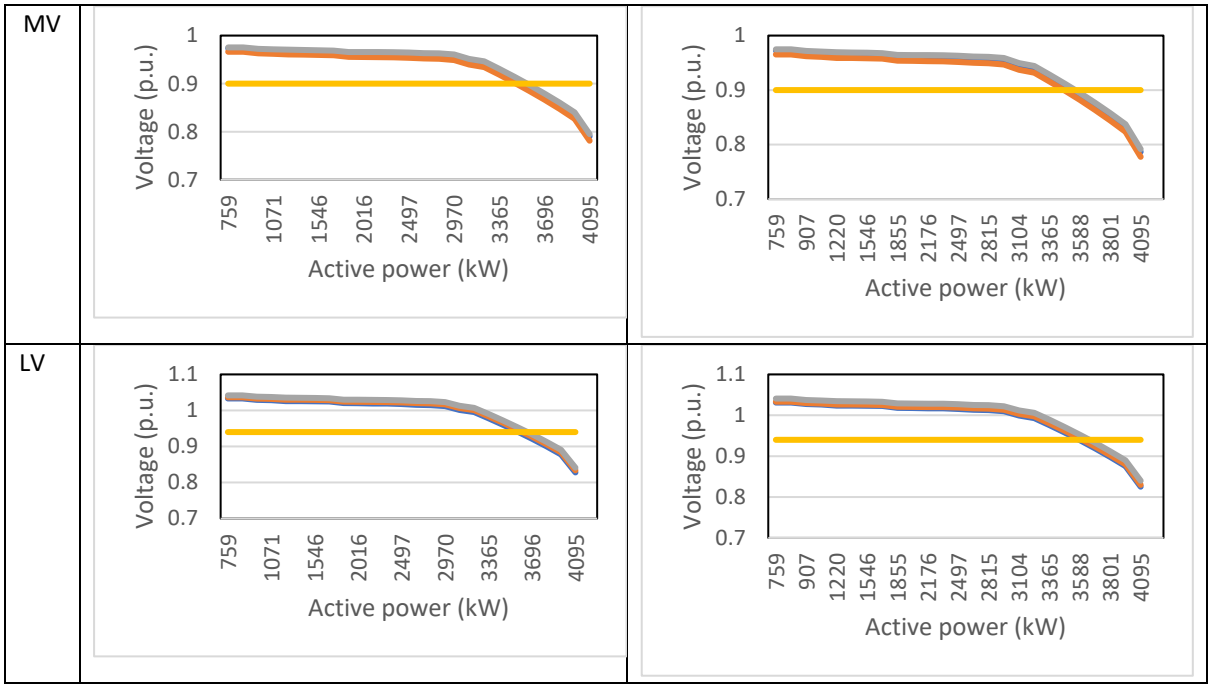

Fig. 4.5.15 Donald time-sweep integration scenario 8

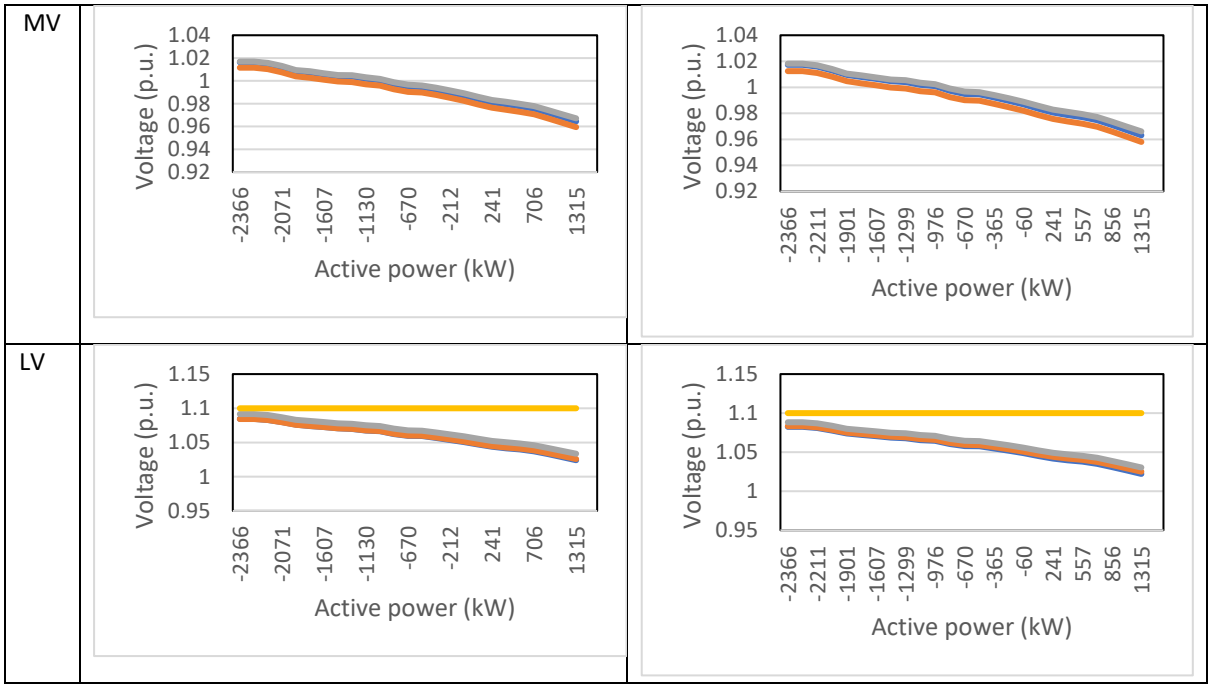

Fig. 4.5.16 Donald time-sweep integration scenario 9

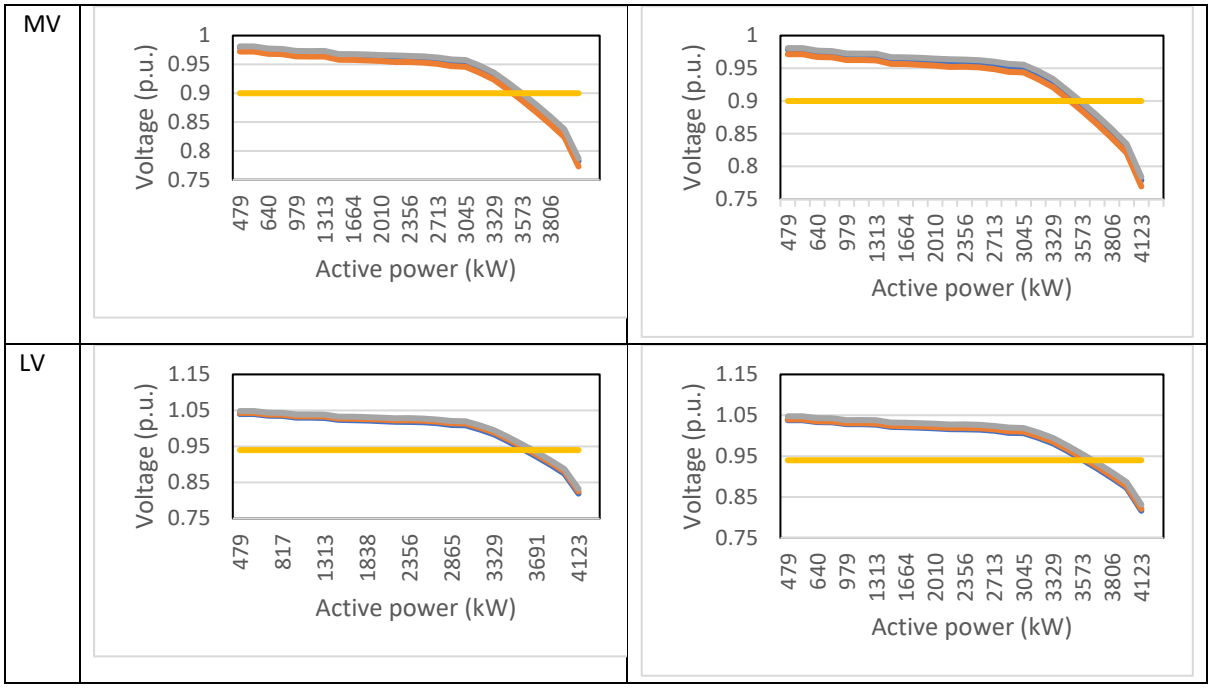

Fig. 4.5.17 Donald time-sweep integration scenario 10

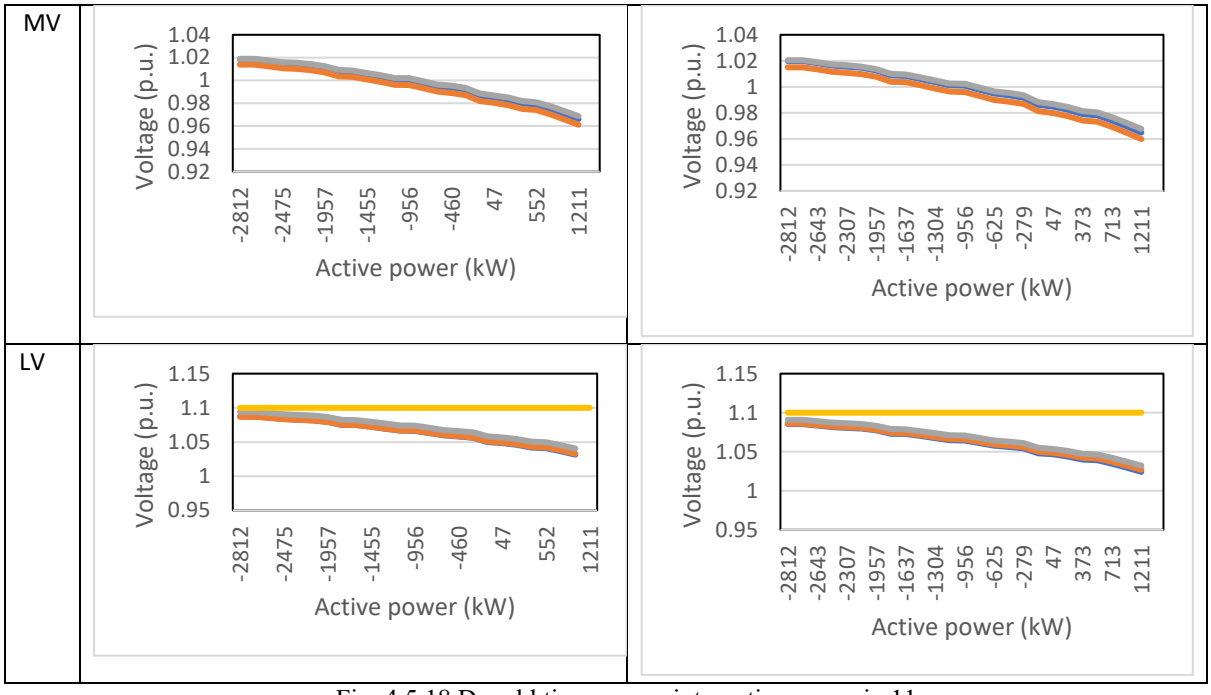

Fig. 4.5.18 Donald time-sweep integration scenario 11

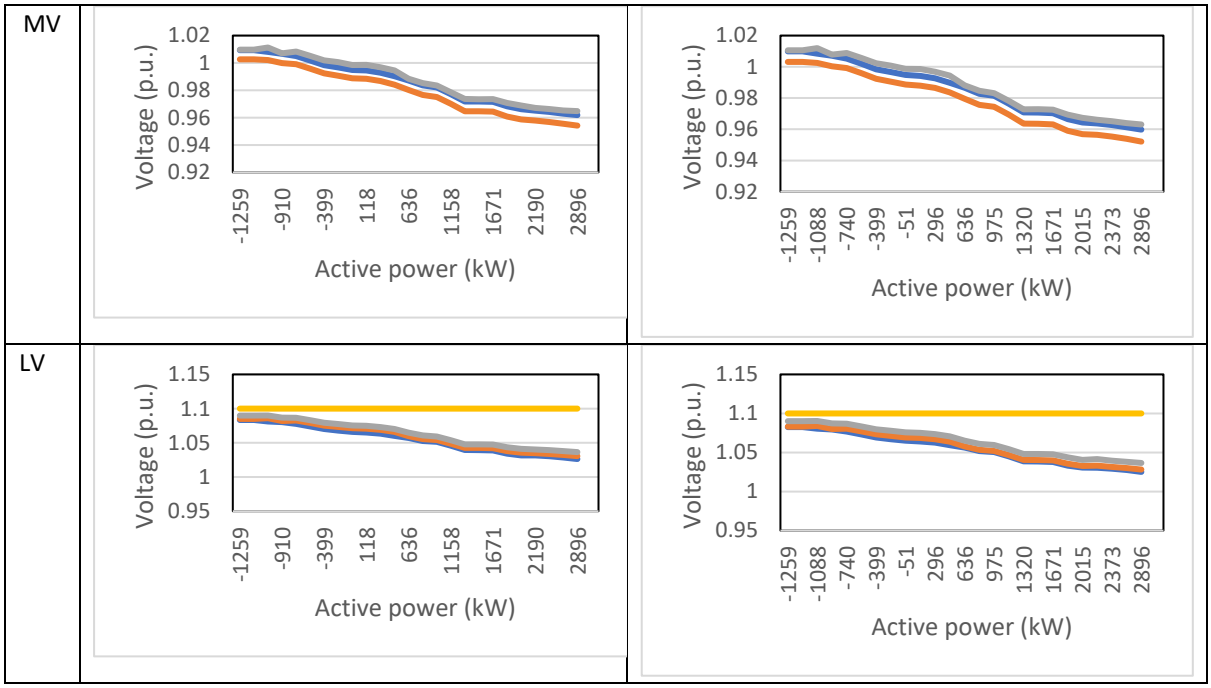

Fig. 4.5.19 Donald time-sweep integration scenario 12

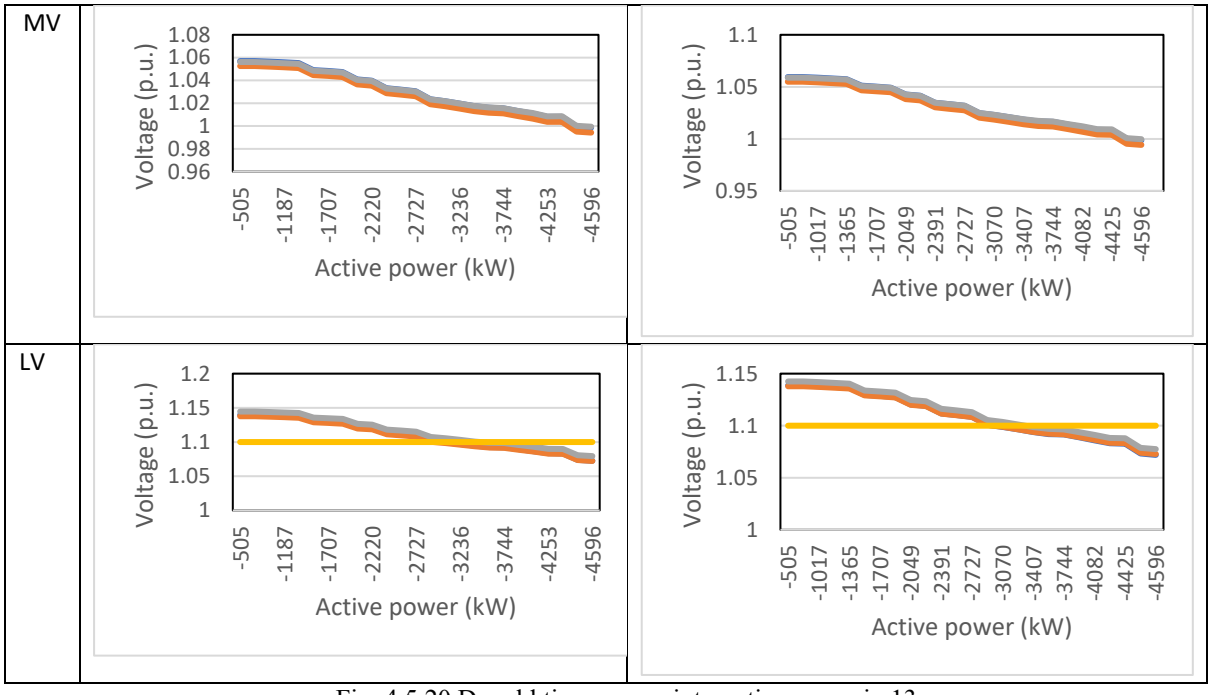

Fig. 4.5.20 Donald time-sweep integration scenario 13

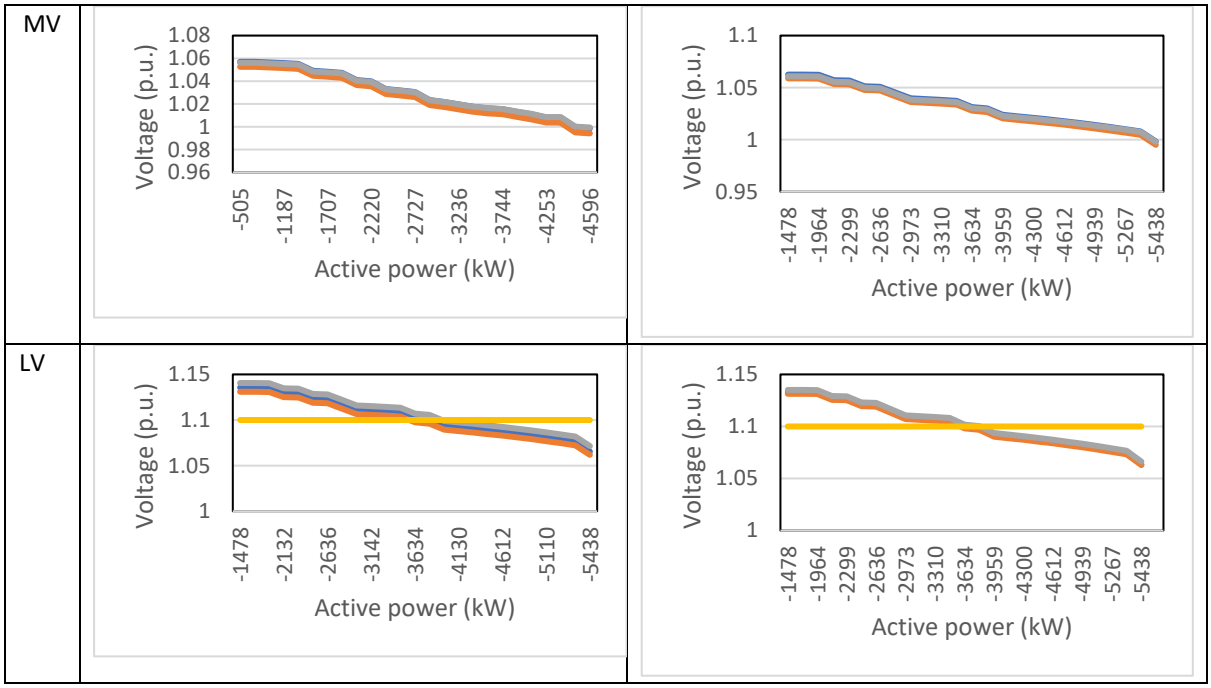

Fig. 4.5.21 Donald time-sweep integration scenario 14

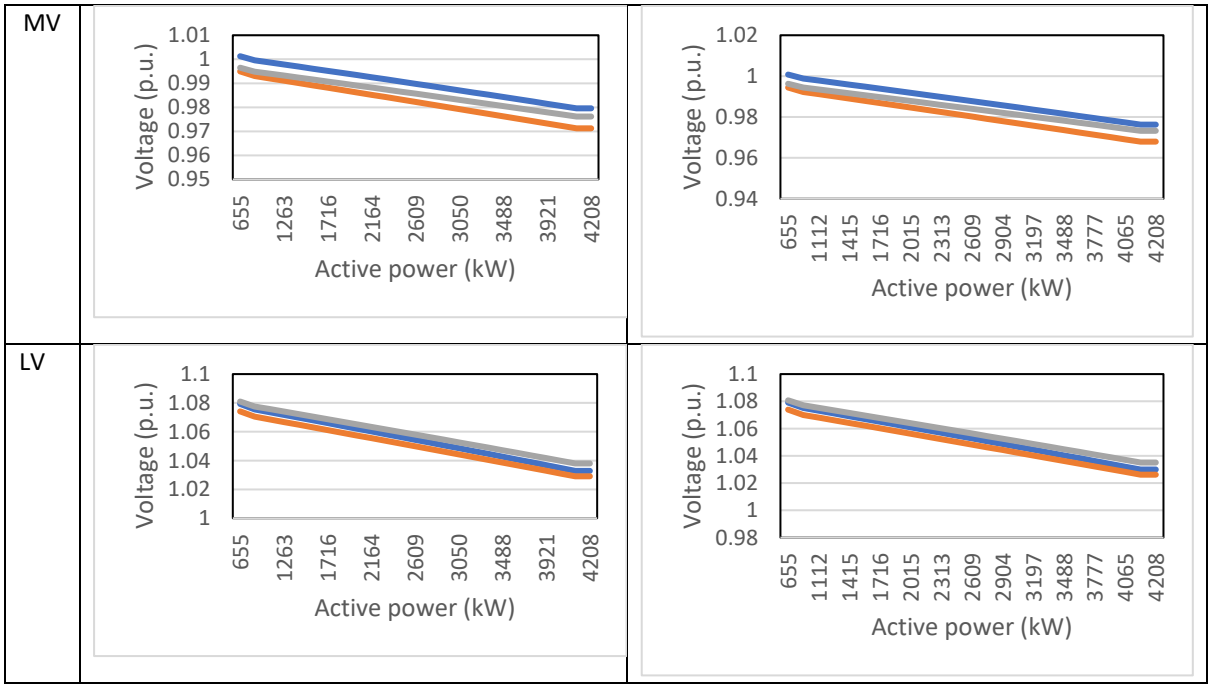

Fig. 4.5.22 Donald time-sweep integration scenario 15

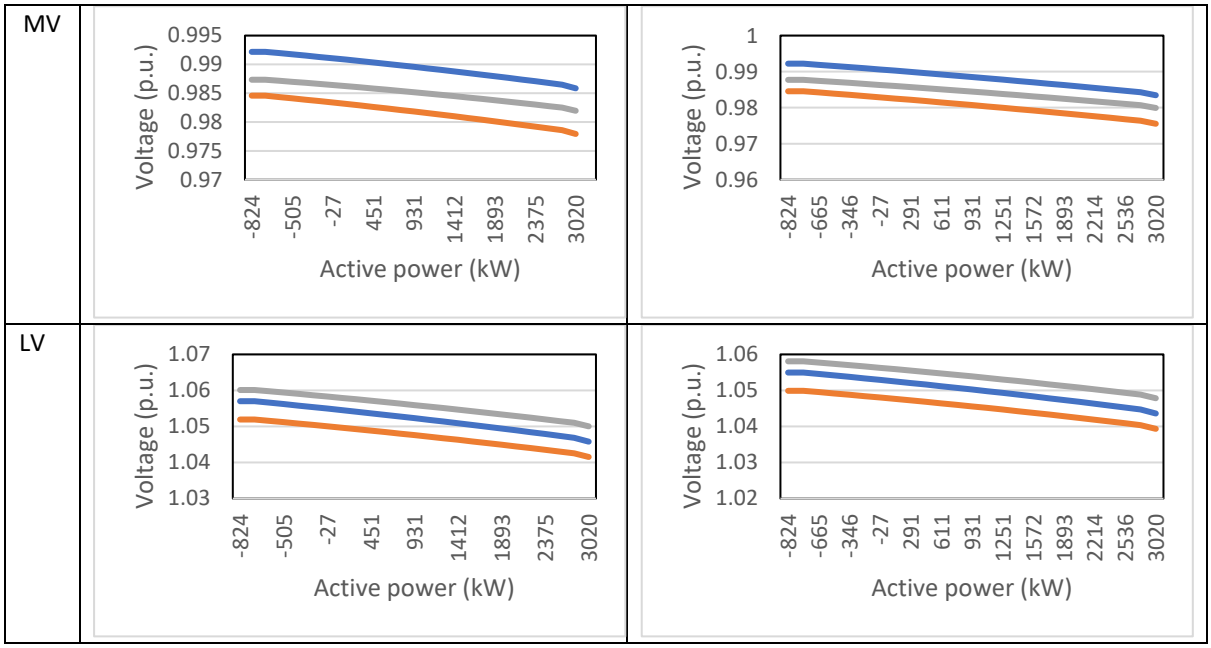

Fig. 4.5.23 Donald time-sweep integration scenario 16

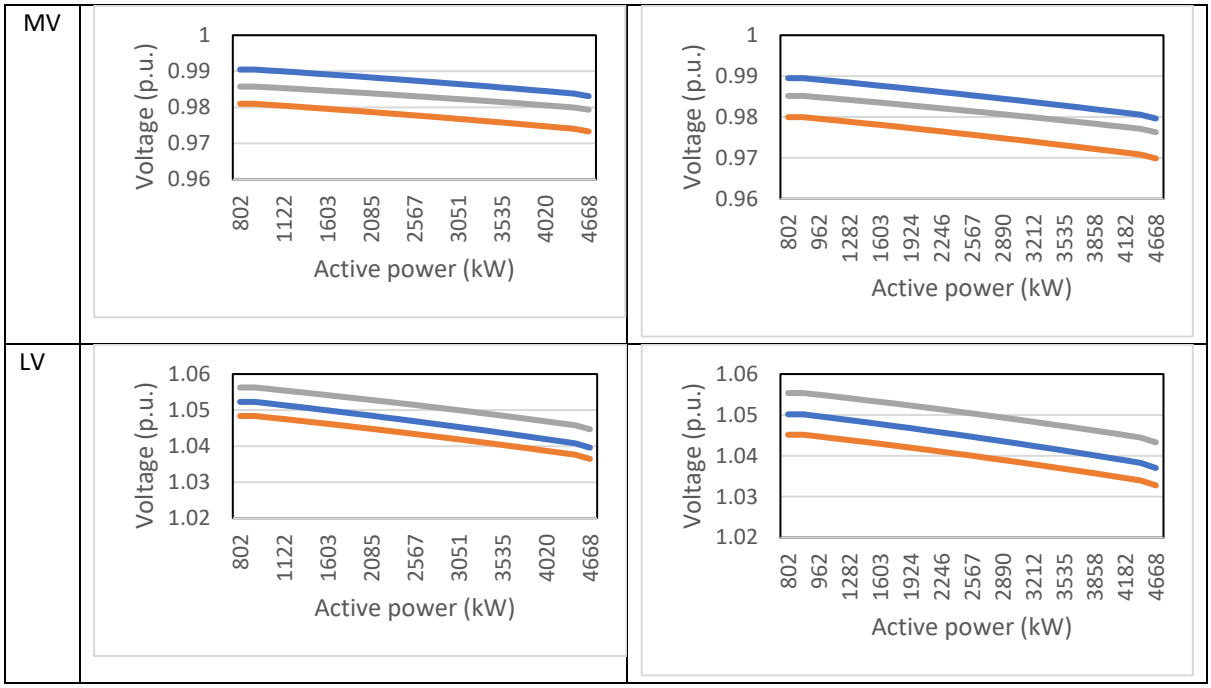

Fig. 4.5.24 Donald time-sweep integration scenario 17

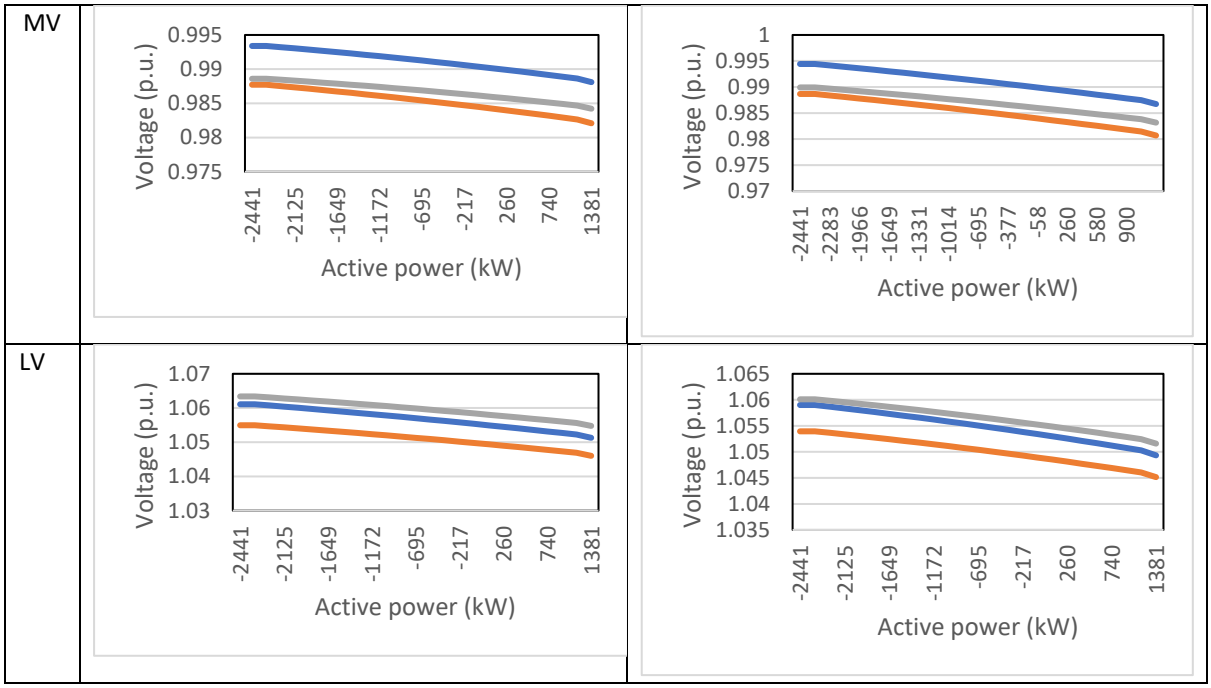

Fig. 4.2.25 Donald time-sweep integration scenario 18

The results show that the MV and LV systems of Donald can supply the load well above the peak load of the network and host the PV and battery as identified in hosting capacity assessment studies. Furthermore, the studies on the stand-alone operation of microgrid shows the Donald network is capable of hosting more loads, PVs and batteries and the voltage variations were reduced due to the availability of the back-up generator which could supply the incoming feeder with more consistent voltage level. This highlights that the supply feeder is the main limiting factor in the hosting capacity of load and local generation of this town.

In order to investigate more realistic operational scenarios following the time-sweep analysis, quasi-dynamic simulations are performed on the Donald network considering the realistic daily load and generation profiles obtained through data analysis. In order to provide consistent results, these data sets were modified to represent normalized load and PV generation profiles of the customers while the typical battery profiles were generated using the literature and the network PV generation profiles (charging and discharging in the 24 hour window). The preliminary results showed that the hot and cold days need to be further studied due to the customers' possible impact of load and generation. Therefore, the results of 2 temperature zones for cold days (15 degrees) and hot days (40 degrees) for various operational scenarios detailed in Table 4.5.2 are demonstrated here.

TABLE 4.5.2 - INTEGRATION AND OPERATIONAL SCENARIOS FOR Quasi–Dynamic Studies of Donald

Operational Scenario	Maximum Load (KW)	Maximum PV (KW)	Maximum Battery Inveter (KW)	Temperature Zone
1	1172	0	0	15 degrees
2	1172	3216	0	15 degrees
3	1172	3216	1639 (c & d)	15 degrees
4	2949.6	0	0	15 degrees
5	2949.6	3216	0	15 degrees
6	2949.6	3216	1639 (c & d)	15 degrees
7	1172	0	0	40 degrees
8	1172	3216	0	40 degrees
9	1172	3216	1639 (c & d)	40 degrees
10	2949.6	0	0	40 degrees
11	2949.6	3216	0	40 degrees
12	2949.6	3216	1639 (c & d)	40 degrees

In each scenario, the loads, generations and batteries are assigned to the relevant clusters considering the weighting of each cluster as defined through the data analysis and the results demonstrate the different voltage profiles at the same buses as the time-sweep analysis for the various studied scenarios as illustrated in Fig. 4.5.26 – 4.5.37.

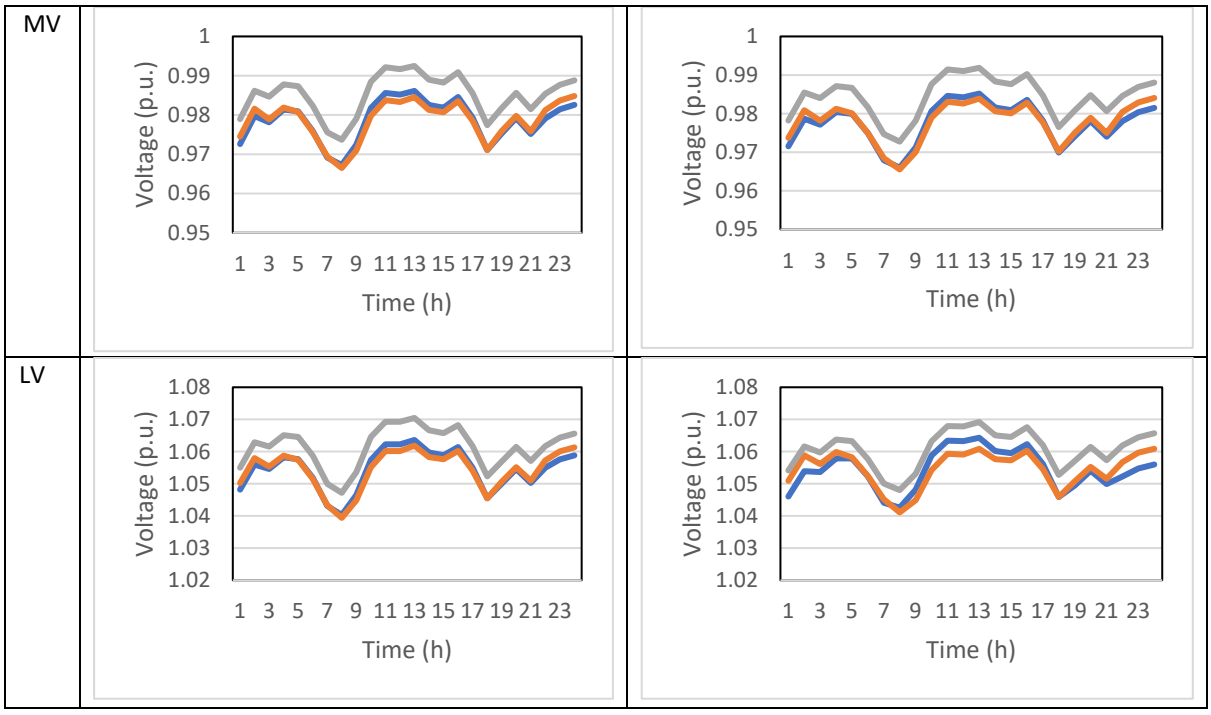

Fig. 4.5.26 Donald quasi-dynamic integration scenario 1

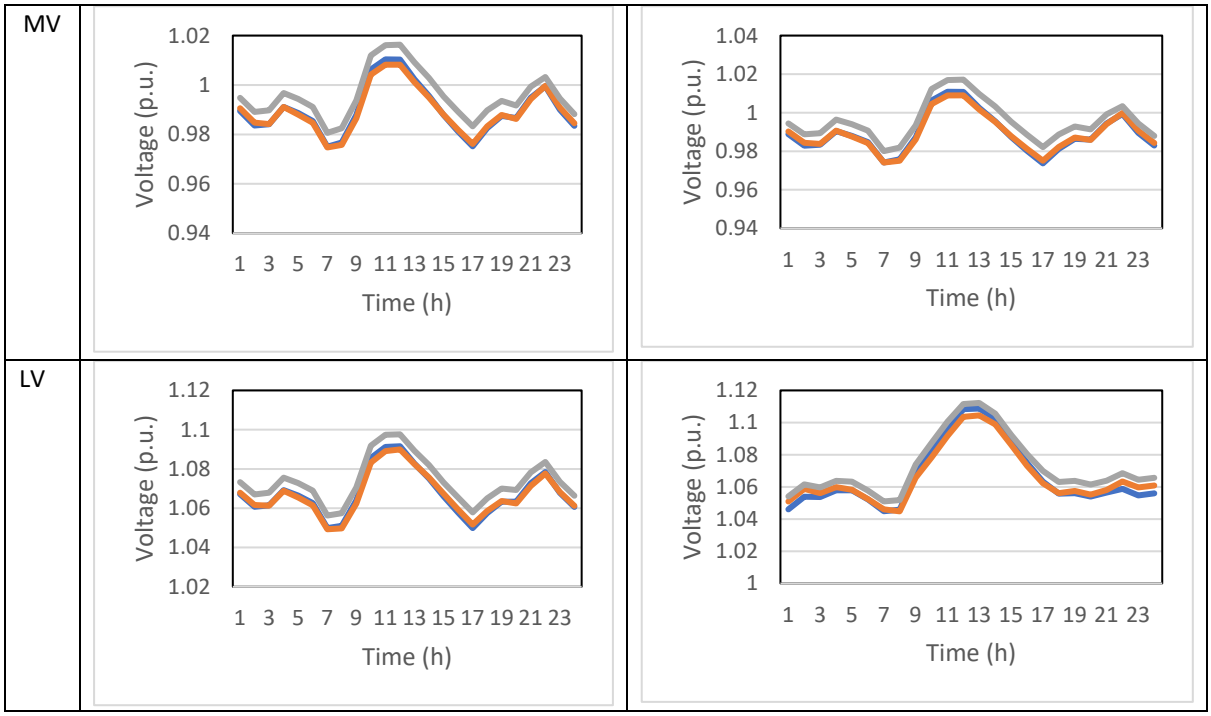

Fig. 4.5.27 Donald quasi-dynamic integration scenario 2

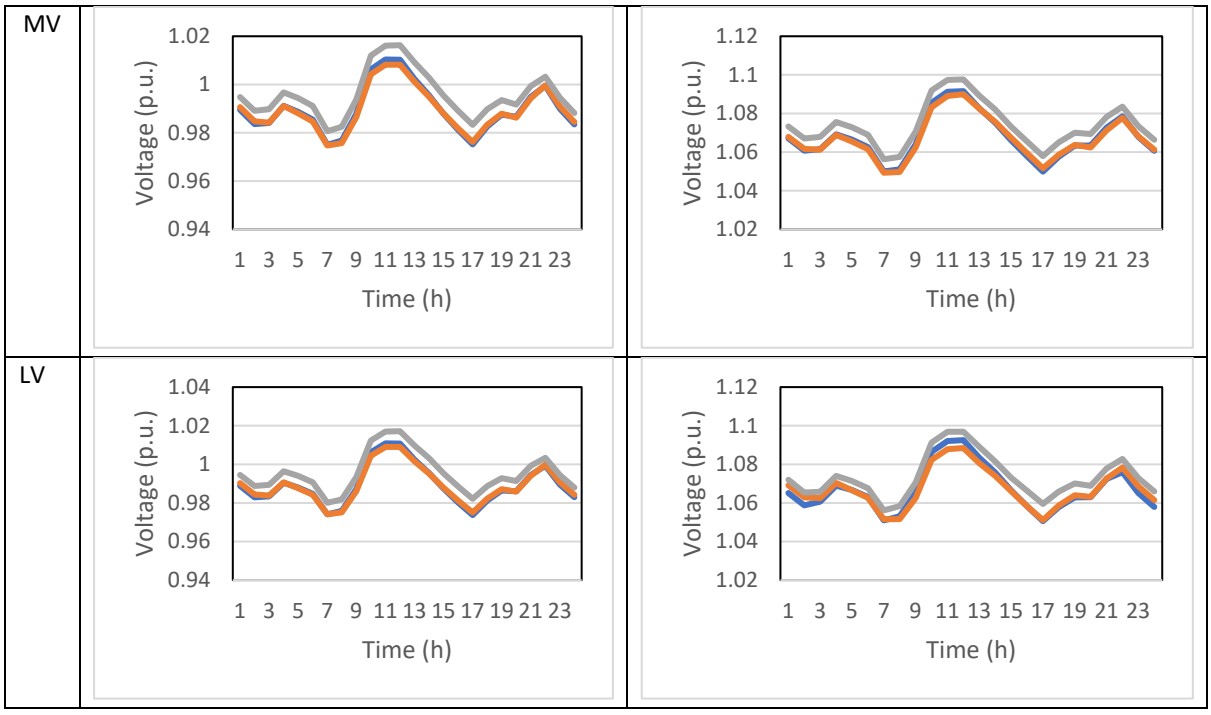

Fig. 4.5.28 Donald quasi-dynamic integration scenario 3

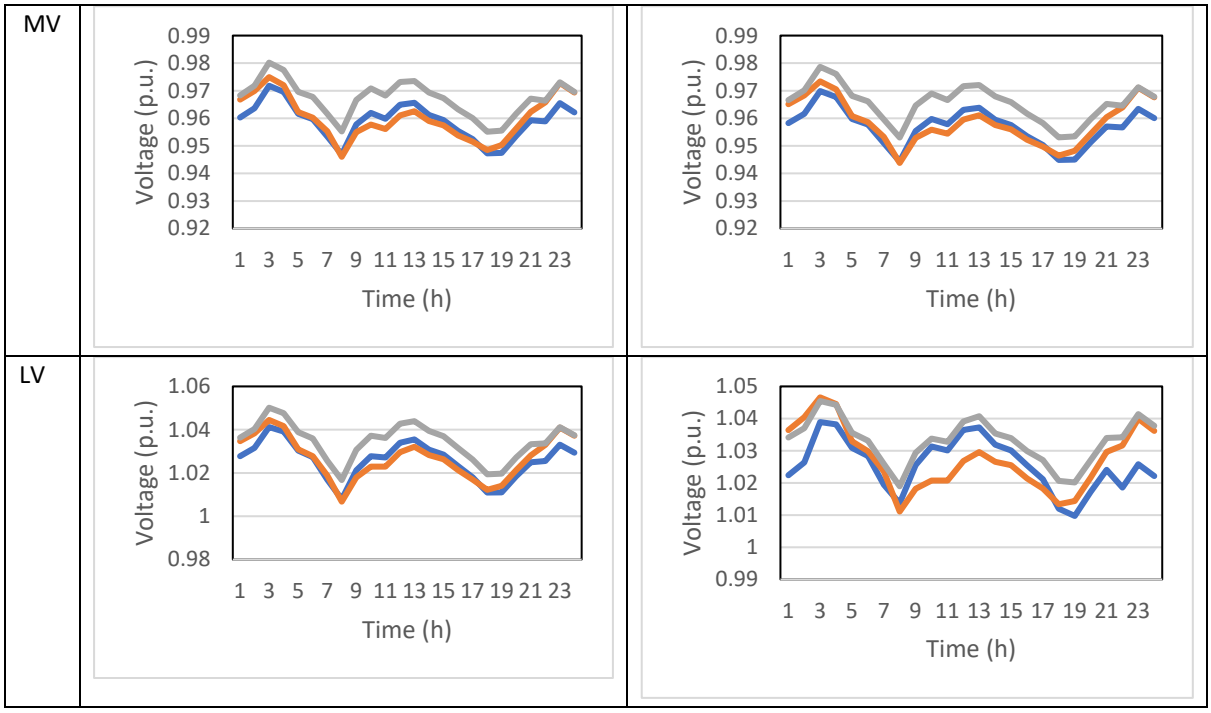

Fig. 4.5.29 Donald quasi-dynamic integration scenario 4

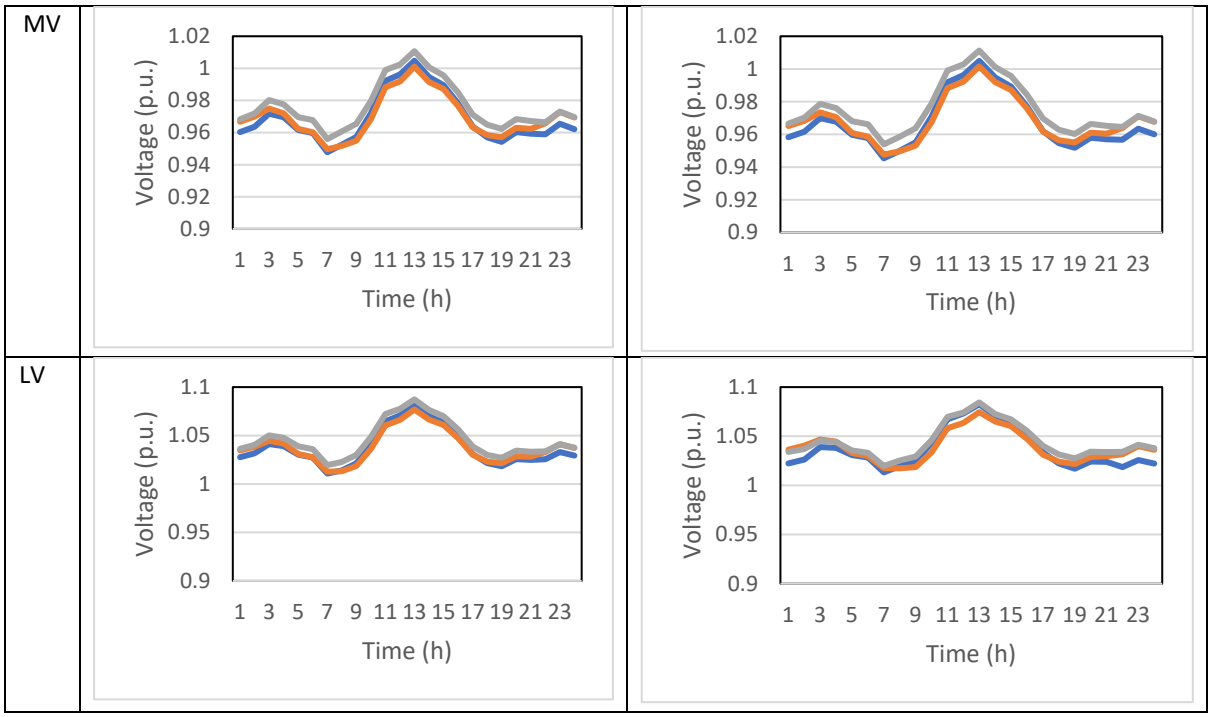

Fig. 4.5.30 Donald quasi-dynamic integration scenario 5

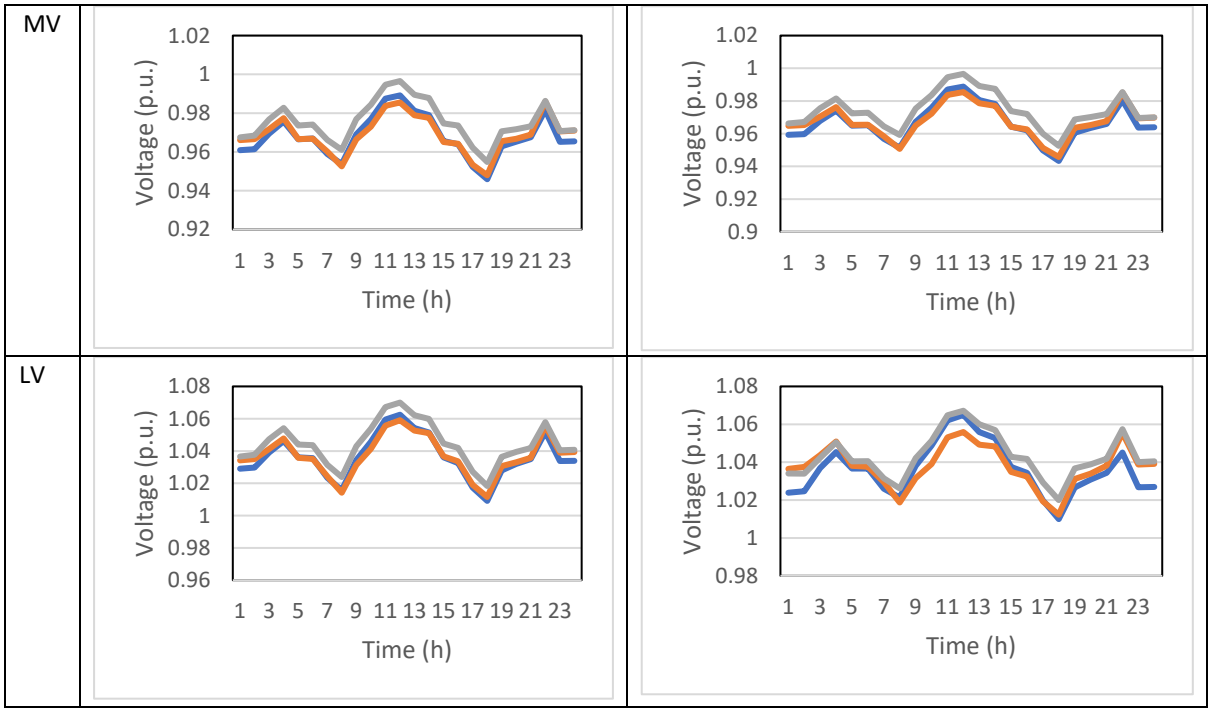

Fig. 4.5.31 Donald quasi-dynamic integration scenario 6

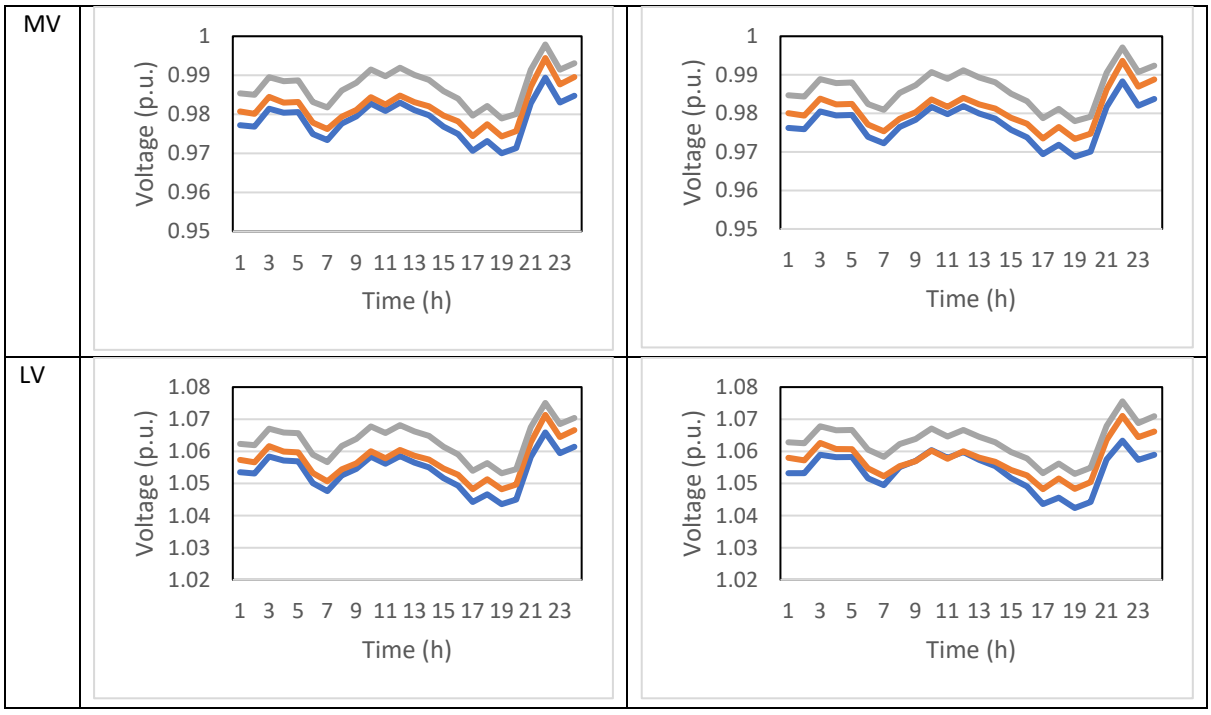

Fig. 4.5.32 Donald quasi-dynamic integration scenario 7

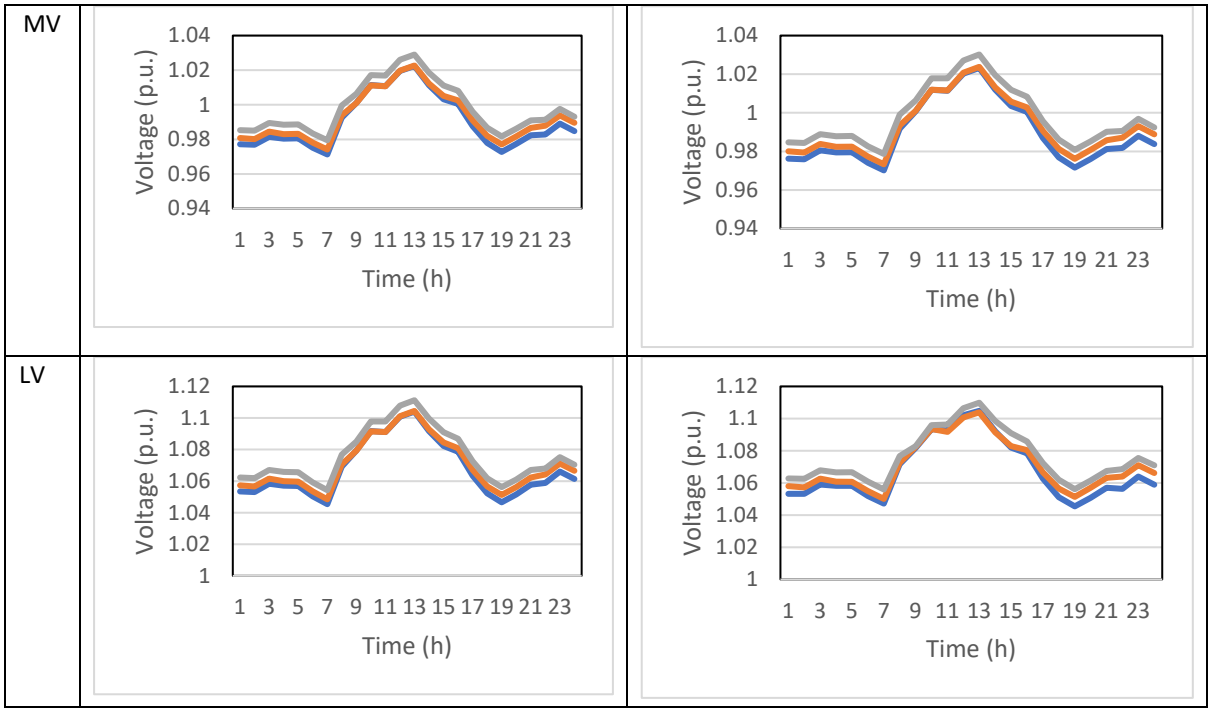

Fig. 4.5.33 Donald quasi-dynamic integration scenario 8

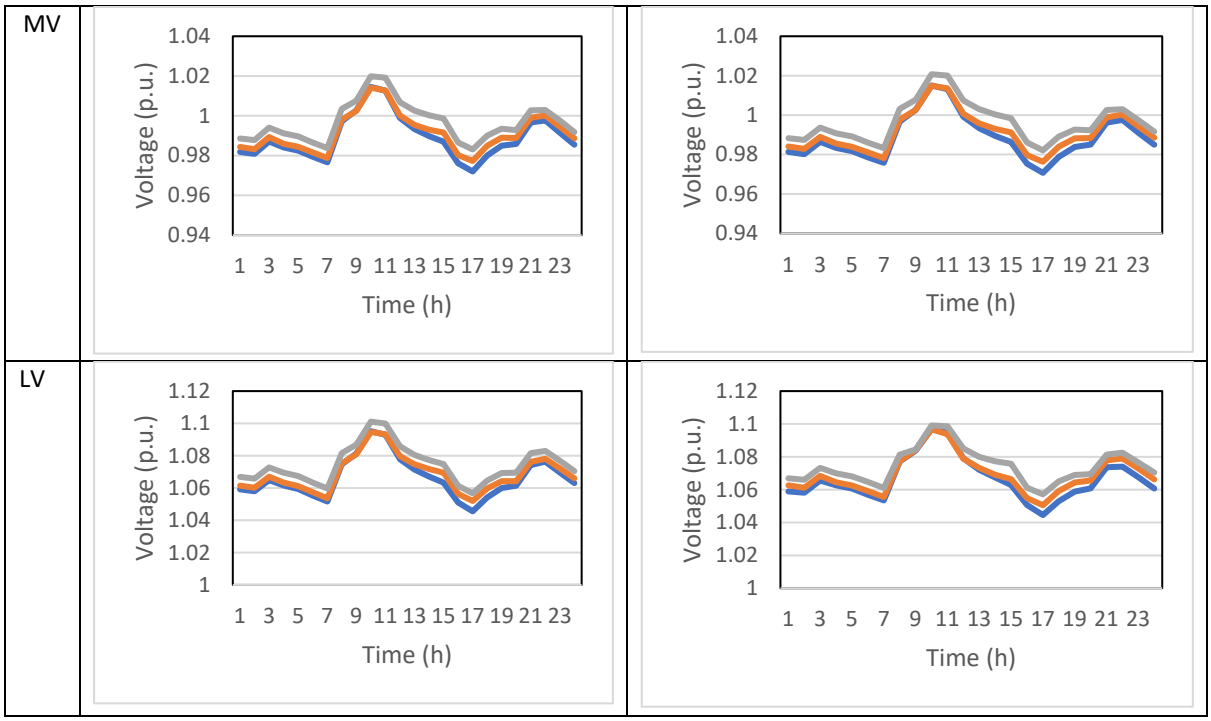

Fig. 4.5.34 Donald quasi-dynamic integration scenario 9

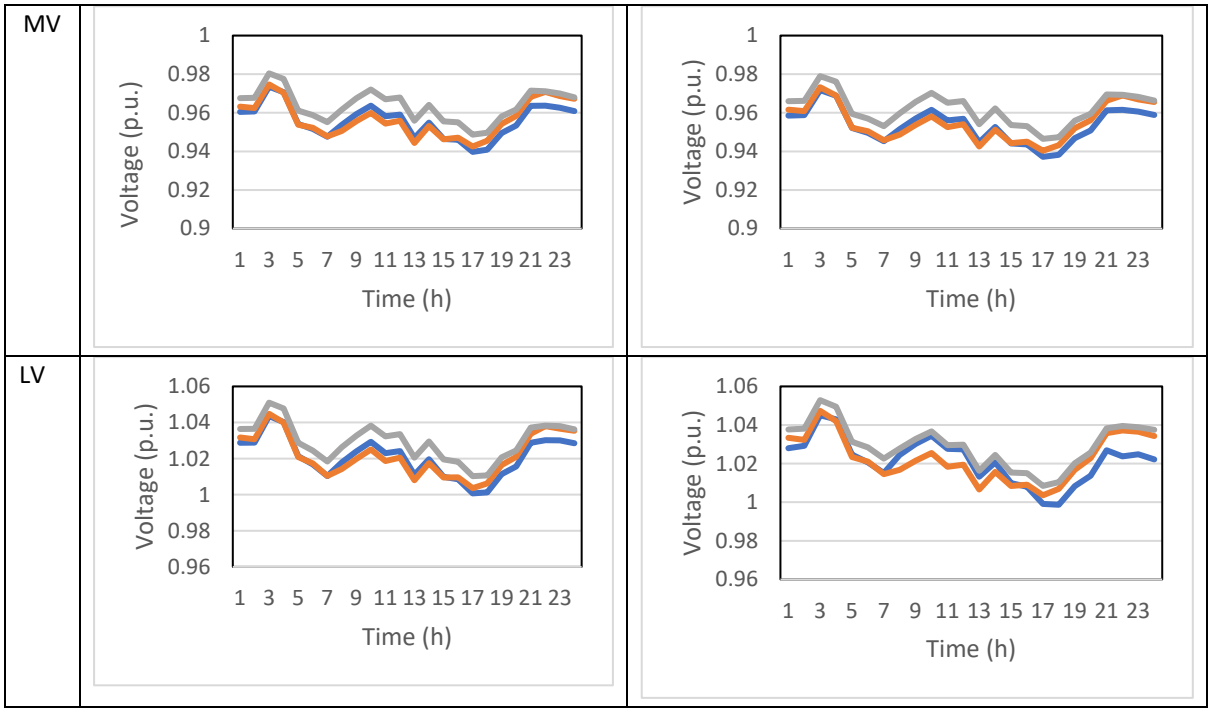

Fig. 4.5.35 Donald quasi-dynamic integration scenario 10

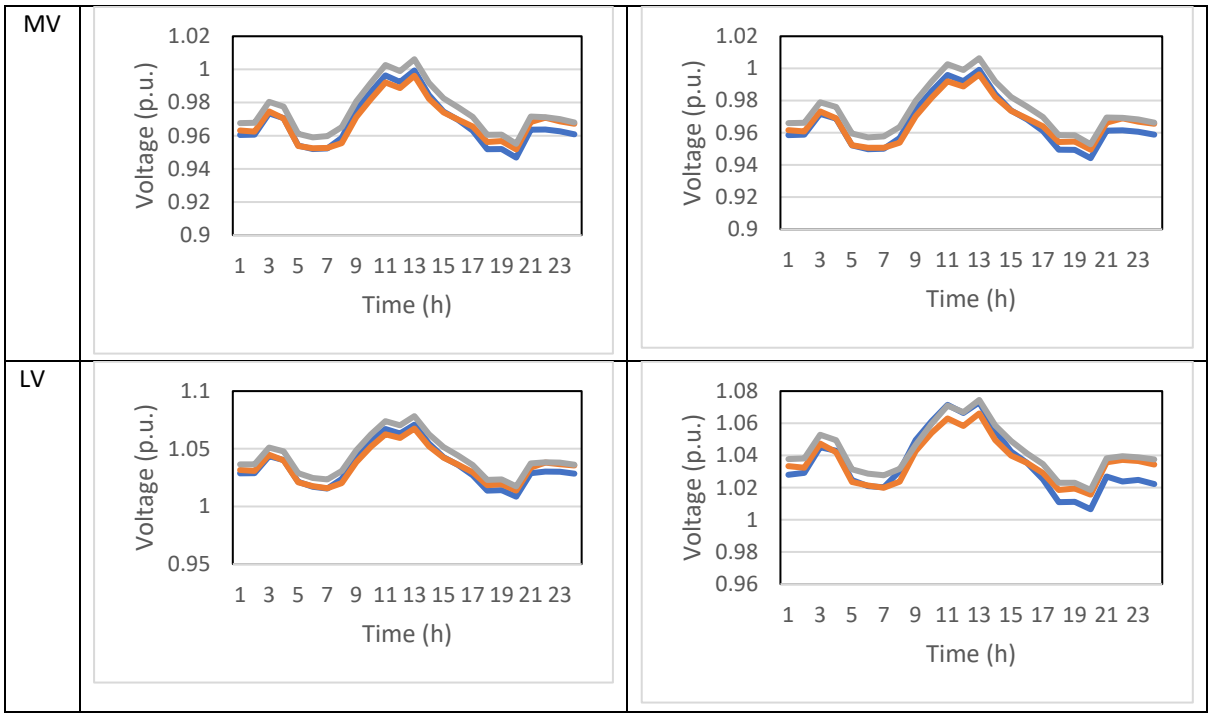

Fig. 4.5.36 Donald quasi-dynamic integration scenario 11

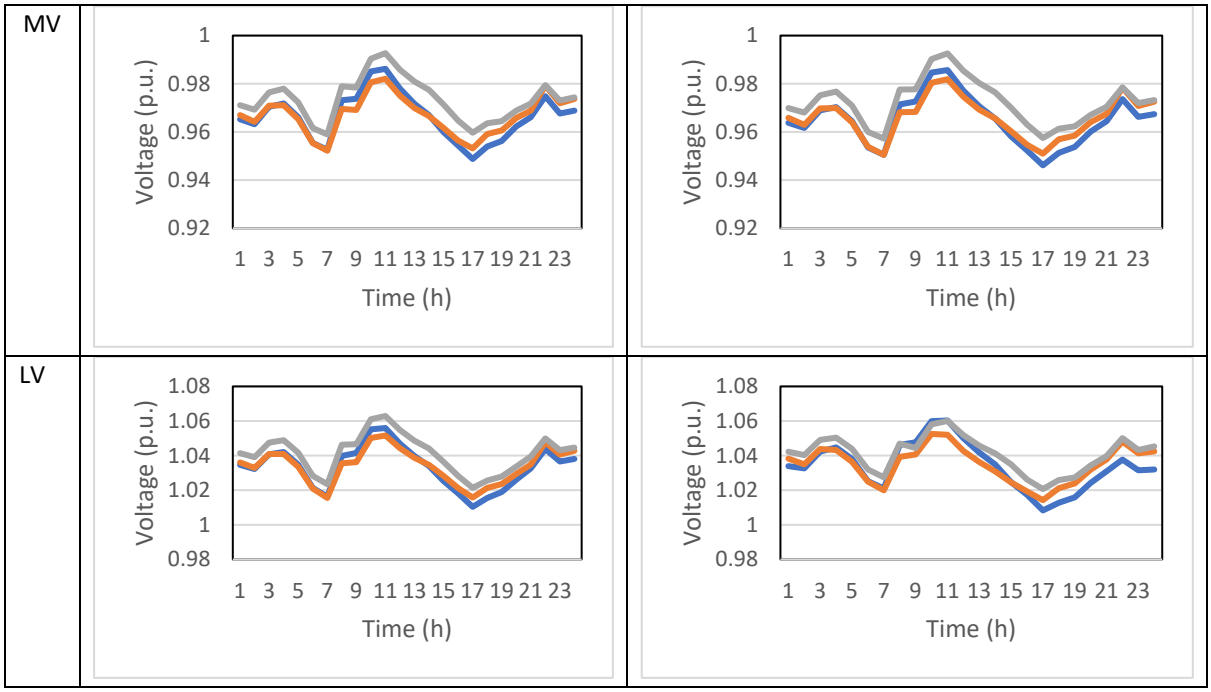

Fig. 4.5.37 Donald quasi-dynamic integration scenario 12

The quasi-dynamic simulations support the findings through time-sweep analysis as the network did not experience a major over or under voltage in many realistic operational scenarios. Minor overvoltage was experienced in the LV network during low load and high PV generation conditions with no batteries (scenario 2 and 8) which were improved by considering the batteries in the system (scenario 3 and 9).

4.5.2. Analysis of Tarnagulla Network

Similar to the Donald network, the yearly smart meter and consumption data of Tarnagulla are analyzed and the peak and average load of the network are obtained to be used for hosting capacity assessment through HOMER Pro Microgrid Analysis Tool. The outcome of the hosting capacity assessment is used to create various grid-connected and stand-alone microgrid operation scenarios which are summarized in Table 4.5.3.

TABLE 4.5.3 - INTEGRATION AND OPERATIONAL SCENARIOS FOR Time-Sweep Studies of Tarnagulla

Integration Scenario	Total Load (KW)	Load Variation	Total PV (KW)	PV Variation	Total Battery Inveter (KW)	Battery Variation	Backup Generator
1	267.48	0-130%	0	0	0	0	
2	267.48		155	0-130%			
3	267.48		0		111 (c)	0-130%	
4	267.48		0		111 (d)	0-130%	
5	267.48		0		55.5 (c)	0-130%	

6	267.48		0		55.5 (d)	0-130%	
7	81.1		155	0-130%			
8	81.1		155	0-130%	111 (c)		
9	81.1		155	0-130%	111 (d)		
10	267.48		155	0-130%	111 (c)		
11	267.48		155	0-130%	111 (d)		
12	267.48	0-130%	0	0	0	0	320 kW
13	267.48		131	0-130%			320 kW
14	267.48		131	0-130%	101 (c)		320 kW
15	267.48		131	0-130%	101 (d)		320 kW

In the developed scenarios, the loads, PV generation and Battery have changed between 0 and 130% of the nominal capacity of each scenario as shown in Table 4.5.3 through time-weep analysis. The batteries were considered in both charging (c) and discharging (d) modes. The backup generators were also used in some scenarios to investigate the stand-alone operation of the microgrid. In the stand-alone mode, the microgrid was isolated from the supply feeder at the PCC and the back-up generator was placed to support the network. In the simulated cases, voltages across different parts of the MV and LV network were analysed and the 3 phase voltage variations at 2 MV buses (**B_MV_PCC_Local** and **B_MV.VR**) and 2 LV buses (**B_LV.W2.5** and **B_LV.C2.5**) with respect to the total net load of the system (as seen from the PCC supply point) are illustrated in Figs. 4.5.38 – 4.5.52 to demonstrate the system operational capacities in various scenarios.

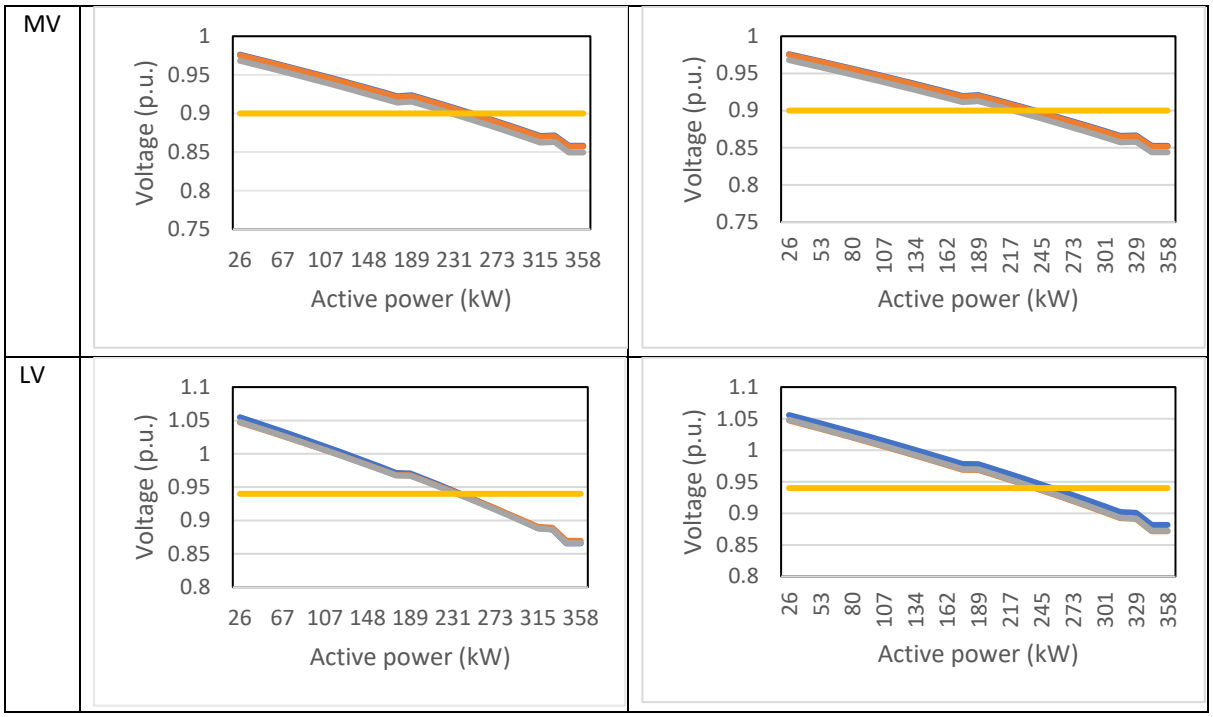

Fig. 4.5.38 Tarnagulla time-sweep integration scenario 1

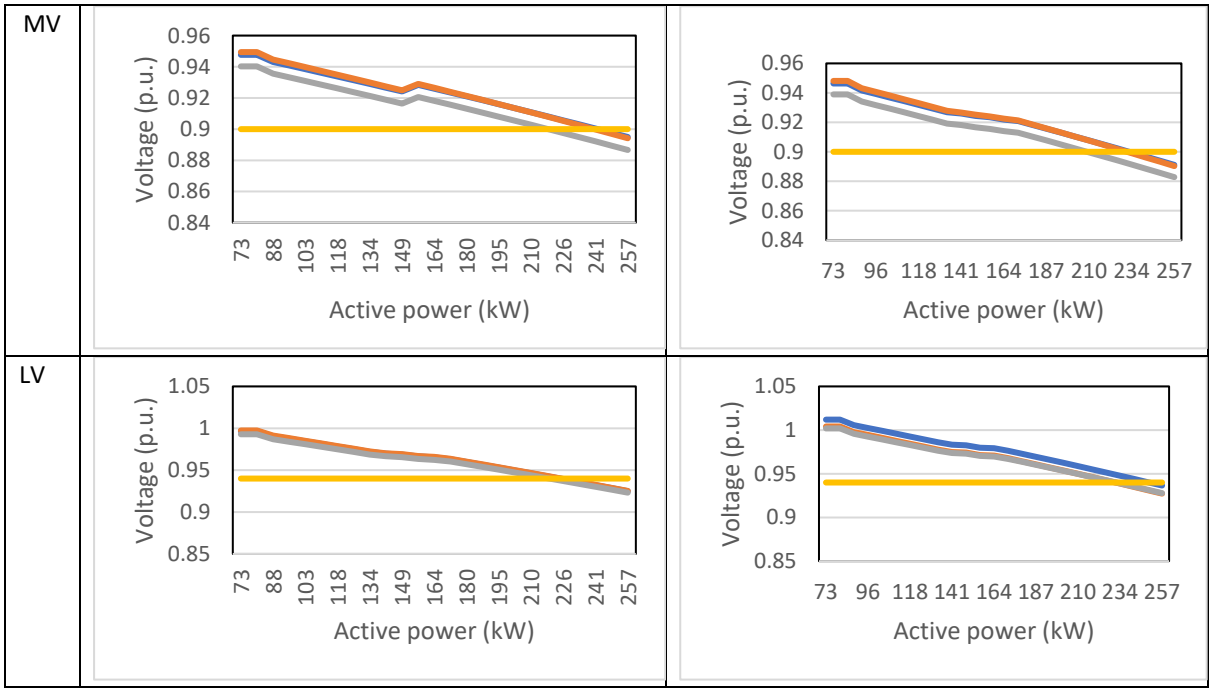

Fig. 4.5.39 Tarnagulla time-sweep integration scenario 2

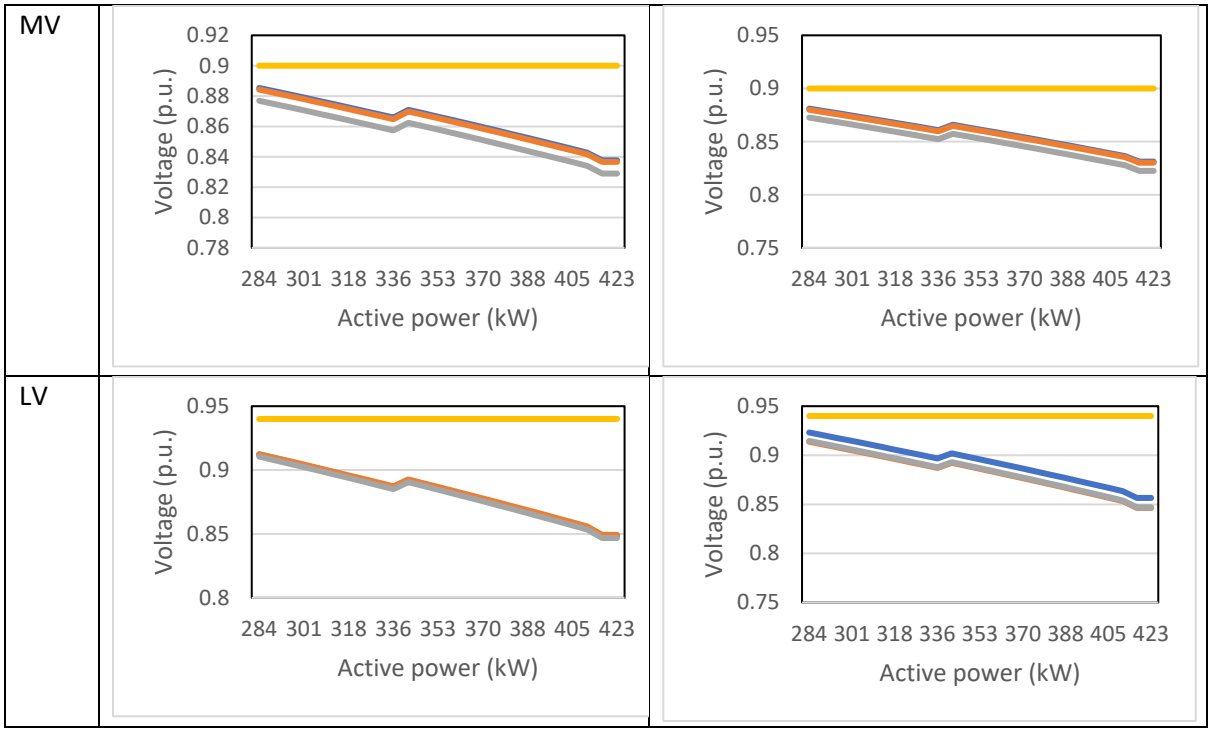

Fig. 4.5.40 Tarnagulla time-sweep integration scenario 3

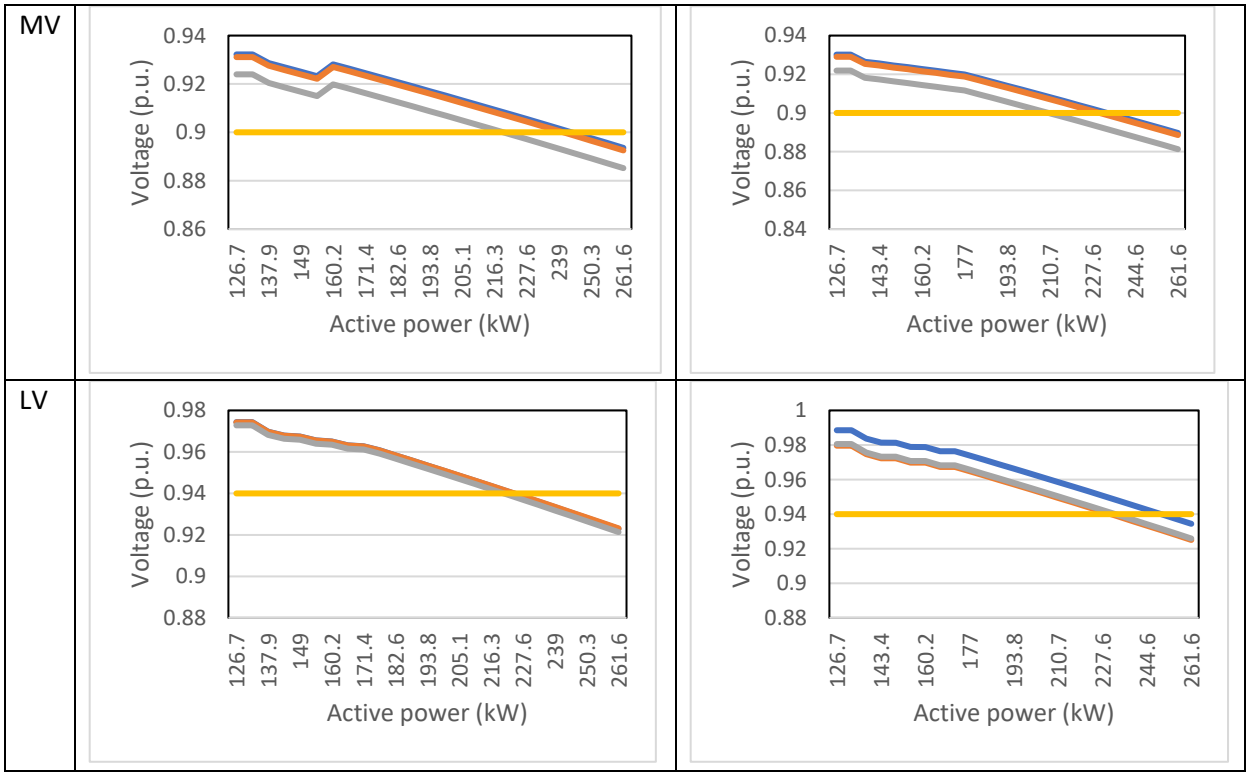

Fig. 4.5.41 Tarnagulla time-sweep integration scenario 4

Fig. 4.5.42 Tarnagulla time-sweep integration scenario 5

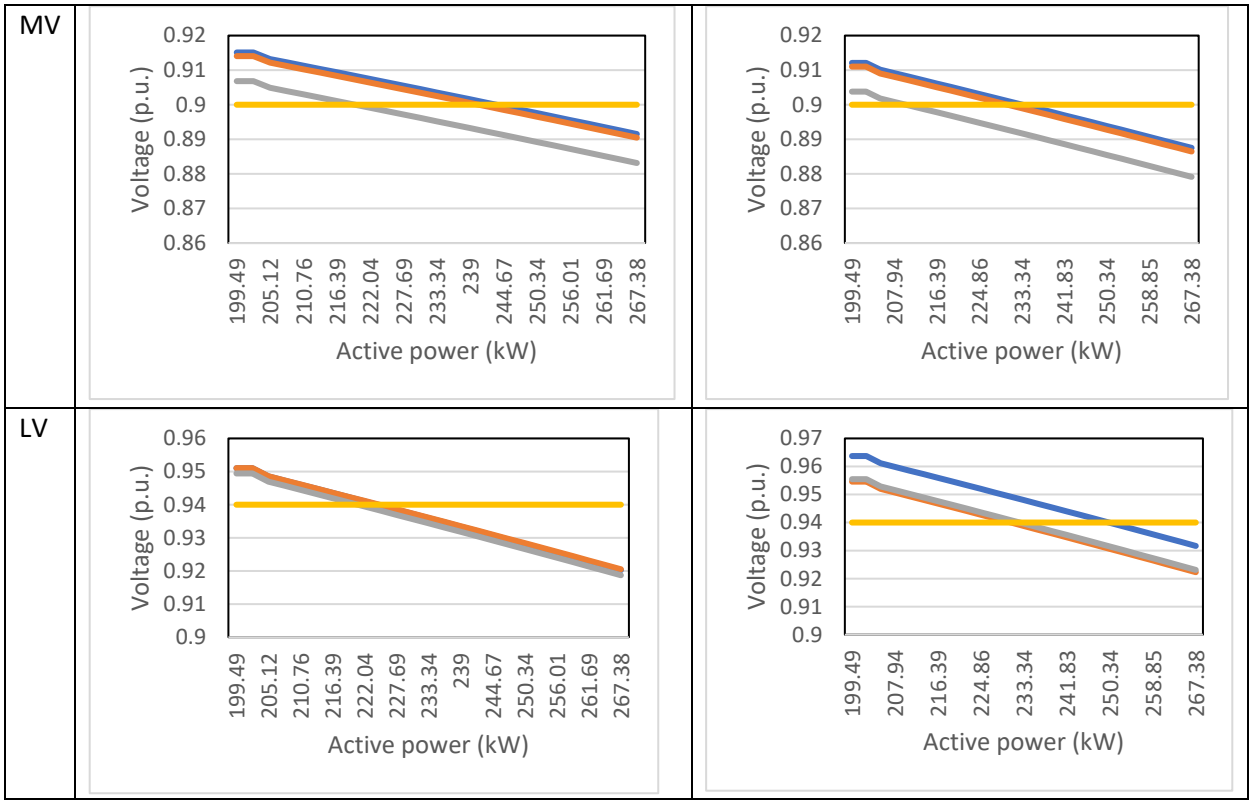

Fig. 4.5.43 Tarnagulla time-sweep integration scenario 6

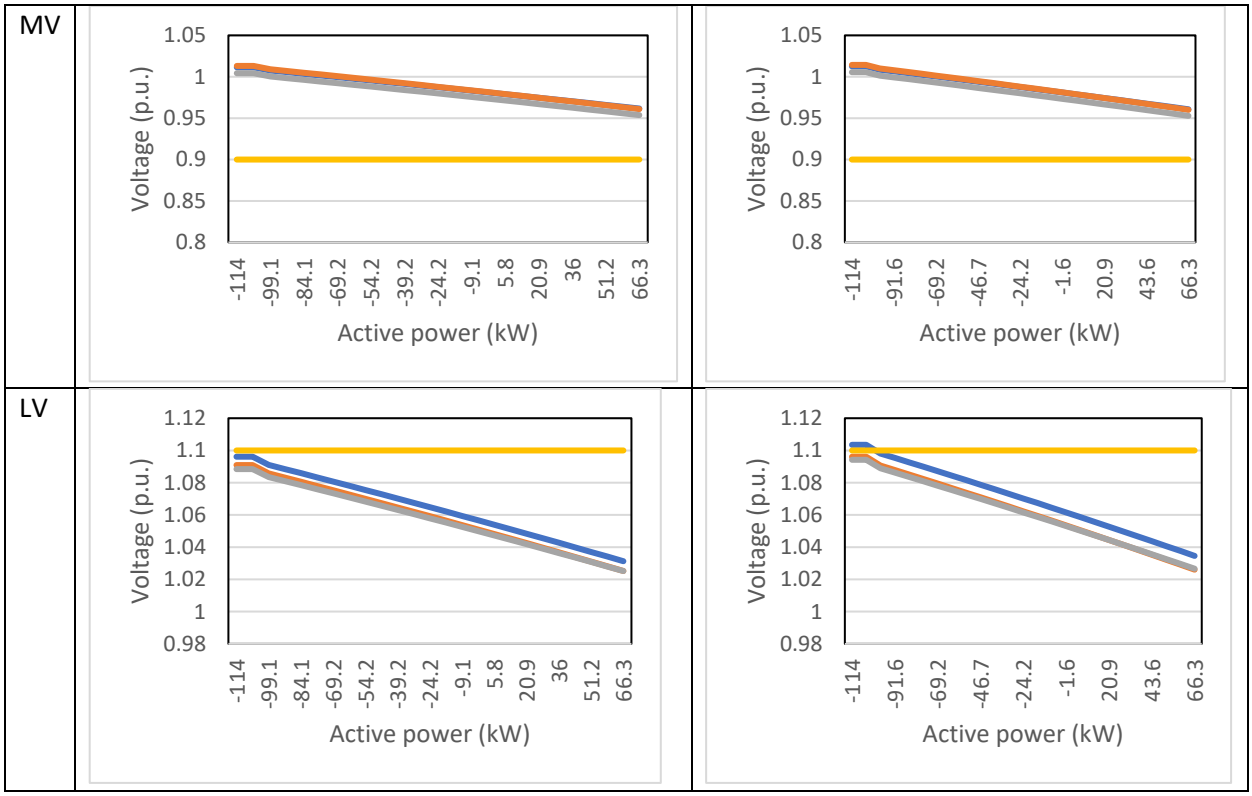

Fig. 4.5.44 Tarnagulla time-sweep integration scenario 7

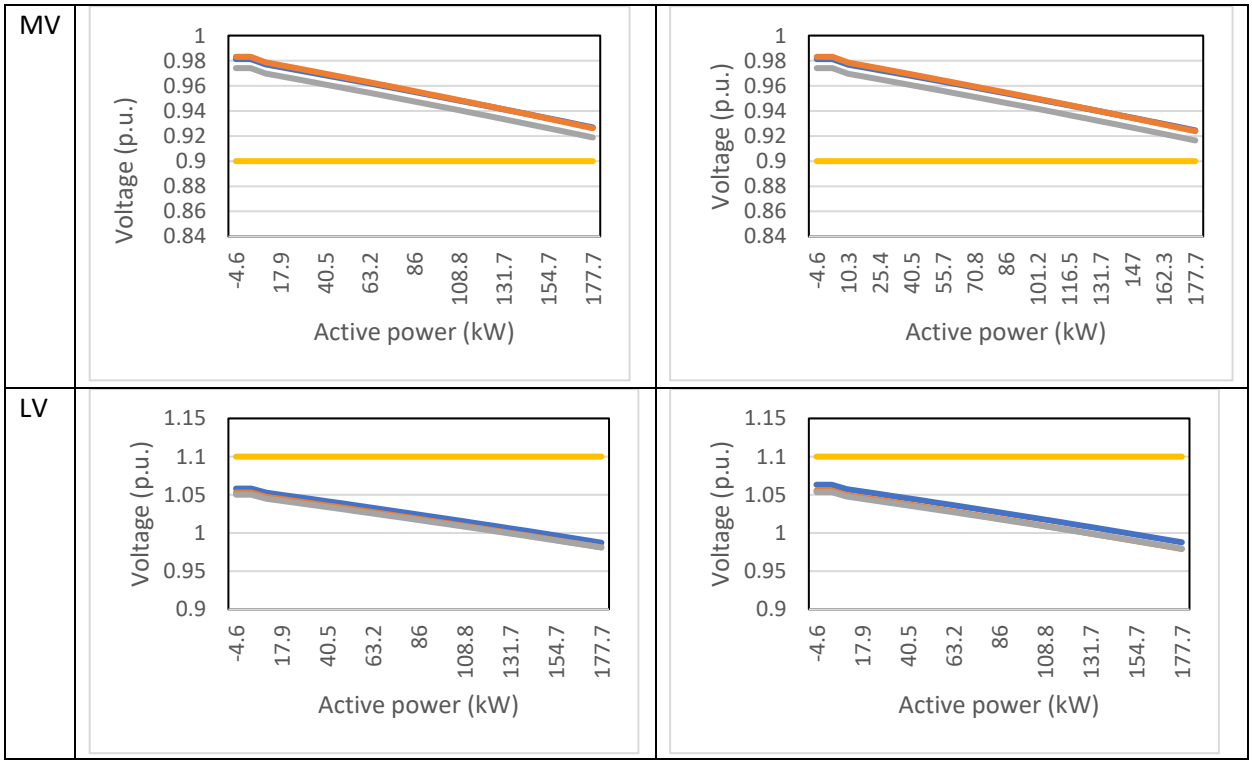

Fig. 4.5.45 Tarnagulla time-sweep integration scenario 8

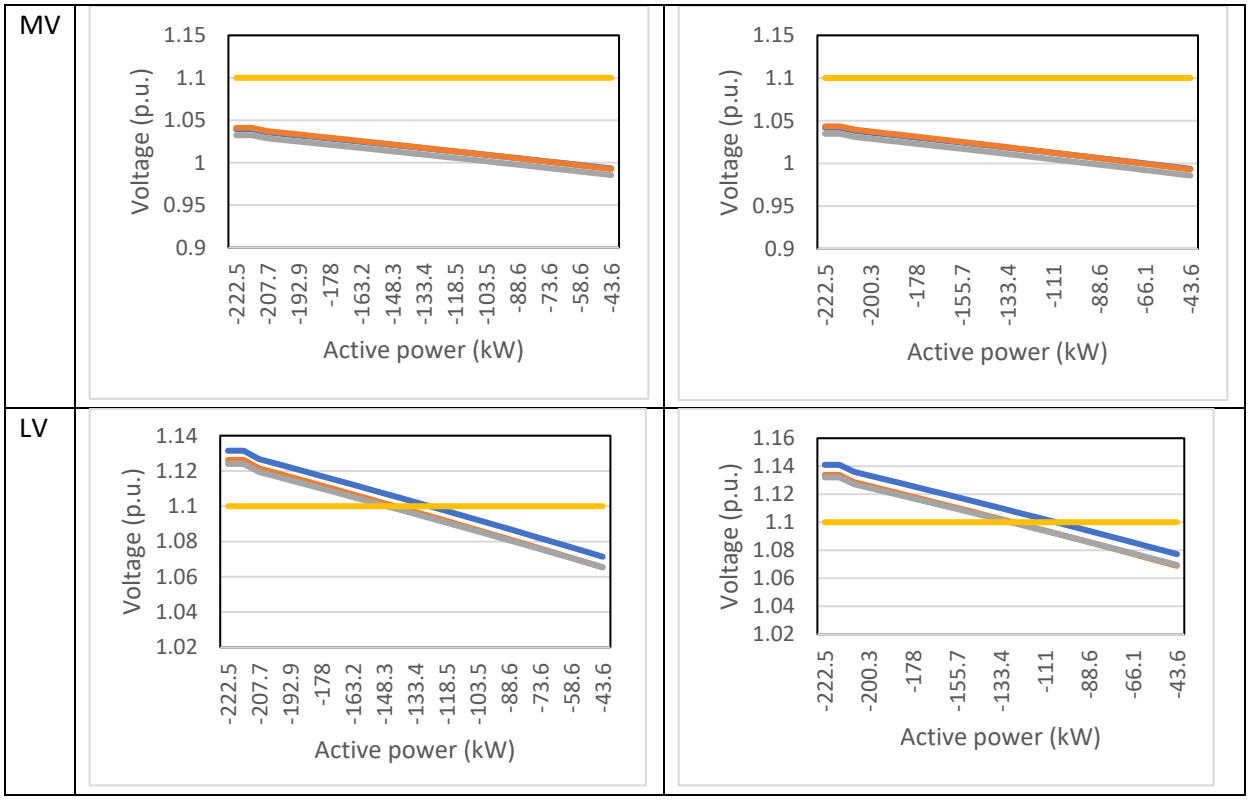

Fig. 4.5.46 Tarnagulla time-sweep integration scenario 9

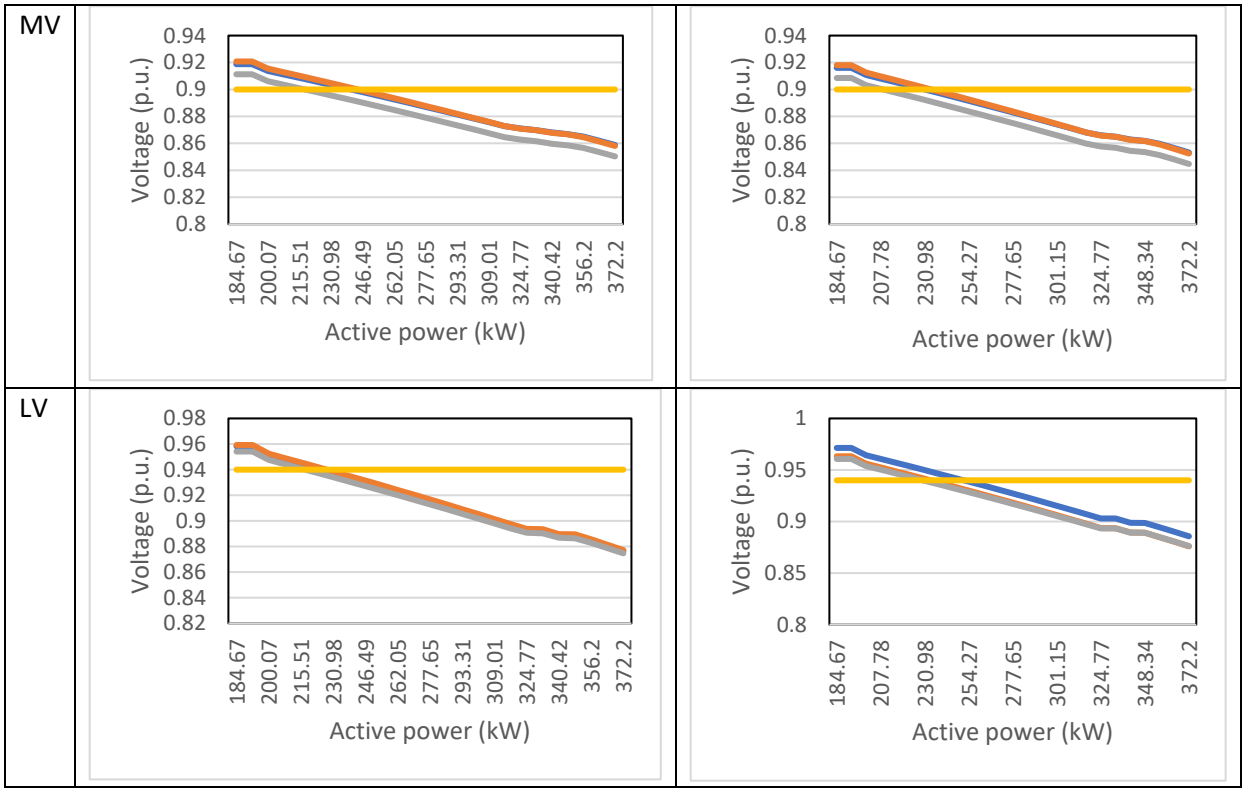

Fig. 4.5.47 Tarnagulla time-sweep integration scenario 10

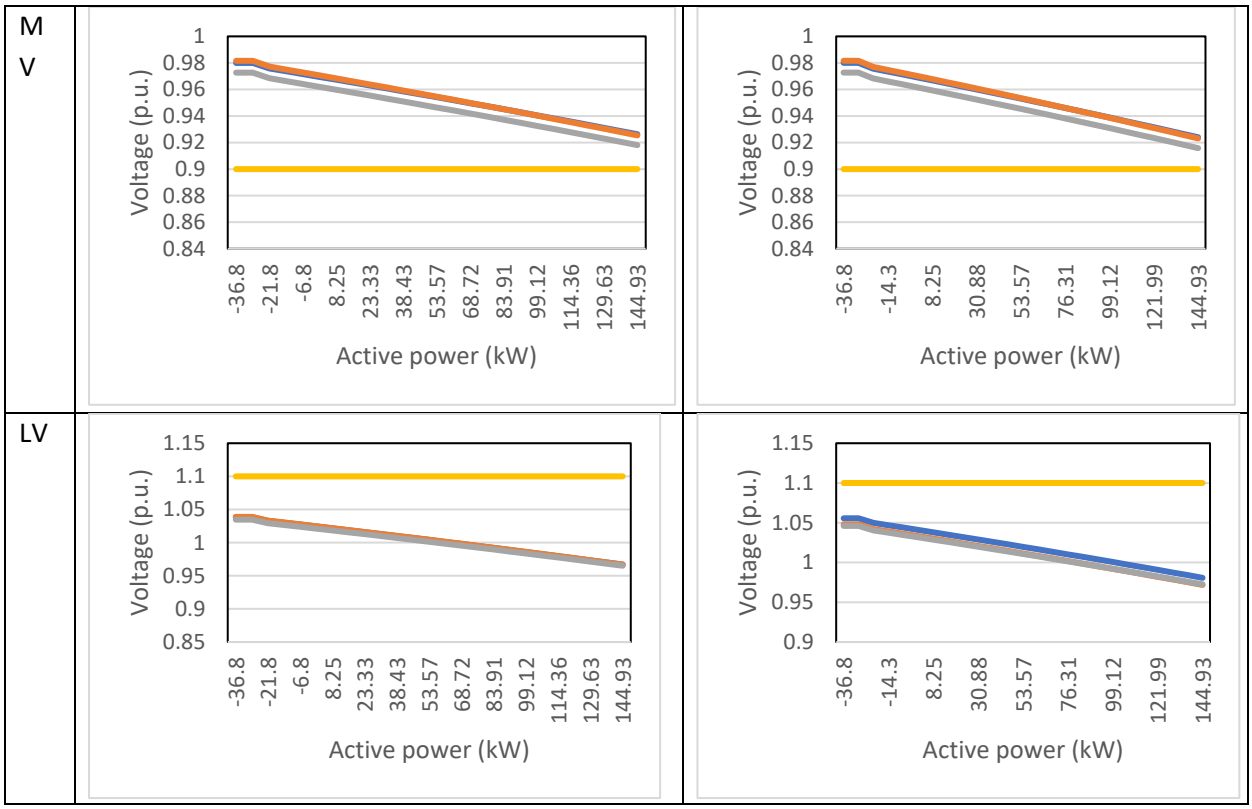

Fig. 4.5.48 Tarnagulla time-sweep integration scenario 11

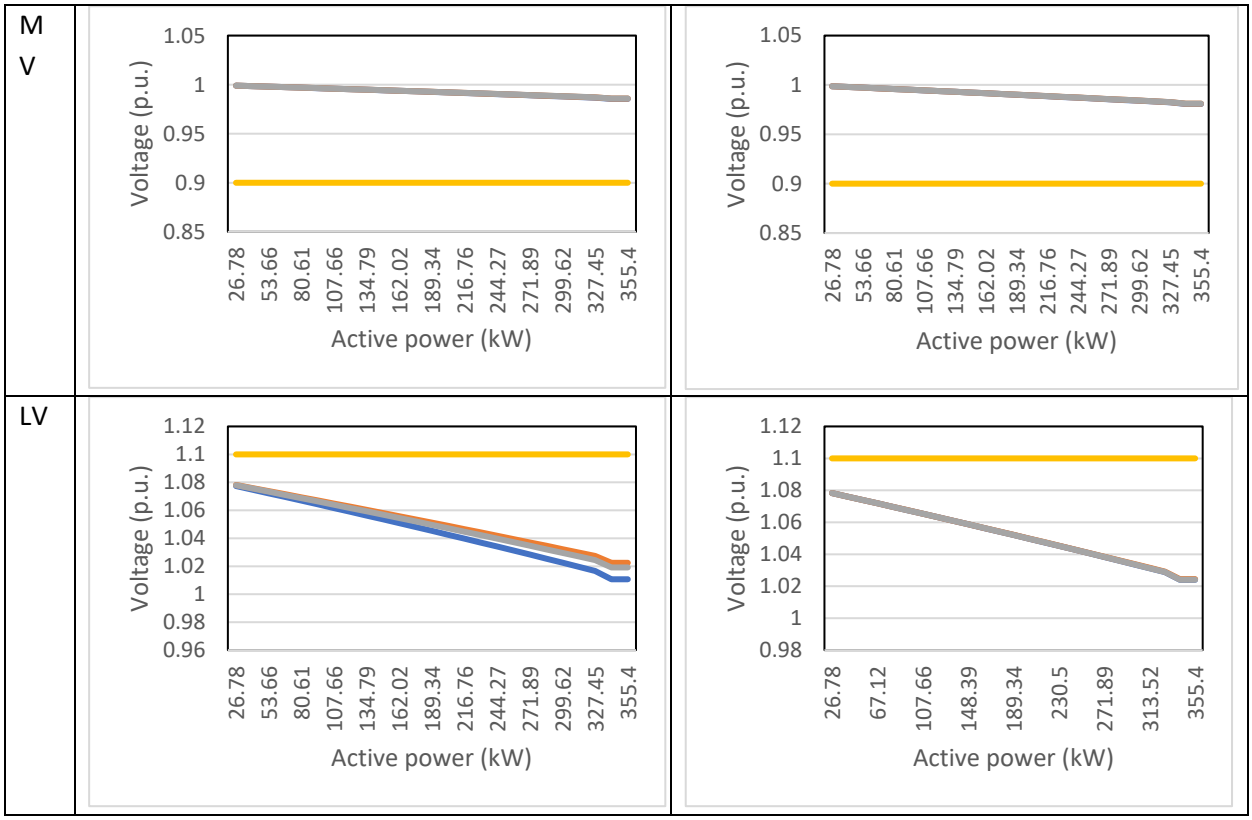

Fig. 4.5.49 Tarnagulla time-sweep integration scenario 12

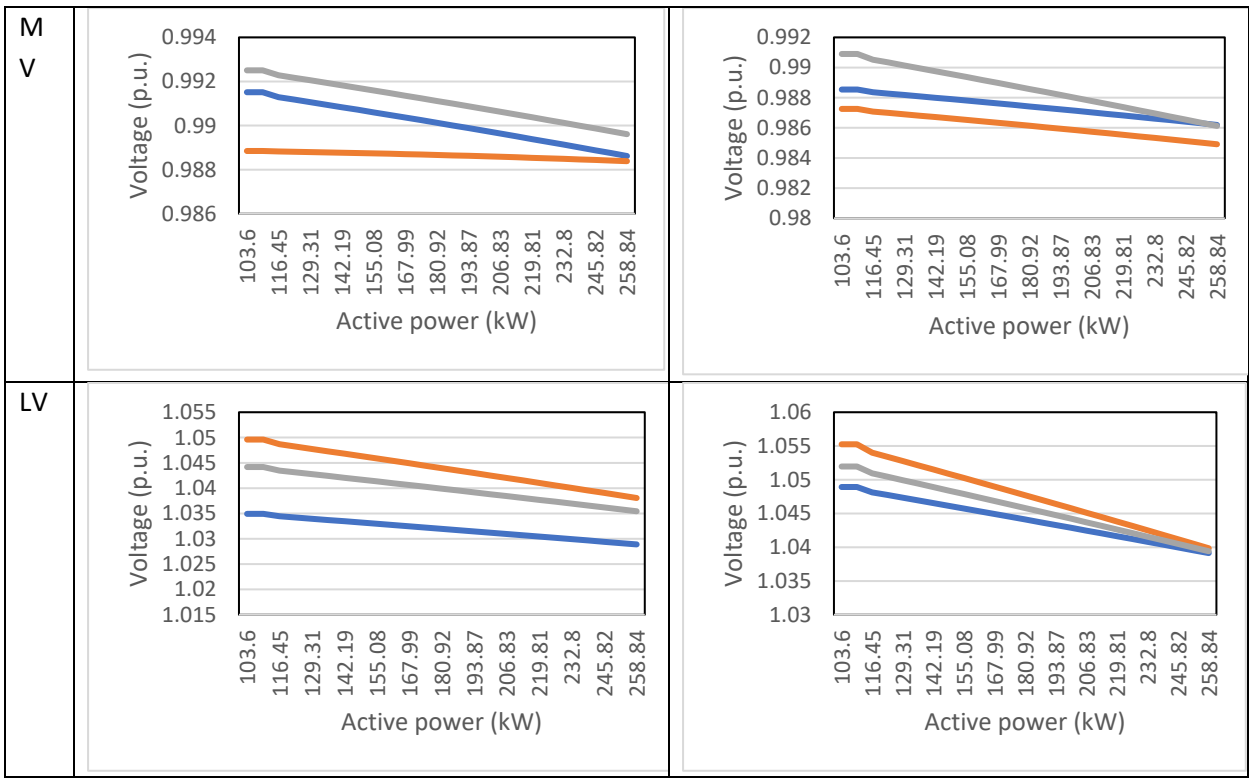

Fig. 4.5.50 Tarnagulla time-sweep integration scenario 13

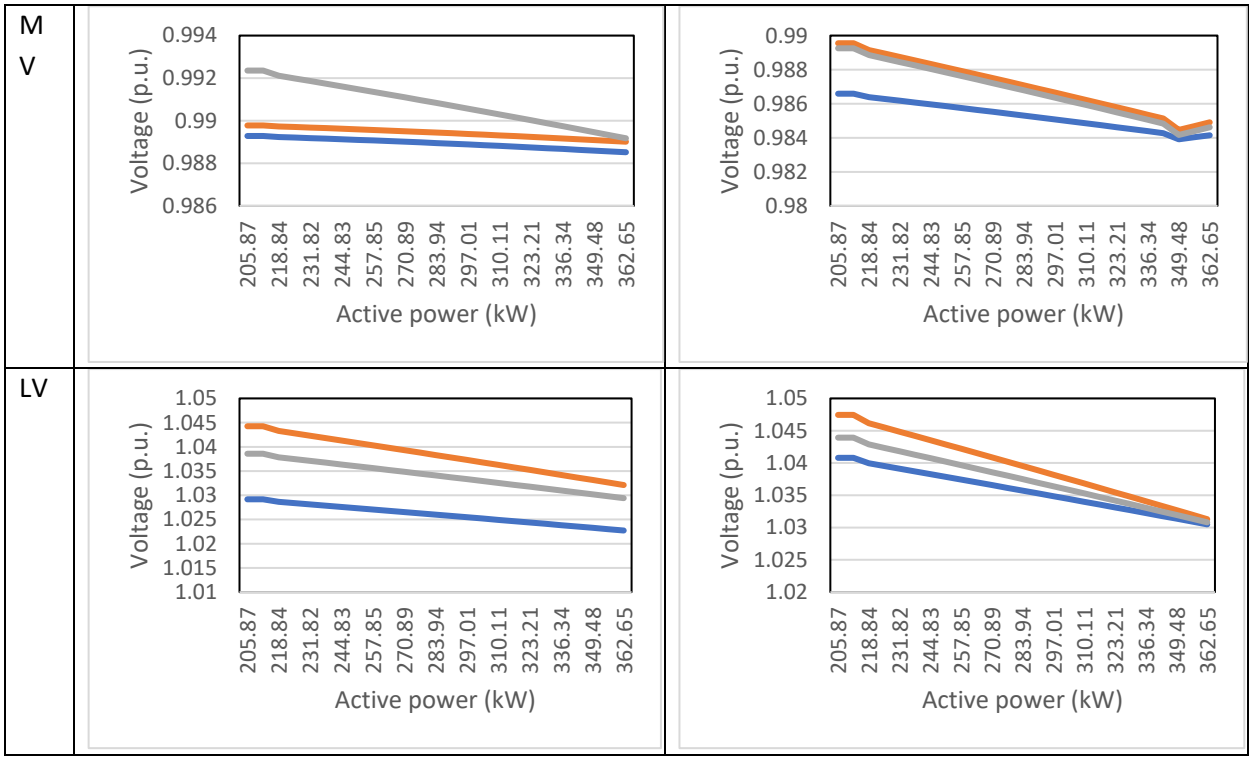

Fig. 4.5.51 Tarnagulla time-sweep integration scenario 14

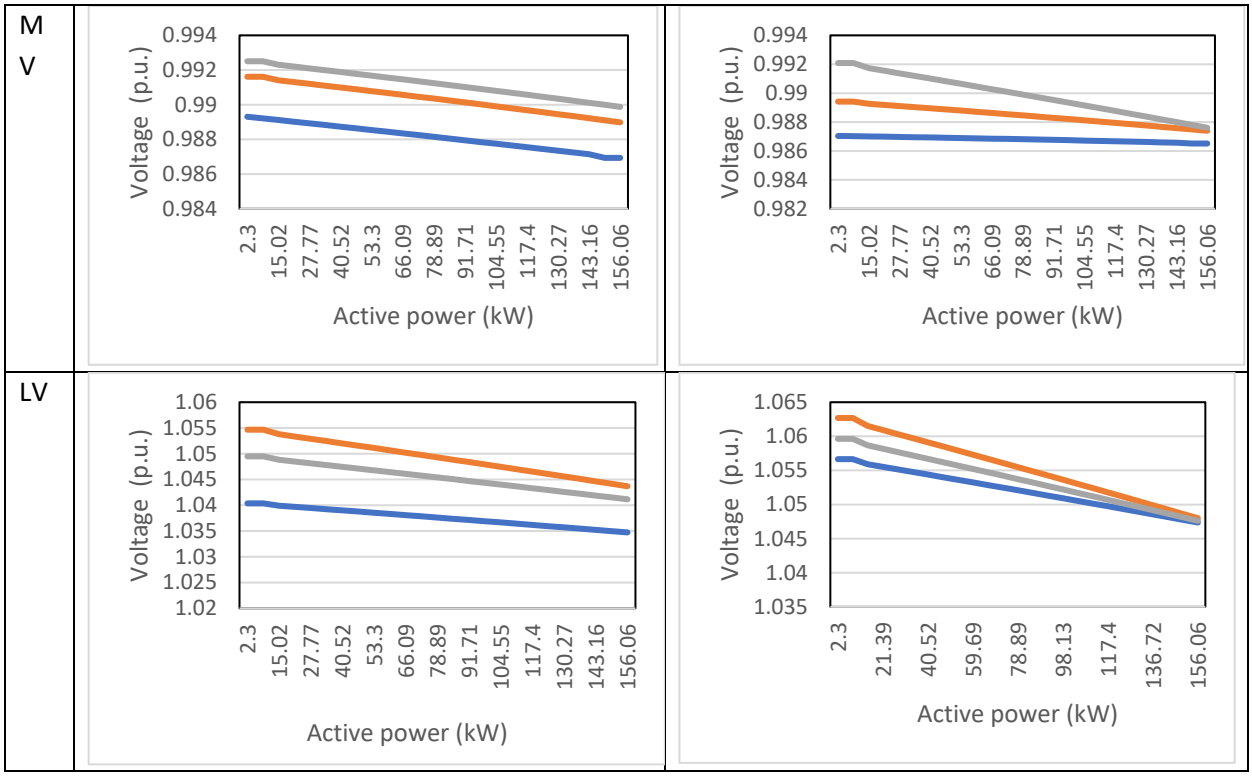

Fig. 4.5.52 Tarnagulla time-sweep integration scenario 15

The results show that the MV and LV systems of Tarnagulla are capable of supplying the load and can also host the PV and battery as identified in hosting capacity assessment studies. However, due to the smaller size of the network (compared to Donald) the system has been more sensitive to load and generation

changes. Furthermore, the studies on the stand-alone operation of microgrid shows the Tarnagulla network is capable of hosting more loads, PVs and batteries as the voltage variations were reduced due to the availability of the back-up generator which could supply the incoming feeder with more consistent voltage level. This highlights that the supply feeder is the main limiting factor in the hosting capacity of load and local generation of Tarnagulla (similar to Donald).

In order to investigate more realistic operational scenarios following the time-sweep analysis, quasi-dynamic simulations are performed on the Tarnagulla network considering the realistic daily load and generation profiles obtained through data analysis. In order to provide consistent results, these data sets were modified to represent normalized load and PV generation profiles of the customers while the typical battery profiles were generated using the literature and the network PV generation profiles (charging and discharging in the 24 hour window). The preliminary results showed that the hot and cold days need to be further studied due the possible impact of load and generation by the customers. Therefore, the results of 2 temperature zones for cold days (15 degrees) and hot days (40 degrees) for various operational scenarios detailed in Table 4.5.4 are demonstrated here.

TABLE 4.5.4 - INTEGRATION AND OPERATIONAL SCENARIOS FOR Quasi–Dynamic Studies of Tarnagulla

Operational Scenario	Maximum Load (KW)	Maximum PV (KW)	Maximum Battery Inveter (KW)	Temperature Zone
1	81	0	0	15 degrees
2	81	155	0	15 degrees
3	81	155	101 (c & d)	15 degrees
4	267	0	0	15 degrees
5	267	155	0	15 degrees
6	267	155	101 (c & d)	15 degrees
7	81	0	0	40 degrees
8	81	155	0	40 degrees
9	81	155	101 (c & d)	40 degrees
10	267	0	0	40 degrees
11	267	155	0	40 degrees
12	267	155	101 (c & d)	40 degrees

In each scenario similar to Donald, the loads, generations and batteries are assigned to the relevant clusters considering the weighting of each cluster as defined through the data analysis and the results demonstrate the different voltage profiles at the same buses as the time-sweep analysis for the various studied scenarios as illustrated in Fig. 4.5.53 – 4.5.64.

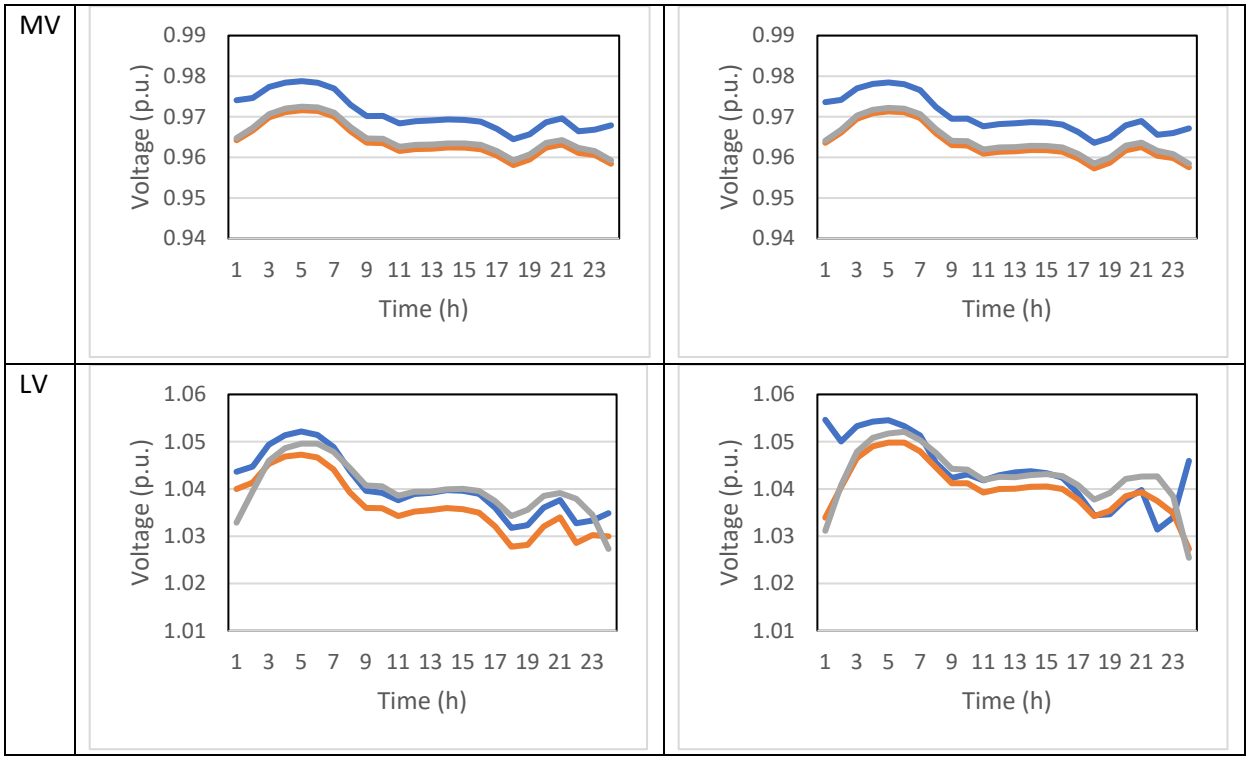

Fig. 4.5.53 Tarnagulla quasi-dynamic integration scenario 1

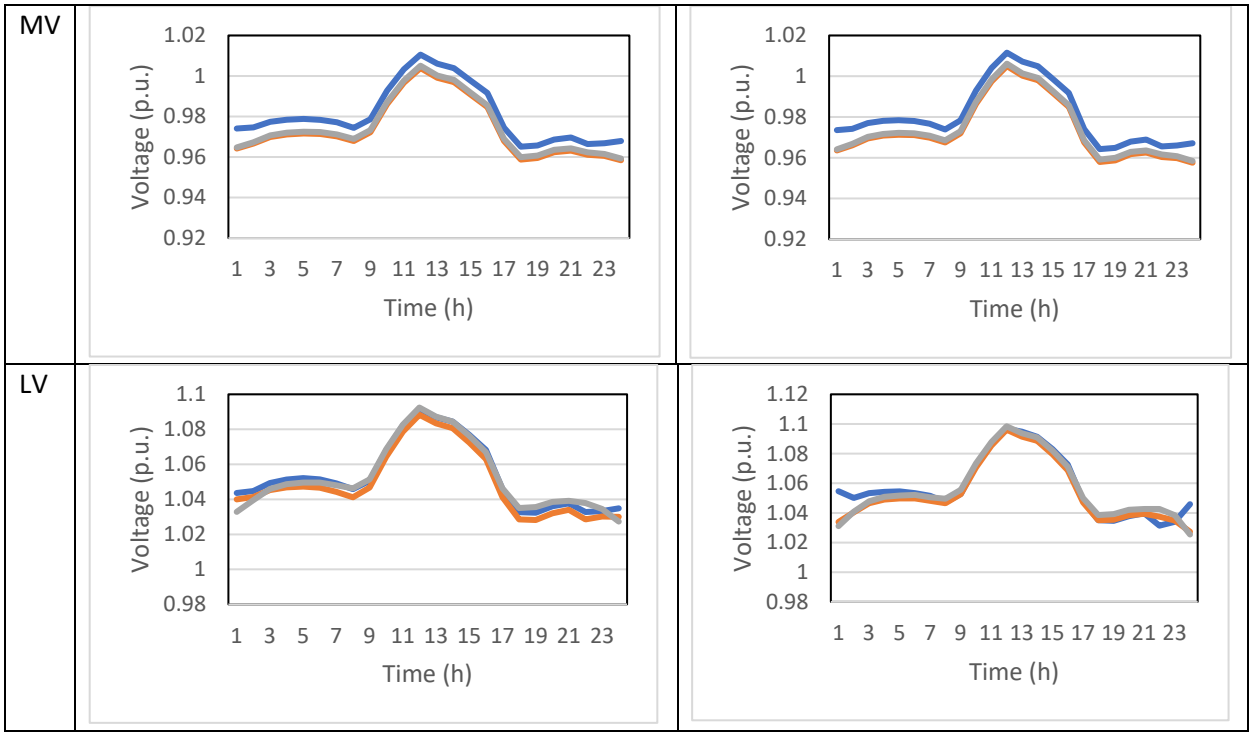

Fig. 4.5.54 Tarnagulla quasi-dynamic integration scenario 2

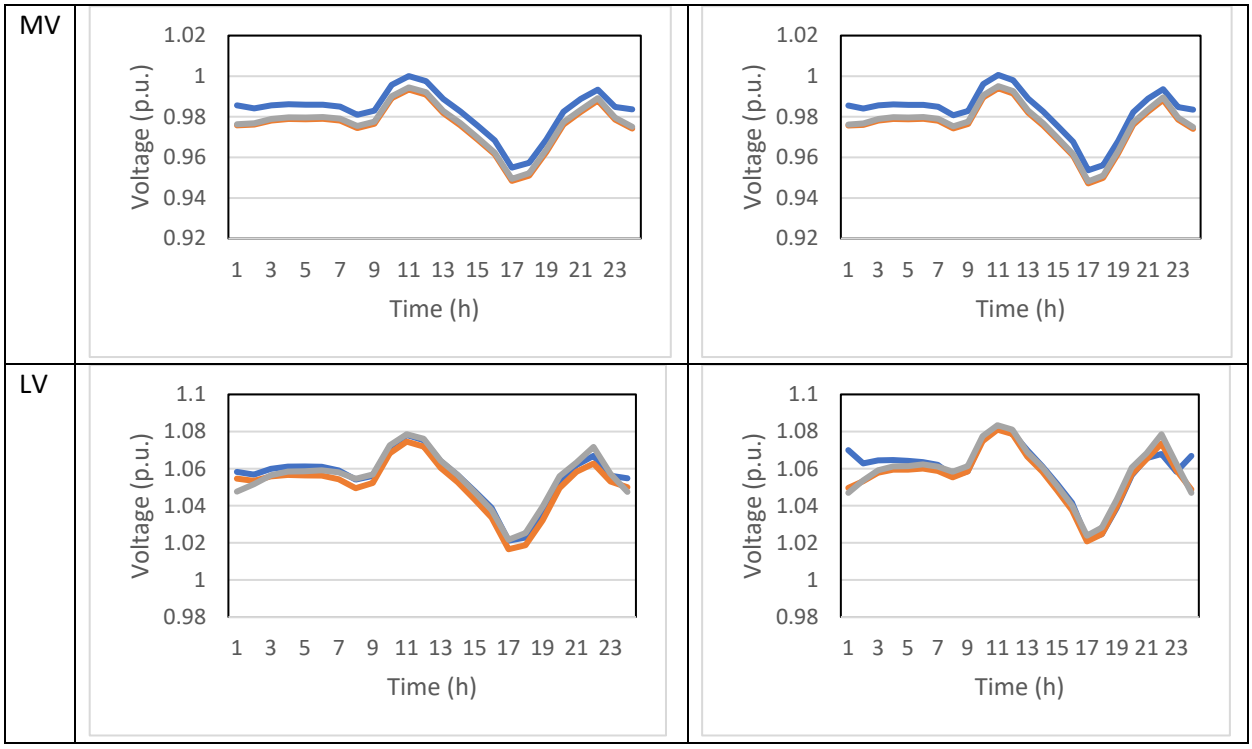

Fig. 4.5.55 Tarnagulla quasi-dynamic integration scenario 3

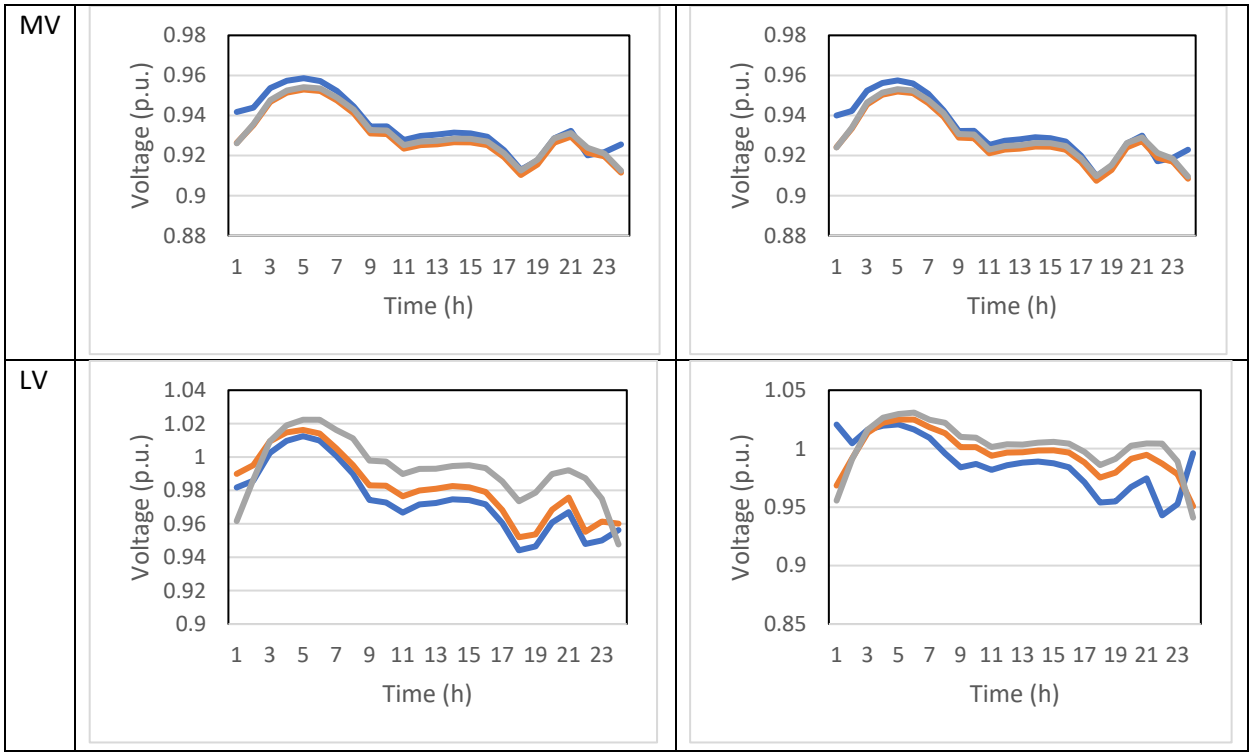

Fig. 4.5.56 Tarnagulla quasi-dynamic integration scenario 4

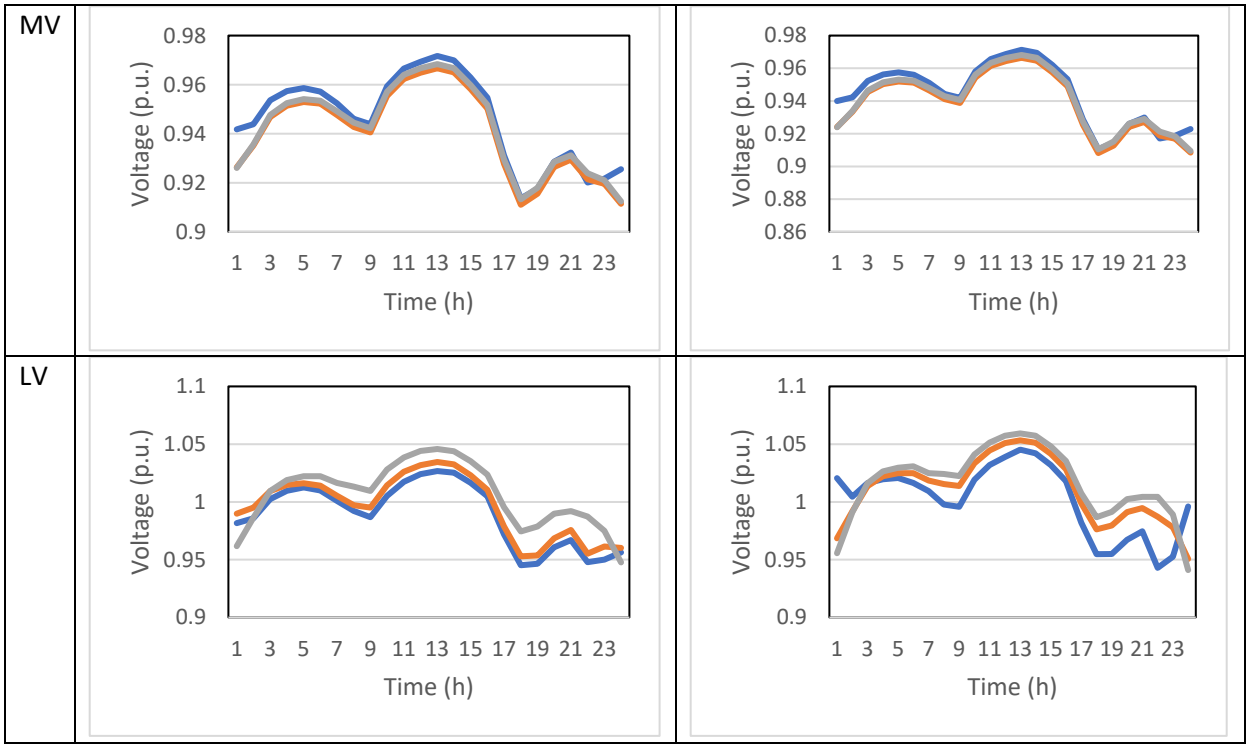

Fig. 4.5.57 Tarnagulla quasi-dynamic integration scenario 5

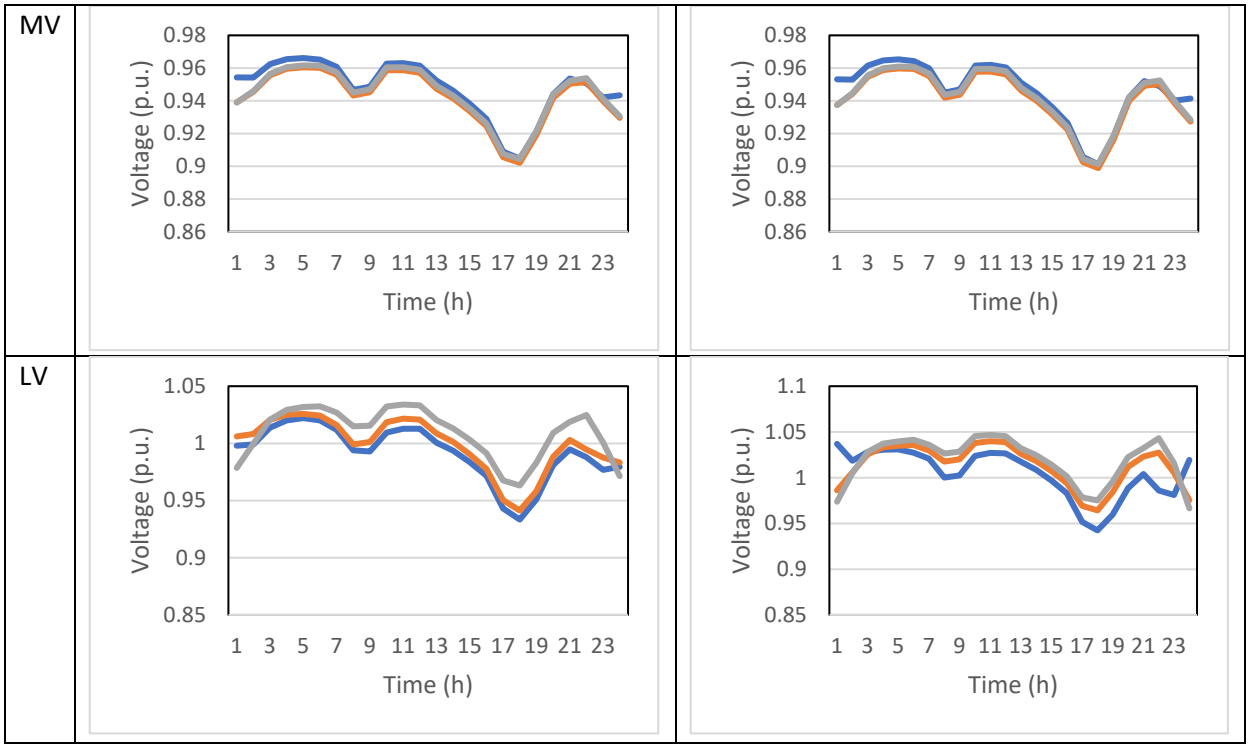

Fig. 4.5.58 Tarnagulla quasi-dynamic integration scenario 6

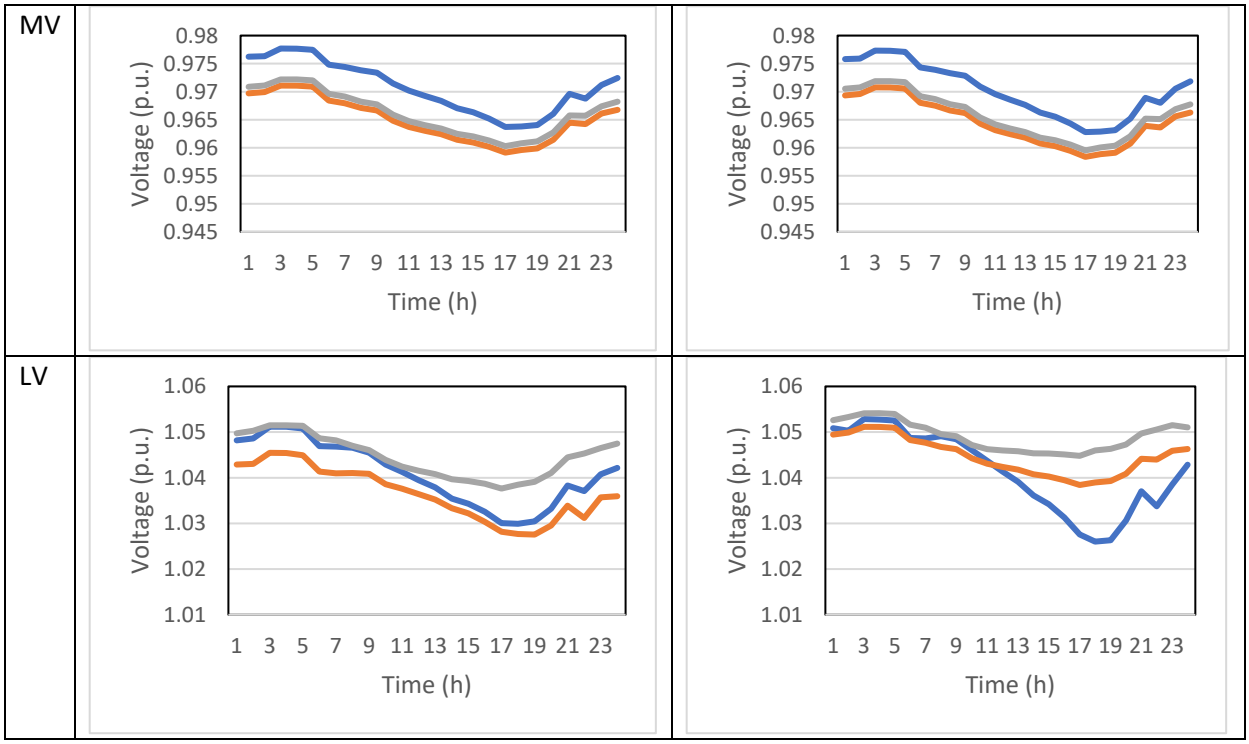

Fig. 4.5.59 Tarnagulla quasi-dynamic integration scenario 7

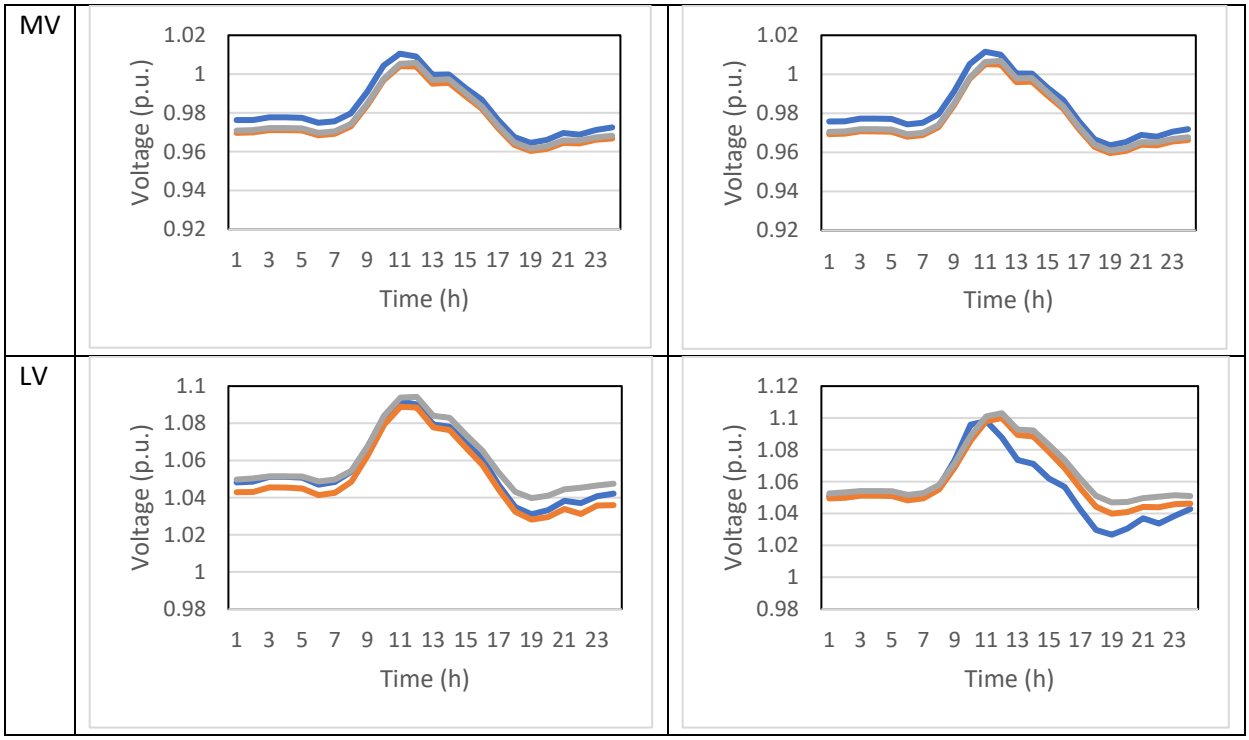

Fig. 4.5.60 Tarnagulla quasi-dynamic integration scenario 8

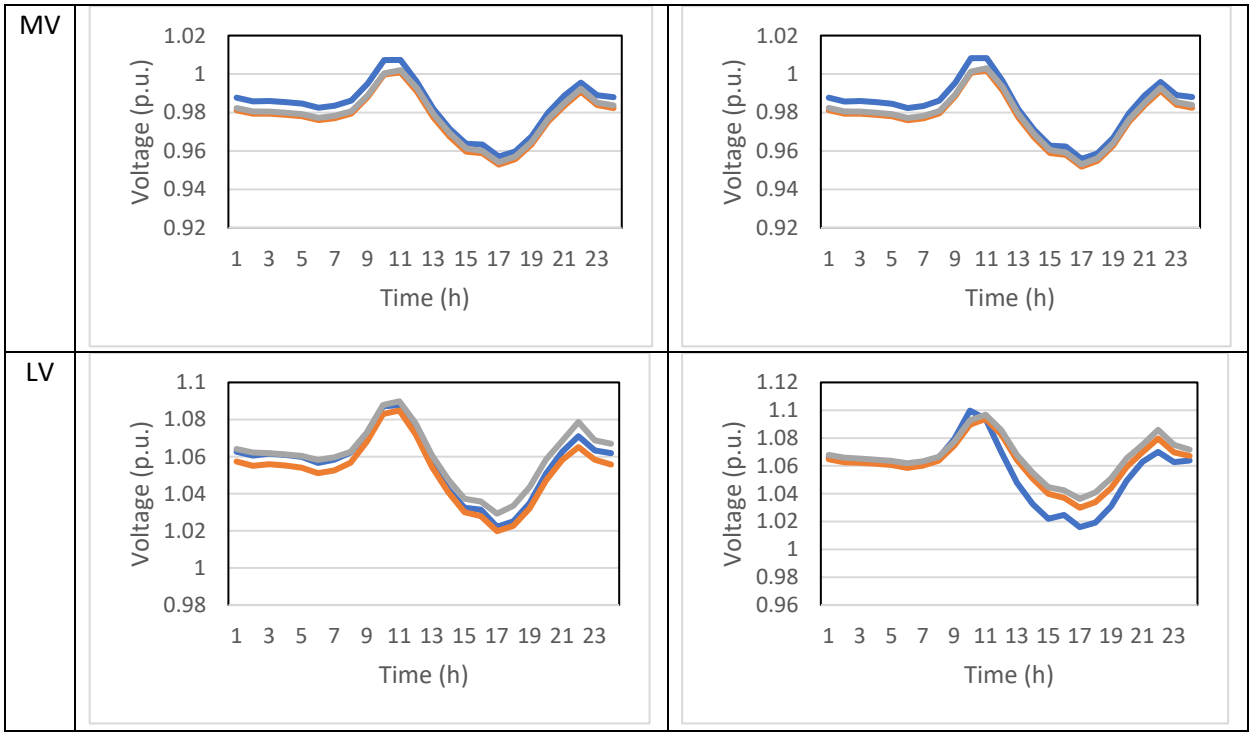

Fig. 4.5.61 Tarnagulla quasi-dynamic integration scenario 9

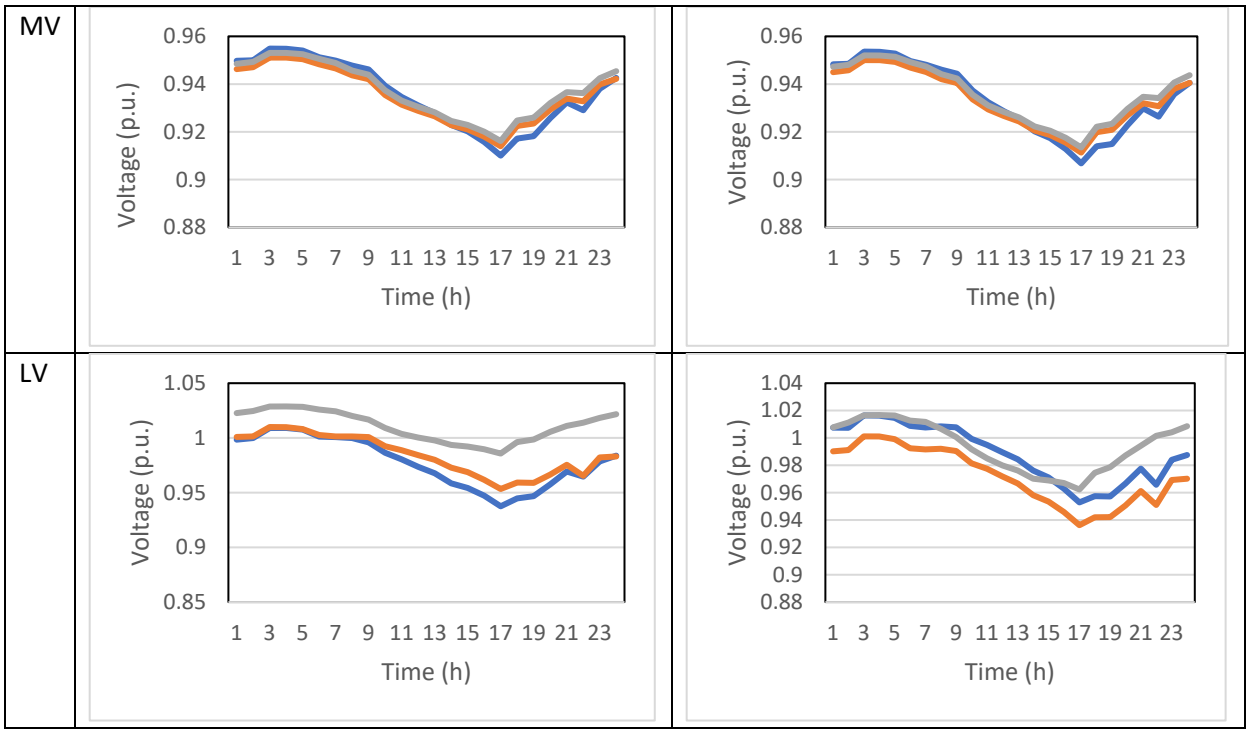

Fig. 4.5.62 Tarnagulla quasi-dynamic integration scenario 10

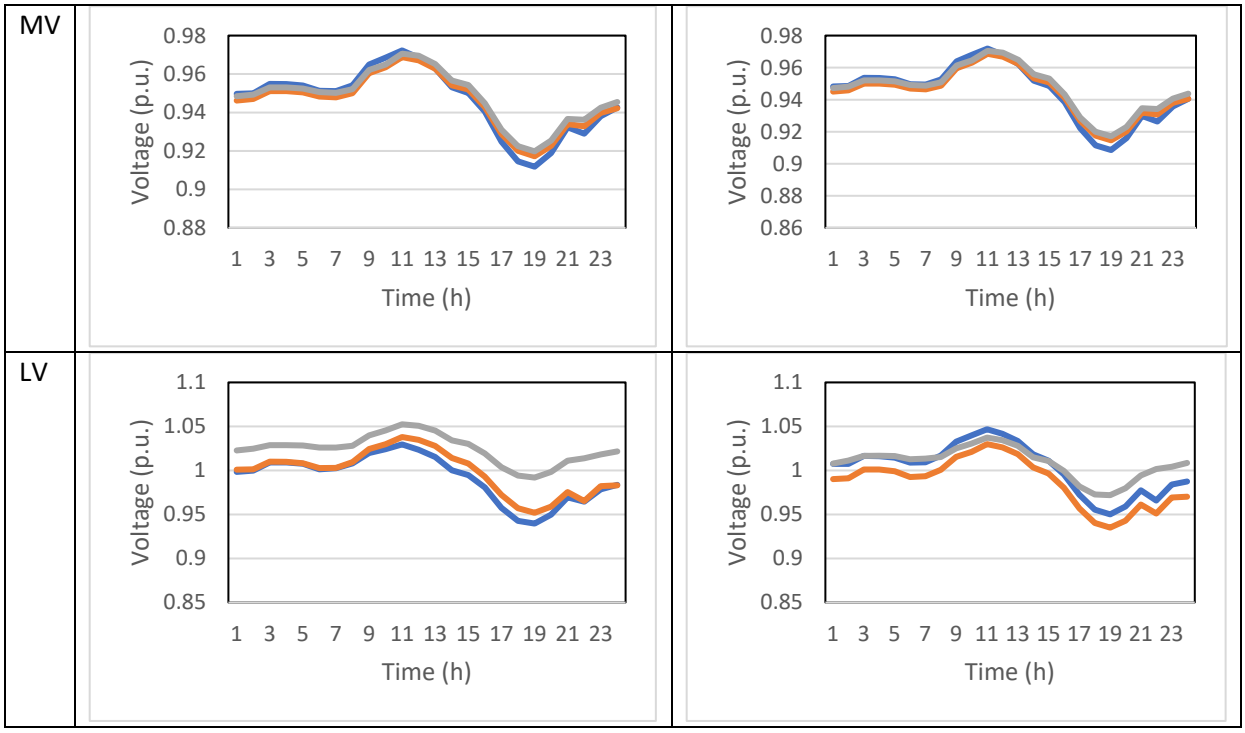

Fig. 4.5.63 Tarnagulla quasi-dynamic integration scenario 11

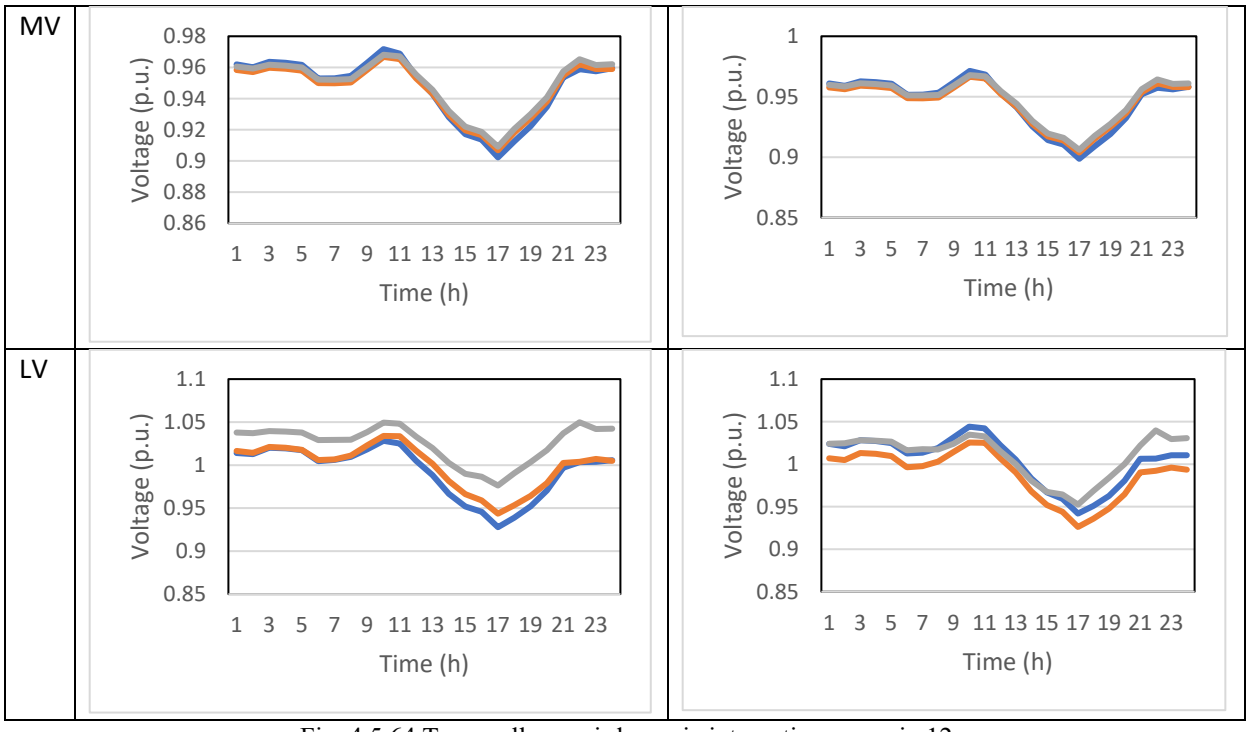

Fig. 4.5.64 Tarnagulla quasi-dynamic integration scenario 12

The quasi-dynamic simulations support the findings through time-sweep analysis as the network did not experience a major over or under voltage in many realistic operational scenarios. As shown in the quasi-dynamic results, the batteries can improve the voltage profile by observing the extra energy output of PVs during low load conditions and injecting back the energy to the microgrid during high load conditions.

4.5.3. Summary and Conclusions

- The MV and LV systems of Donald are capable of supplying the load well above the peak load of the network can also host the PV and battery as identified in hosting capacity assessment studies.
- The Tarnagulla network has been more sensitive to load and generation changes
- Supply feeder is the main limiting factor in the hosting capacity of load and local generation of both Donald and Tarnagulla
- The voltages across the network in stand-alone operation modes were more consistent due to the voltage support of the back-up generator
- The quasi-dynamic simulations support the findings through time-sweep analysis as the networks did not experienced major over or under voltages in many realistic operational scenarios
- Minor overvoltage was observed in the LV network during low load and high PV generation conditions with no batteries which were improved by considering the batteries in the system

4.6. Hosting Capacity Improvement

In this section, several hosting capacity improvement techniques have been implemented and evaluated. First, a base scenario is defined in which no hosting capacity improvement technique has been implemented. The analysis is used later as a benchmark to evaluate the effectiveness of the improvement techniques. The benchmark metrics used in this section are:

- The maximum total active power that can be generated in the network by PV systems (P_{Gen});
- The maximum total active power that the network can inject to the upstream network (P_{Net}).

These values have been calculated by sweeping the PV generation from 0 to100%, until any of the following limiting conditions arises:

- The farthest LV bus of the network reaches the upper-band voltage limit (1.1 pu);
- One of the MV/LV transformers reaches its maximum capacity.

4.6.1. Methodology:

As shown in Fig. 4.6.1, the considered techniques can be classified into network and customer side solutions. In the network-side solutions, typically, networks implement the improvement techniques, and the methods are generally centralised. While in the customer-side solutions, DER owners are participating in the solution, and methods are more likely to be decentralised or distributed.

❖ **Network-Side Methods:**
- ➢ MV/LV transformers' tap changer to control LV side voltage;
- ➢ A community battery in LV feeders to absorb power generated by PV systems.

❖ **Customer-Side Methods:**
- ➢ *volt/var* control in smart inverters;
- ➢ Residential batteries to absorb the generated active power by the PV inverter.

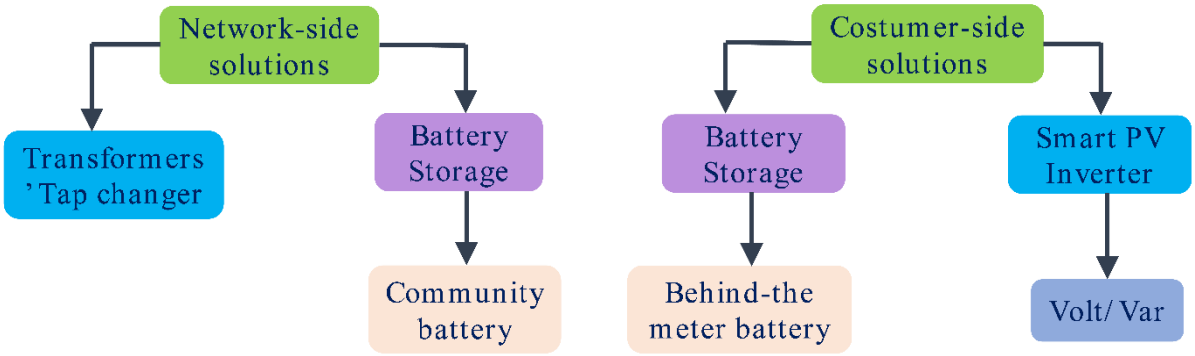

Fig. 4.6.1. Methodology diagram of this improving hosting capacity.

4.6.2. Tarnagulla Network

Base Case:

In Table 4.6.1, for four levels of load with a power factor of 0.85, the maximum total active power that can be generated in the network (PGen) and the maximum total active power it can inject to its upstream network (P_{Net}) are shown. Furthermore, the detailed results, the variation of the voltage magnitude of bus B_LV.V2.4 and the occupied capacity of the MV/ LV transformer TF-V with respect to the total generated active power in/by the Tarnagulla network are shown in Fig. 4.6.2 and 4.6.3, respectively. It can be seen that, in this case, the overvoltage problem restricts the generation and the capacity of the transformers is not a limiting factor. Moreover, by increasing the load, the networks are able to host more generation, and consequently, inject more power to the upstream networks.

Table 4.6.1. P_{Gen} and P_{Net} in base case of the Tarnagulla network.

		P_{Gen} (kW)	P_{Net} (kW)
Load (%)	25	150	69
	50	270	108
	75	392	149
	100	517	192

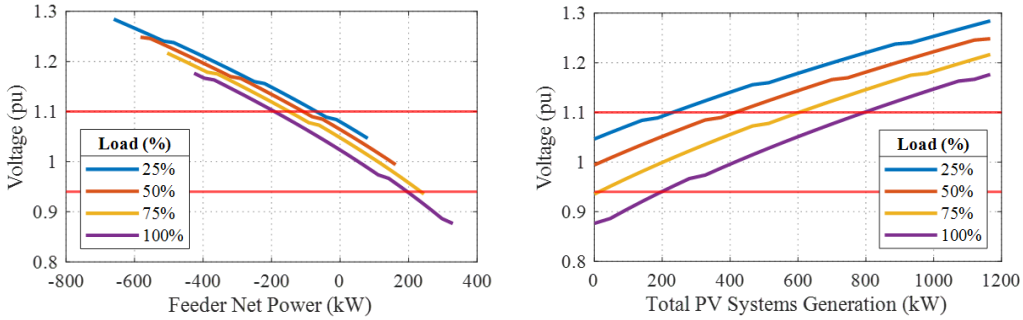

Fig. 4.6.2. Voltage magnitude variation of bus B_LV.V2.4 in the base case of the Tarnagulla network.

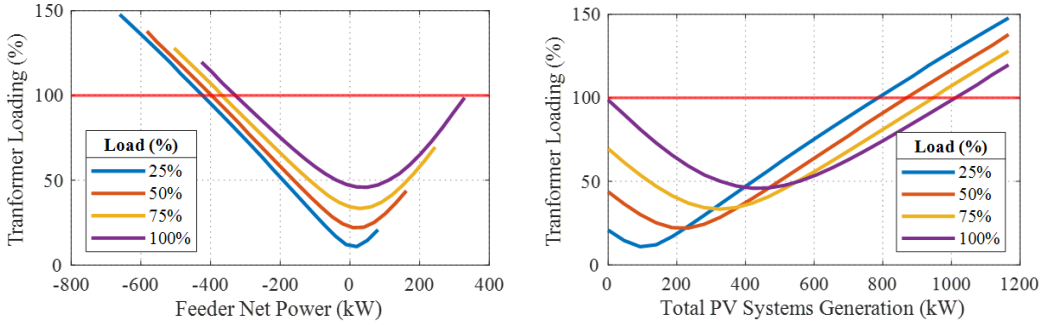

Fig. 4.6.3. The occupied capacity of transformer TF-V in the base case of the Tarnagulla network.

Transformers tap changer

Two tap positions, -1 and -2, have been considered for the MV/LV transformers and P_{Gen} and P_{Net} have been calculated for four levels of load. As shown in Table 4.6.2 and 4.6.3, using lower tap positions, both P_{Gen} and P_{Net} are increased since the voltage magnitude across the LV feeders is reduced. However, this may not be an optimal solution. Since the voltage magnitude at the LV side is reduced, the load hosting capacity can be also adversely affected.

Tap Position=-1

Table 4.6.2. P_{Gen} and P_{Net} when transformers' tap position is -1 in the Tarnagulla network.

		P_{Gen} (kW)	P_{Net} (kW)
Load (%)	25	224 (49% ↑)	143 (107% ↑)
	50	345 (28% ↑)	182 (69% ↑)
	75	467 (19% ↑)	223 (50% ↑)
	100	593 (15% ↑)	265 (38% ↑)

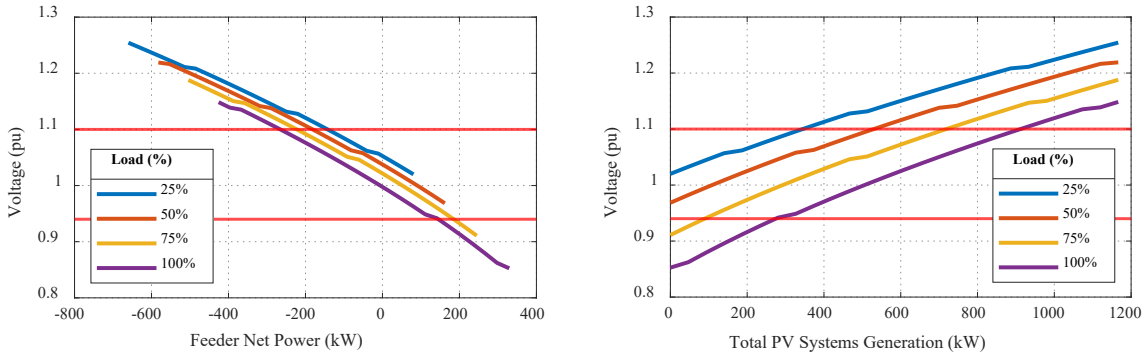

Fig. 4.6.4. Voltage magnitude variation of bus B_LV.V2.4 when transformers' tap position is -1 in the Tarnagulla network.

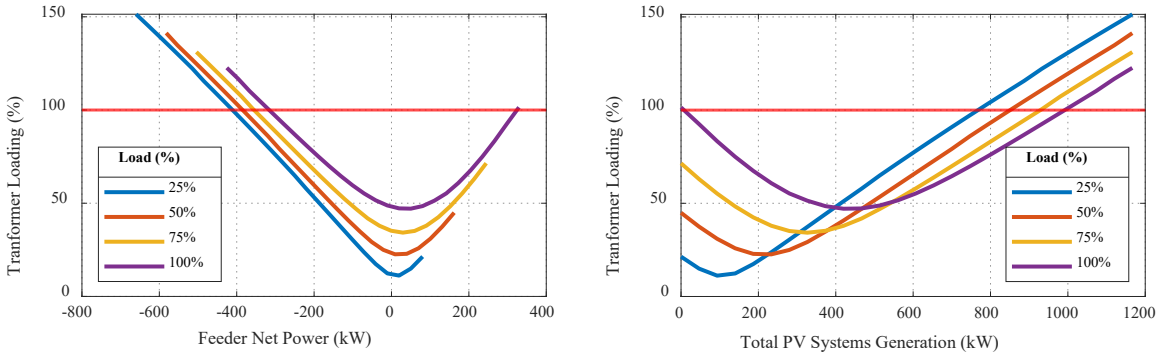

Fig. 4.6.5. The occupied capacity of transformer TF-V when transformers' tap position is -1 in the Tarnagulla network.

❖ Tap Position=-2

Table 4.6.3. P_{Gen} and P_{Net} when transformers' tap position is -2 in the Tarnagulla network

		P_{Gen} (kW)	P_{Net} (kW)
Load (%)	25	306 (103% ↑)	223 (223% ↑)
	50	426 (58% ↑)	260 (141% ↑)
	75	549 (40% ↑)	301 (102% ↑)
	100	632 (22% ↑)	303* (57% ↑)

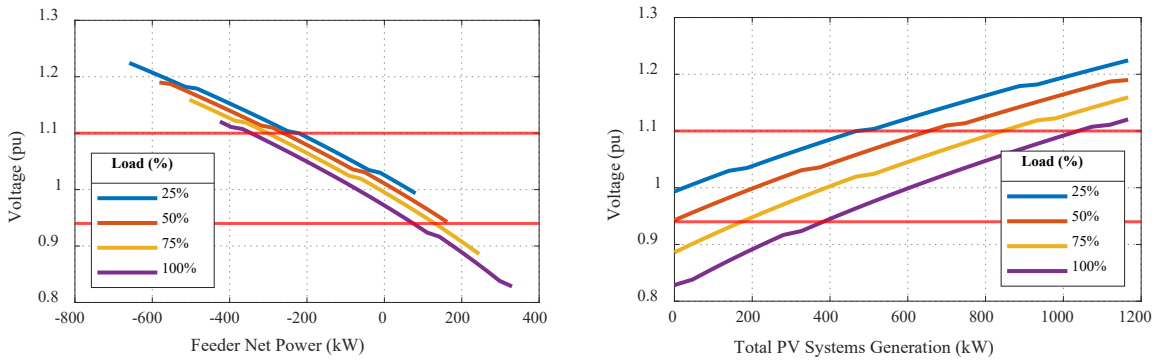

Fig. 4.6.6. Voltage magnitude variation of bus B_LV.V2.4 when transformers' tap position is -2 in the Tarnagulla network

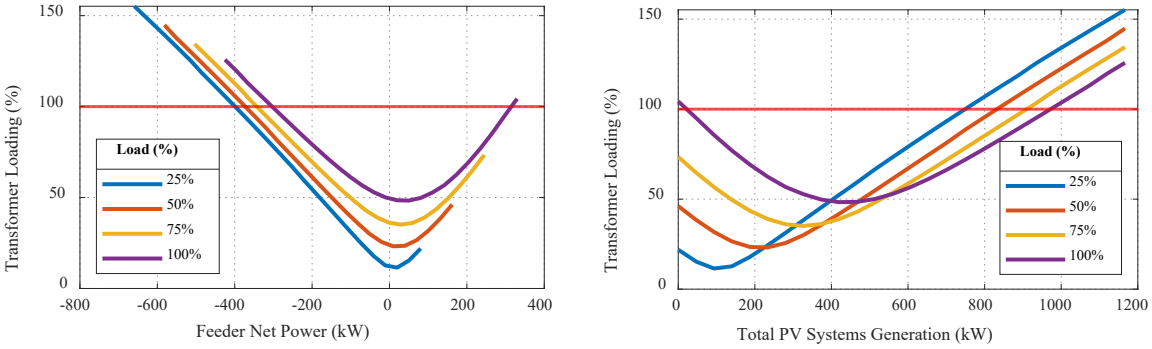

Fig. 4.6.7. The occupied capacity of transformer TF-V when transformers' tap position is -2 in the Tarnagulla network

Smart inverters - volt/var Control

The volt/var curve used for this study is shown in Fig. 4.6.8. This curve is adopted from AS/NZS A4777.2 with the settings shown in Table 4.6.4. Moreover, it is assumed that the inverters are over-sized by 10% in order to provide var control.

Table 4.6.4. Applied *volt/var* setting

	Voltage (pu)	Var % rated VA
V_1	0.9	30%
V_2	0.96	0%
V_3	1.08	0%
V_4	1.15	-30%

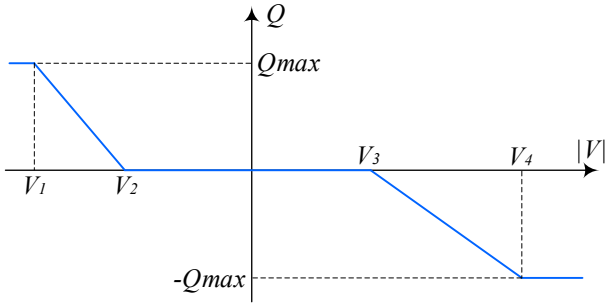

Fig. 4.6.8. Adopted *volt/var* curve from AS/NZS A4777.2

Two case studies have been carried out utilising *volt/var* control for PV inverters. In the first case, it is considered that all PV inverters are smart (with var control capability) while in the second case, half of them are legacy ones (without var control capability) and half of them are smart. It can be seen in Tables 4.6.5 and 4.6.6 that *volt/var* can improve both P_{Gen} and P_{Net} without decreasing the load hosting capacity of network. In the second case, however, since fewer smart PV inverters are installed, the absorbed reactive power by PV inverters is less, therefore, the improvement is not as much as the first case. Furthermore, when there is active power generation, as PV inverters are using reactive power to improve the voltage profile, the transformers capacity is occupied more compared to the base case.

- **All PV inverters are smart**

Table 4.6.5. P_{Gen} and P_{Net} when all PV inverters are equipped with volt/var control in the Tarnagulla network.

		P_{Gen} (kW)	P_{Net} (kW)
Load (%)	25	170 (13% ↑)	89 (29% ↑)
	50	289 (7% ↑)	127 (18% ↑)
	75	411 (5% ↑)	167 (12% ↑)
	100	534 (3% ↑)	208 (8% ↑)

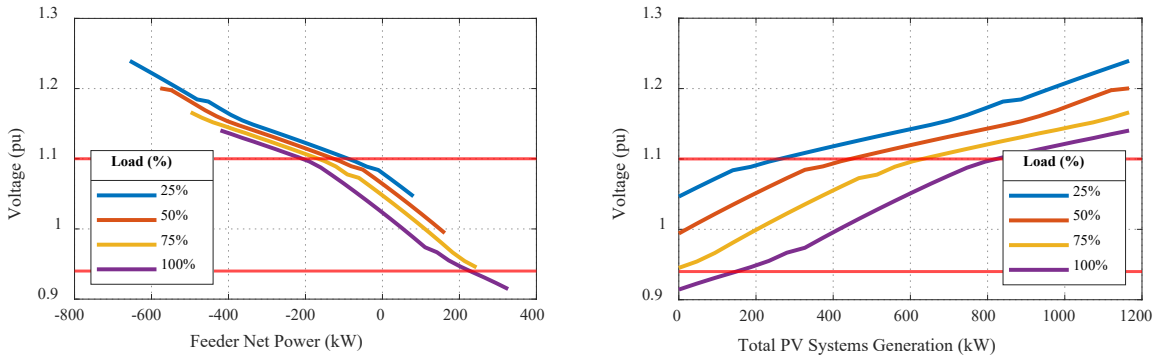

Fig. 4.6.9. Voltage magnitude variation of bus B_LV.V2.4 when all PV inverters are equipped with volt/var control in the Tarnagulla network.

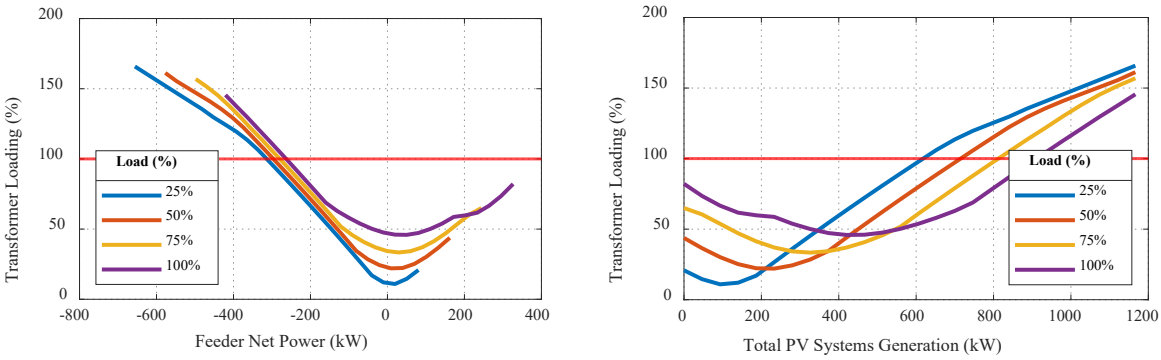

Fig. 4.6.10. The occupied capacity of transformer TF-V when all PV inverters are equipped with volt/var control in the Tarnagulla network.

❖ Half of PV inverters are smart

Table 4.6.6. P_{Gen} and P_{Net} when half of PV inverters are equipped with volt/var control in Tarnagulla network

		P_{Gen} (kW)	P_{Net} (kW)
Load (%)	25	159 (6% ↑)	78 (13% ↑)
	50	278 (3% ↑)	117 (8% ↑)
	75	400 (2% ↑)	157 (5% ↑)
	100	525 (2% ↑)	199 (4% ↑)

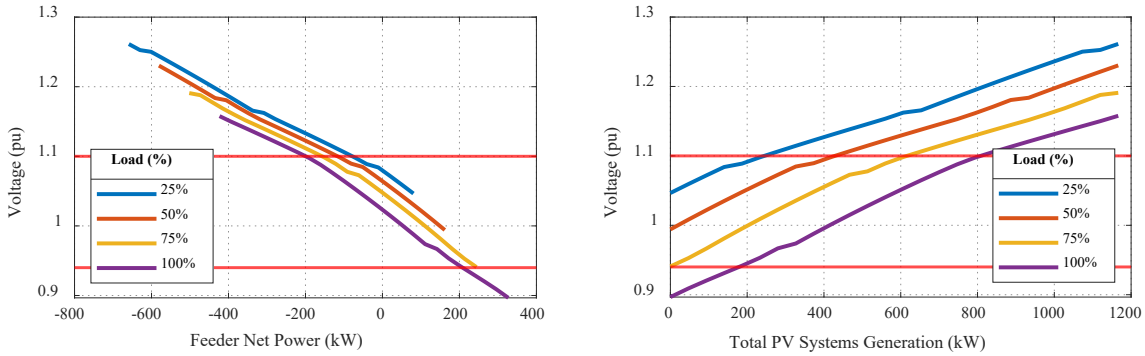

Fig. 4.6.11. Voltage magnitude variation of bus B_LV.V2.4 when half of PV inverters are equipped with volt/var control in the Tarnagulla network

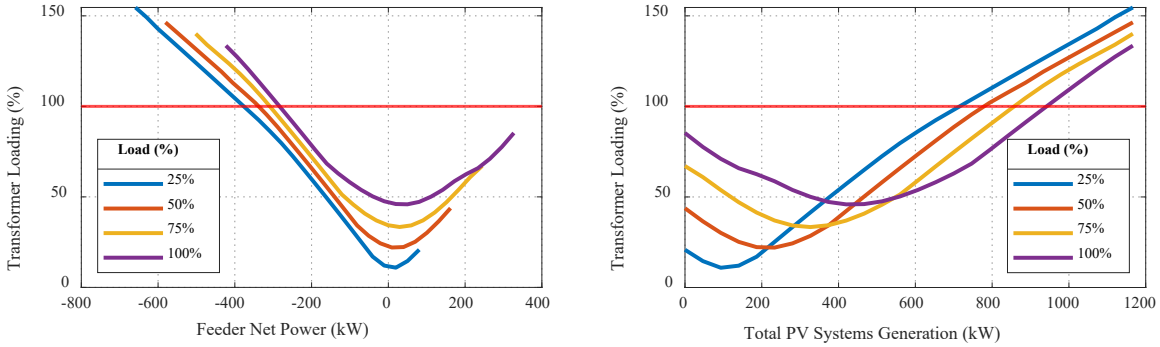

Fig. 4.6.12. The occupied capacity of transformer TF-V when half of PV inverters are equipped with volt/var control in the Tarnagulla network.

Community Battery

Two locations for the community battery storage are considered, at the head and at the end of the LV feeders. Then, P_{Gen} and P_{Net} have been calculated for the cases in which the battery storages absorb 5, 10, or 15% of the total generated active power of the feeder they are installed on. From Table 4.6.7 and 4.6.9 it is observed that from the perspective of improving P_{Gen}, installing community batteries at the end of the feeder is more effective than installing it at the head of the feeder. This is due to the fact that the overvoltage problem generally is more severe at the end of a feeder. Furthermore, from the perspective of improving P_{Net} (Table 4.6.8 and 4.6.10), installing community batteries at the head of the feeders has a negative impact while by installing them at the end of the feeder, P_{Net} improves noticeably.

- **The head of the feeder**

Table 4.6.7. P_{Gen} when community batteries are installed at the head of the LV feeder in the Tarnagulla network.

		P_{Gen} (kW)		
		Battery storage absorption ratio		
		5%	10%	15%
Load (%)	25	156 (4% ↑)	163 (8% ↑)	170 (13% ↑)
	50	281 (4% ↑)	293 (8% ↑)	306 (13% ↑)

	75	408 (4% ↑)	426 (9% ↑)	445 (13% ↑)
	100	538 (4% ↑)	562 (9% ↑)	586 (13% ↑)

Table 4.6.8. P_{Net} when community batteries are installed at the head of the LV feeder in the Tarnagulla network.

		P_{Net} (kW)		
		Battery storage absorption ratio		
		5%	10%	15%
Load (%)	25	68 (-2% ↓)	66 (-4% ↓)	64 (-7% ↓)
	50	105 (-3% ↓)	102 (-6% ↓)	98 (-9% ↓)
	75	144 (-3% ↓)	140 (-6% ↓)	134 (-10% ↓)
	100	186 (-3% ↓)	180 (-6% ↓)	172 (-10% ↓)

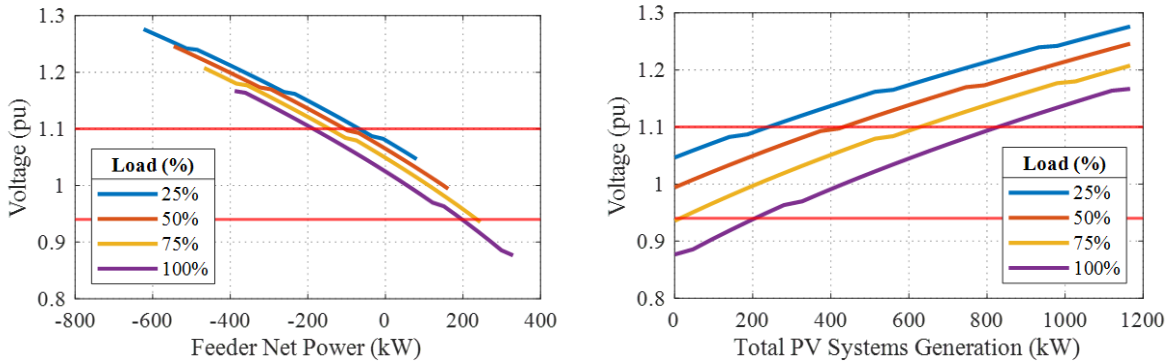

Fig. 4.6.13. Voltage magnitude variation of bus B_LV.V2.4 when community batteries absorb 5% of total generated active power of the feeder they are installed at.

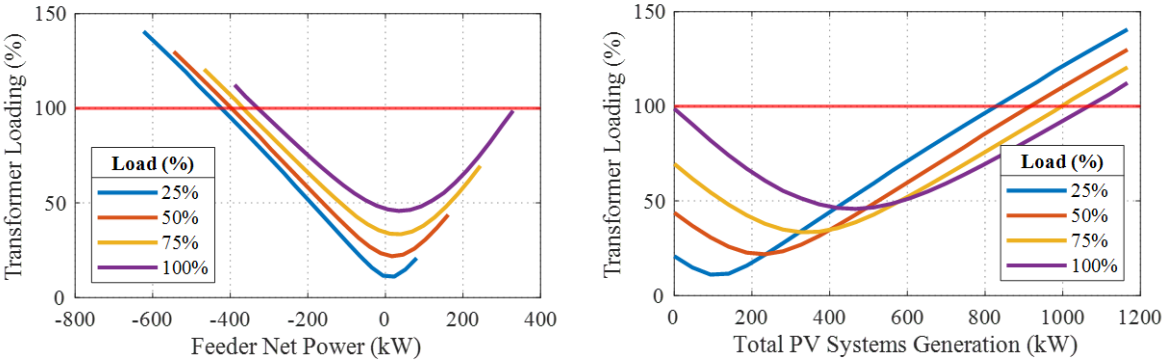

Fig. 4.6.14. The occupied capacity of transformer TF-V when community batteries absorb 5% of total generated active power of the feeder they are installed at.

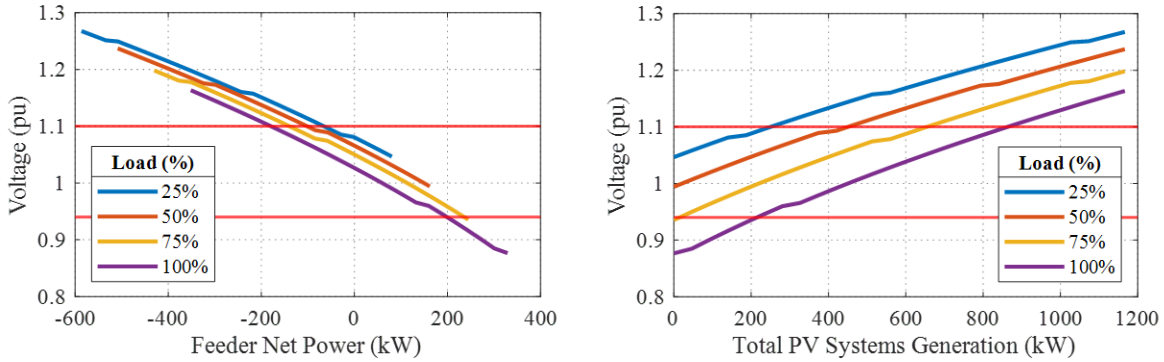

Fig. 4.6.15. Voltage magnitude variation of bus B_LV.V2.4 when community batteries absorb 10% of total generated active power of the feeder they are installed on

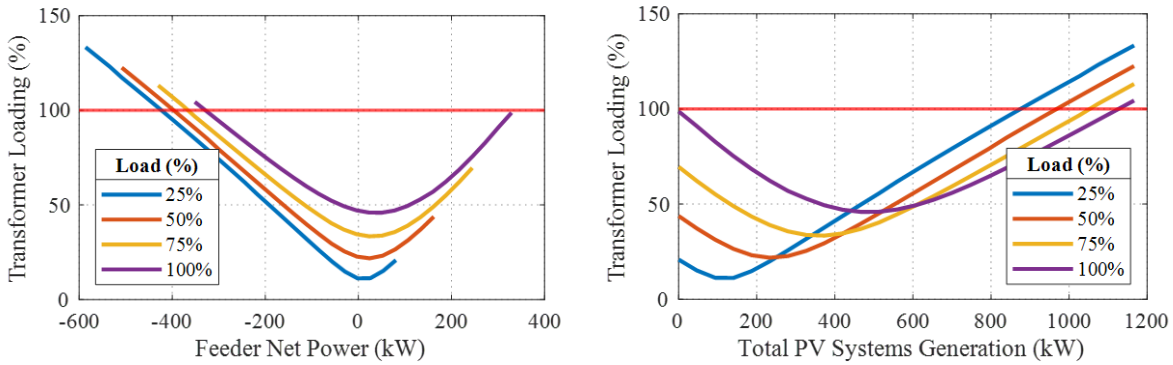

Fig. 4.6.16. The occupied capacity of transformer TF-V when community batteries absorb 10% of total generated active power of the feeder they are installed at.

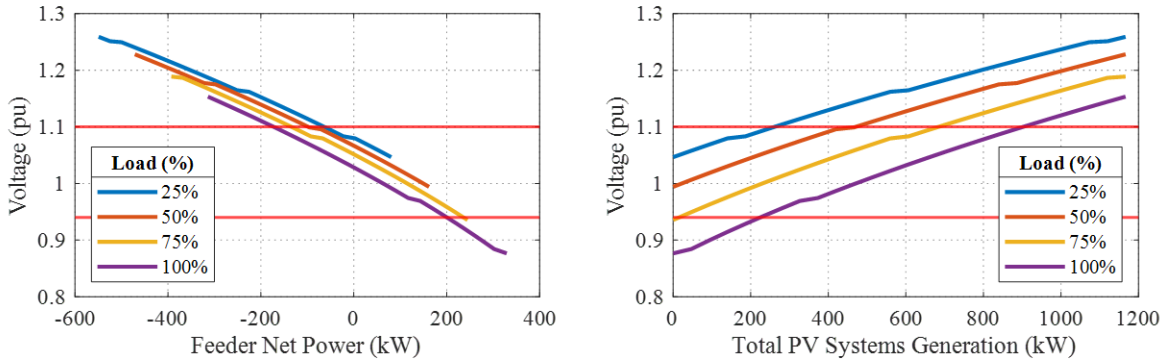

Fig. 4.6.17. Voltage magnitude variation of bus B_LV.V2.4 when community batteries absorb 15% of total generated active power of the feeder they are installed at.

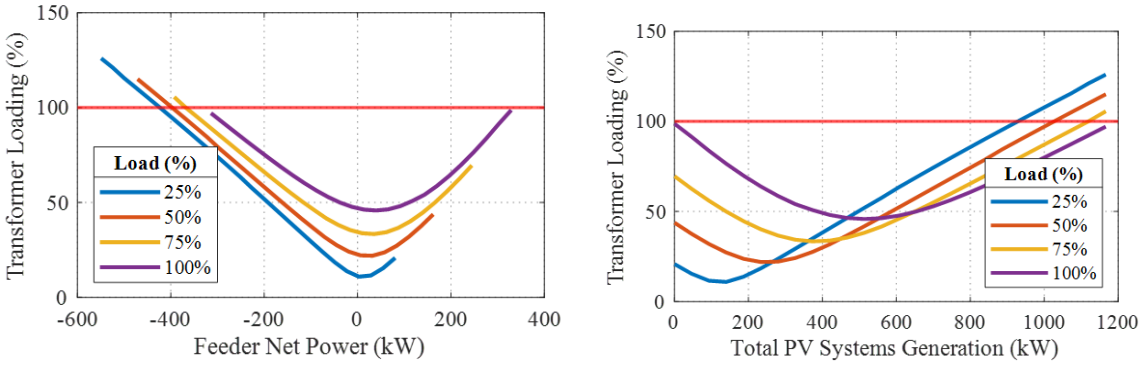

Fig. 4.6.18. The occupied capacity of transformer TF-V when community batteries absorb 15% of total generated active power of the feeder they are installed at.

❖ **End of the feeder**

Table 4.6.9. P_{Gen} when community batteries are installed at the end of the LV feeder in the Tarnagulla network.

		P_{Gen} (kW)		
		Battery storage absorption ratio		
		5%	10%	15%
Load (%)	25	162 (8% ↑)	176 (17% ↑)	192 (28% ↑)
	50	291 (8% ↑)	317 (17% ↑)	347 (29% ↑)
	75	423 (8% ↑)	460 (17% ↑)	505 (29% ↑)
	100	558 (8% ↑)	608 (18% ↑)	667 (29% ↑)

Table 4.6.10. P_{Net} when community batteries are installed at the end of the LV feeder in the Tarnagulla network.

		P_{Net} (kW)		
		Battery storage absorption ratio		
		5%	10%	15%
Load (%)	25	73 (6% ↑)	78 (13% ↑)	83 (20% ↑)
	50	115 (6% ↑)	123 (14% ↑)	133 (23% ↑)
	75	159 (7% ↑)	171 (15% ↑)	186 (25% ↑)
	100	205 (7% ↑)	221 (15% ↑)	241 (26% ↑)

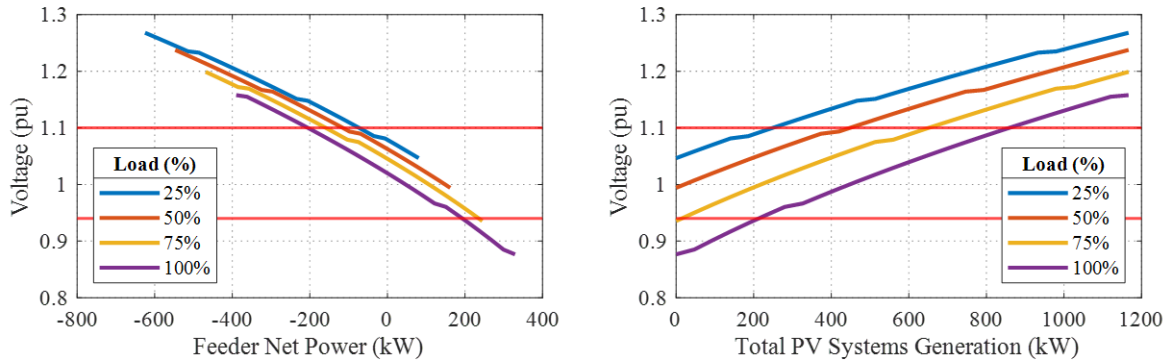

Fig. 4.6.19. Voltage magnitude variation of bus B_LV.V2.4 when community batteries absorb 5% of total generated active power of the feeder they are installed at.

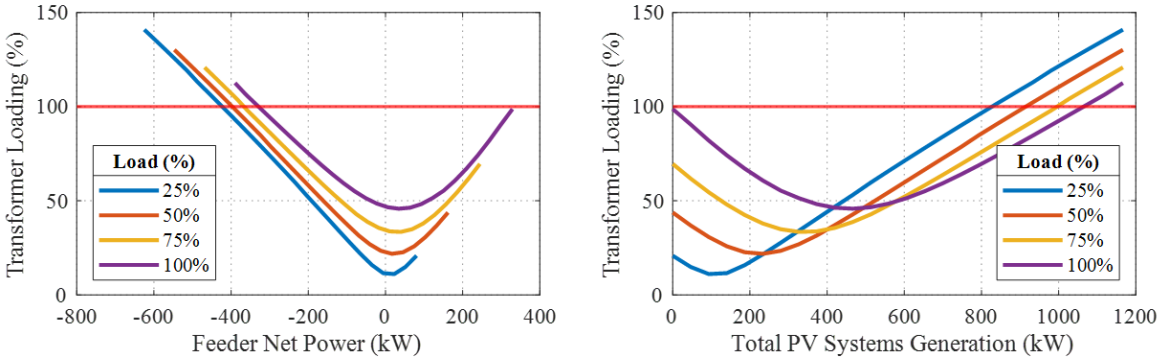

Fig. 4.6.20. The occupied capacity of transformer TF-V when community batteries absorb 5% of total generated active power of the feeder they are installed at.

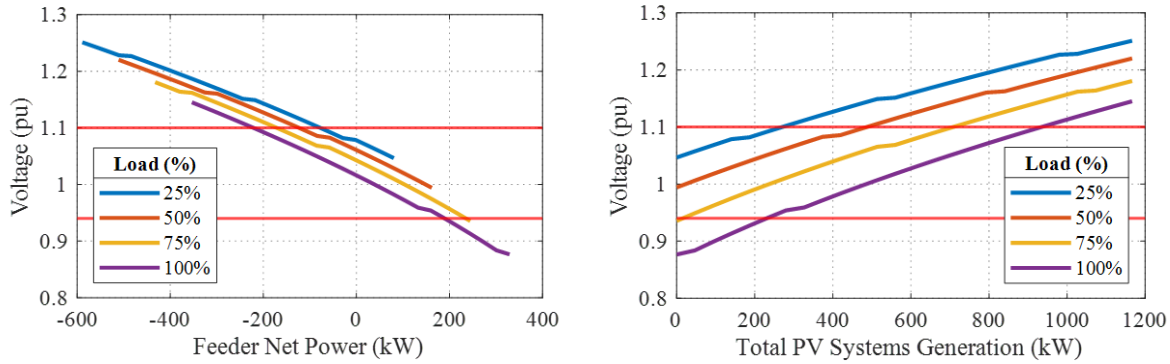

Fig. 4.6.21. Voltage magnitude variation of bus B_LV.V2.4 when community batteries absorb 10% of total generated active power of the feeder they are installed at.

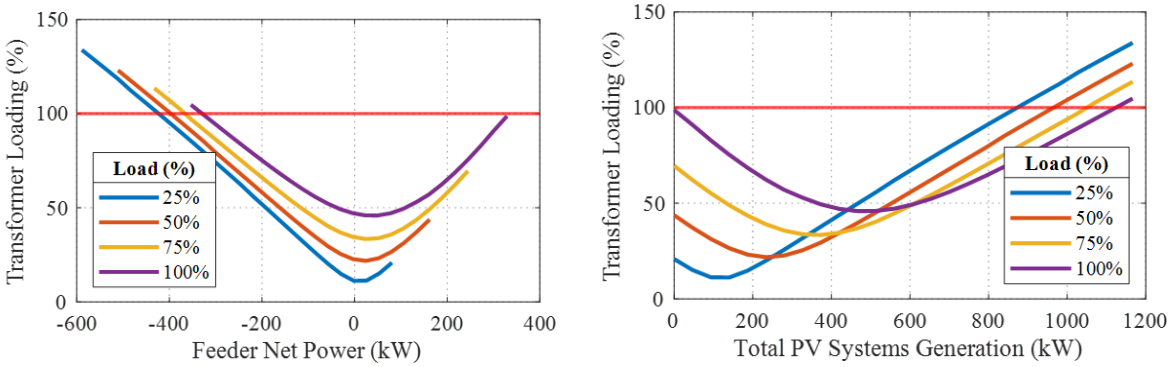

Fig. 4.6.22. The occupied capacity of transformer TF-V when community batteries absorb 10% of total generated active power of the feeder they are installed at.

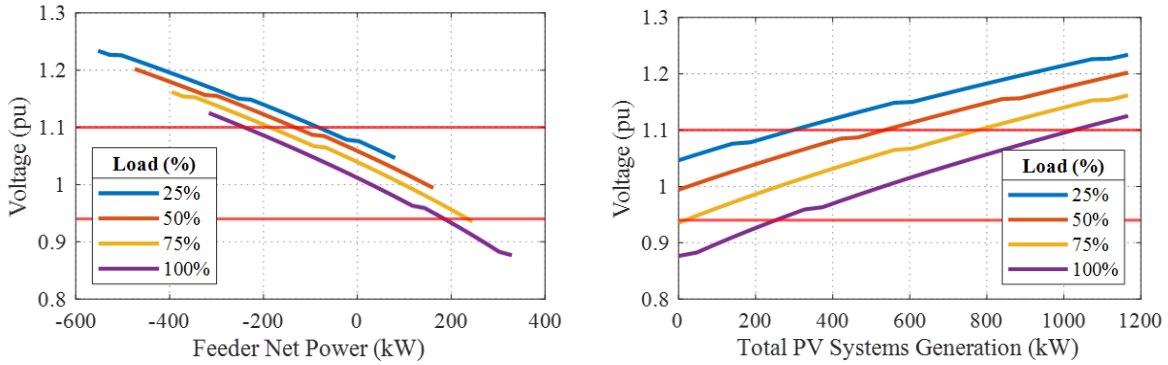

Fig. 4.6.23. Voltage magnitude variation of bus B_LV.V2.4 when community batteries absorb 15% of total generated active power of the feeder they are installed at.

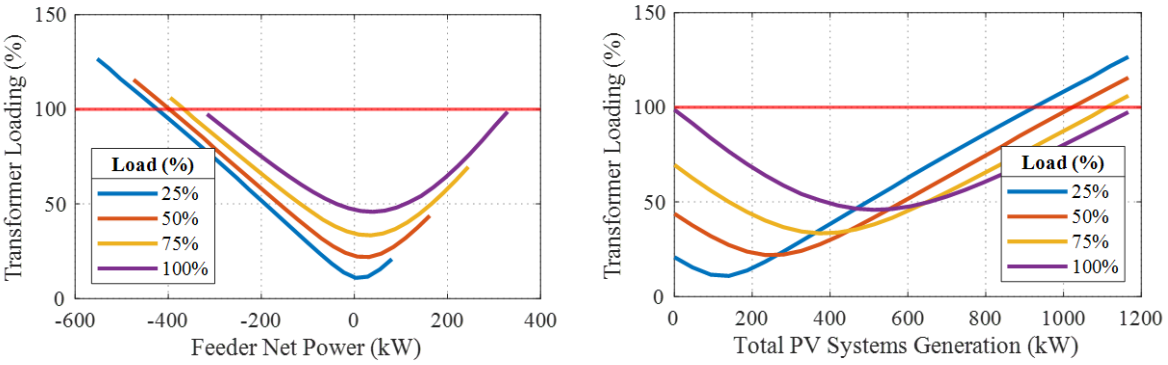

Fig. 4.6.24. The occupied capacity of transformer TF-V when community batteries absorb 15% of total generated active power of the feeder they are installed at.

Residential Battery

It is assumed that a residential battery storage is installed at each bus of the LV feeders. Then, P_{Gen} and P_{Net} have been calculated for the cases in which each battery storage absorbs 10, 20, 30, 40, and 50% of the generated active power by its local PV system. From Table 4.6.11 it can be seen that by increasing the absorption ratio, P_{Gen} is improved. For a few cases, PV systems can inject their full capacity without violating voltage limits. Furthermore, P_{Net} does not change, except for the cases in which PV systems are able to inject their full capacity. In these cases, since a portion of it is being absorbed, the ability of the network to inject active power reduces.

Table 4.6.11. P_{Gen} when houses have residential batteries in the Tarnagulla network.

		P_{Gen} (kW)				
		Battery storage absorption ratio.				
		10%	20%	30%	40%	50%
Load (%)	25	166 (11% ↑)	187 (25% ↑)	214 (42% ↑)	250 (66% ↑)	300 (100% ↑)
	50	300 (11% ↑)	337 (25% ↑)	385 (43% ↑)	449 (67% ↑)	540 (100% ↑)
	75	436 (11% ↑)	490 (25% ↑)	560 (43% ↑)	653 (67% ↑)	758 (93% ↑)

	100	574 (11% ↑)	646 (25% ↑)	738 (43% ↑)	758 (47% ↑)	758 (47% ↑)

Table 4.6.12. P_{Net} when houses have residential batteries in the Tarnagulla network.

		P_{Net} (kW)				
		Battery storage absorption ratio				
		10%	20%	30%	40%	50%
Load (%)	25	69 (0%)	69 (0%)	69 (0%)	69 (0%)	69 (0%)
	50	108 (0%)	108 (0%)	108 (0%)	108 (0%)	108 (0%)
	75	149 (0%)	149 (0%)	149 (0%)	149 (0%)	136 (-9% ↓)
	100	192 (0%)	192 (0%)	192 (0%)	131 (-32% ↓)	55 (-71% ↓)

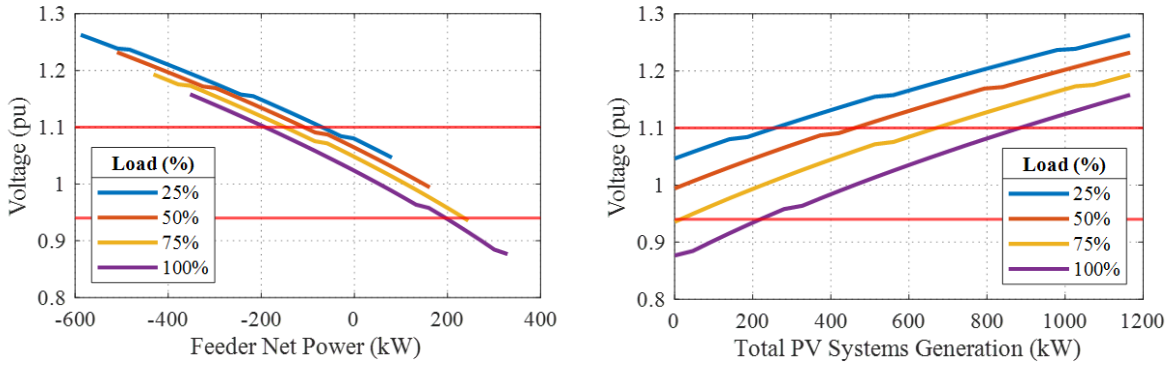

Fig. 4.6.25. Voltage magnitude variation of bus B_LV.V2.4 when residential batteries absorb 10% of their local generated active power.

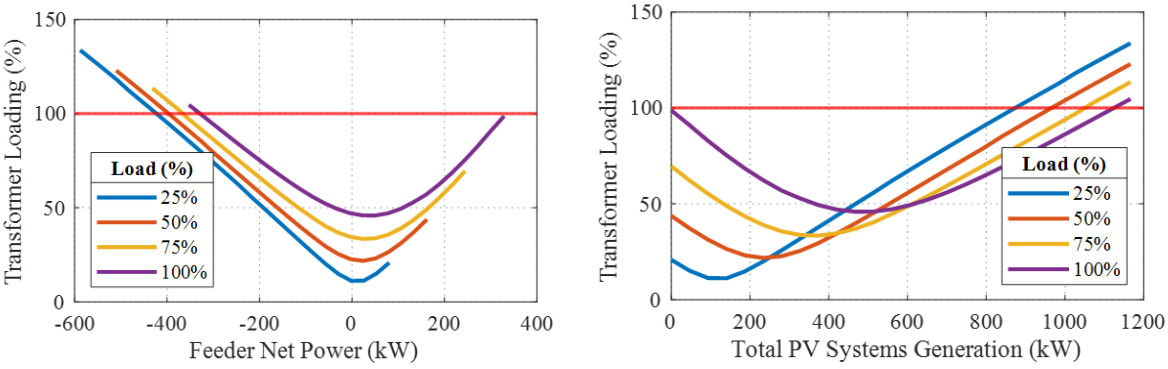

Fig. 4.6.26. The occupied capacity of transformer TF-V when residential batteries absorb 10% of their local generated active power.

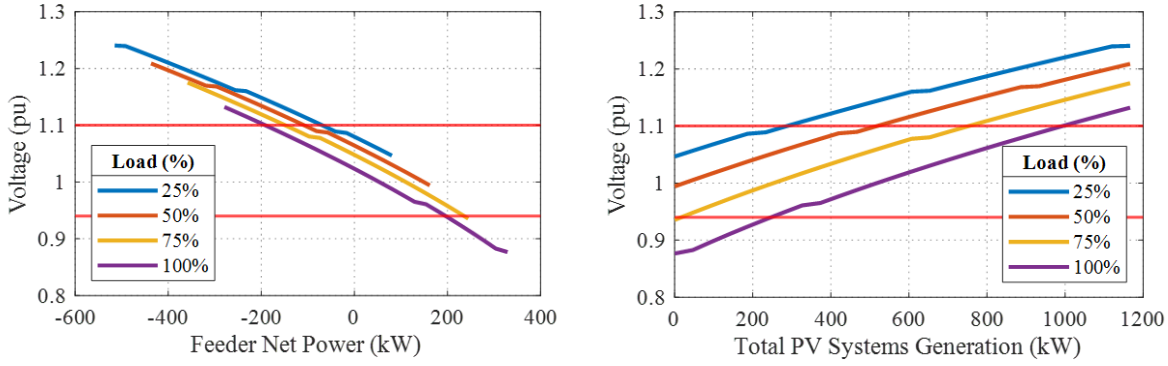

Fig. 4.6.27. Voltage magnitude variation of bus B_LV.V2.4 when residential batteries absorb 20% of their local generated active power.

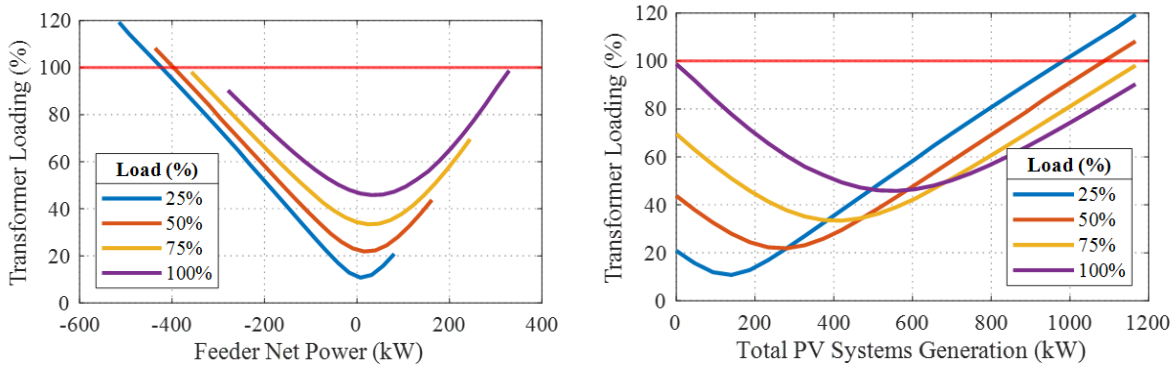

Fig. 4.6.28. The occupied capacity of transformer TF-V when residential batteries absorb 20% of their local generated active power.

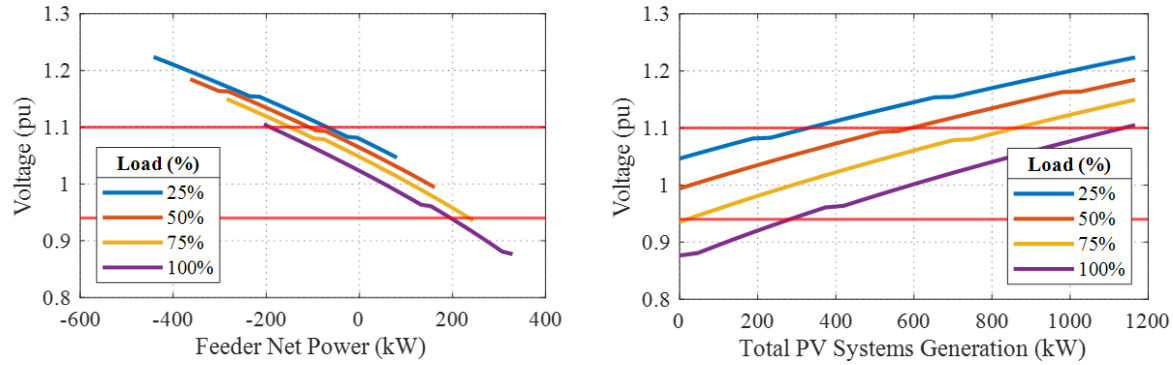

Fig. 4.6.29. Voltage magnitude variation of bus B_LV.V2.4 when residential batteries absorb 30% of their local generated active power.

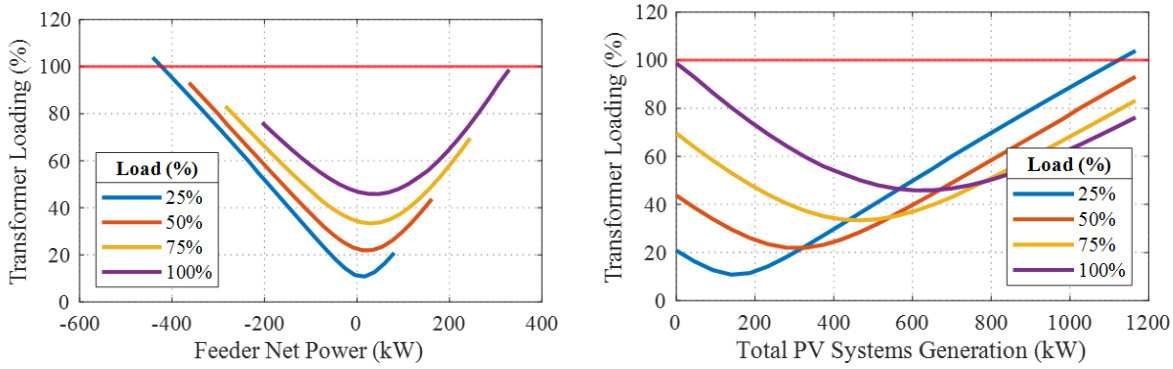

Fig. 4.6.30. The occupied capacity of transformer TF-V when residential batteries absorb 30% of their local generated active power.

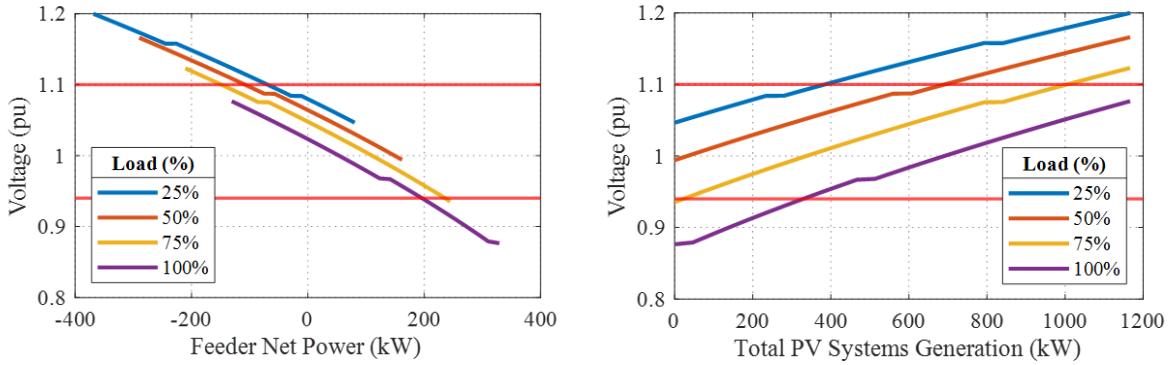

Fig. 4.6.31. Voltage magnitude variation of bus B_LV.V2.4 when residential batteries absorb 40% of their local generated active power.

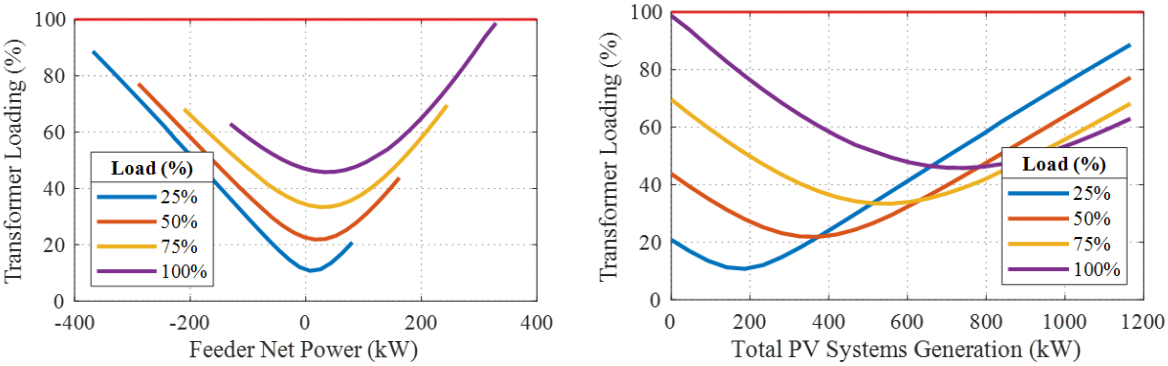

Fig. 4.6.32. The occupied capacity of transformer TF-V when residential batteries absorb 40% of their local generated active power.

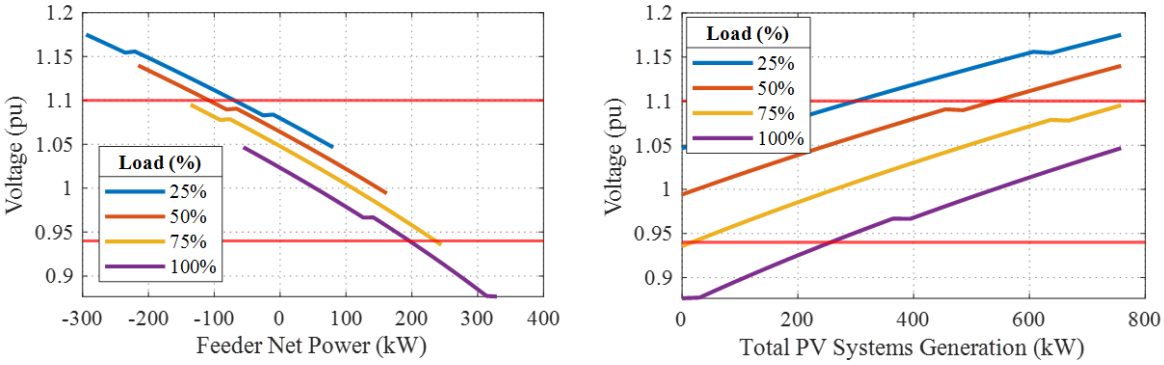

Fig. 4.6.33. Voltage magnitude variation of bus B_LV.V2.4 when residential batteries absorb 50% of their local generated active power.

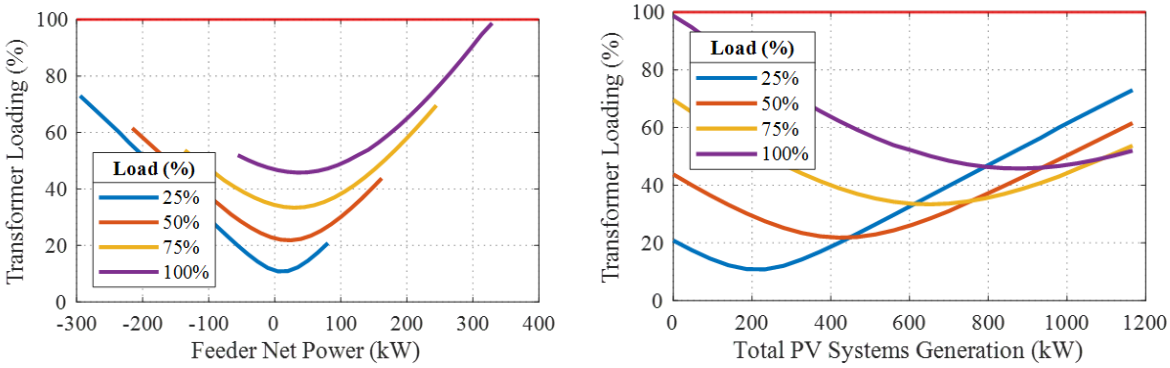

Fig. 4.6.34. The occupied capacity of transformer TF-V when residential batteries absorb 50% of their local generated active power.

4.6.3. Donald Network:

Base Case:

In Table 4.6.13, for two levels of load with power factor of 0.85, P_{Gen} and P_{Net} are shown. Furthermore, the detailed results, the variation of the voltage magnitude of bus B_LV. T09.01.10 and the occupied capacity of the MV/ LV transformer TF-T09 with respect to the total generated active power in/by the Tarnagulla network are shown in Fig. 4.6.35 and 4.6.36, respectively. It can be seen that, in this study, the overvoltage problem is the only limiting factor and it exists only in the light load condition (25%). Therefore, in the rest of the report for the Donald network, the results of the hosting capacity improvement techniques are only reported for this load level. Furthermore, from Fig. 4.6.35, the impact of on-load tap changers of transformers at the upstream network on the voltage magnitude can be observed. In the rest of the report, the first time that the voltage magnitude of bus B_LV. T09.01.10 crosses the 1.1 pu is considered as the reference to calculate P_{Gen} and P_{Net}.

Table 4.6.13. P_{Gen} and P_{Net} in base case of the Donald network.

		P_{Gen} (kW)	P_{Net} (kW)
Load (%)	25	2657	1774
	50	3514	1747

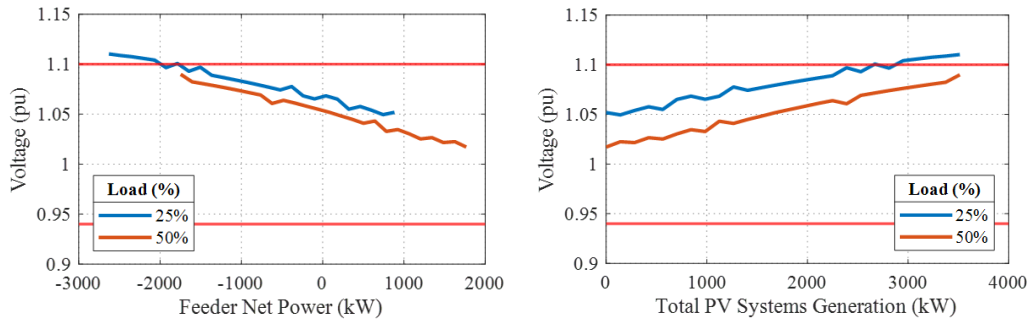

Fig. 4.6.35. Voltage magnitude variation of bus B_LV. T09.01.10 in the base case of the Donald network.

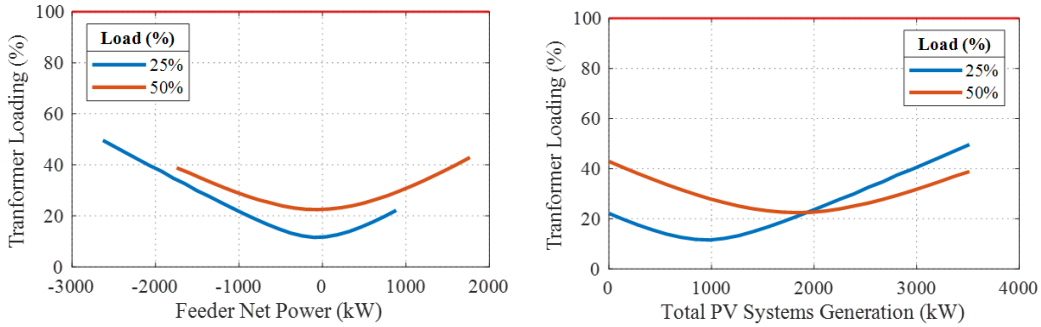

Fig. 4.6.36. The occupied capacity of transformer TF-T09 in the base case of the Donald network.

Transformers tap changer

Two tap positions, -1 and -2, have been selected for the MV/LV transformers and P_{Gen} and P_{Net} have been calculated when the load level is 25%. As shown in Table 4.6.14, in both cases, using lower tap positions, both P_{Gen} and P_{Net} are increased insofar there is no overvoltage in the grid. However, this may not be an optimal solution. Since the voltage magnitude at the LV side is reduced, the load hosting capacity can reduce.

Table 4.6.14. P_{Gen} and P_{Net} when transformers' tap position is -1 and -2 in the Donald network.

	P_{Gen} (kW)	P_{Net} (kW)
Tap Position= -1	3514 (32% ↑)	2631 (48% ↑)
Tap Position= -2	3514 (32% ↑)	2631 (48% ↑)

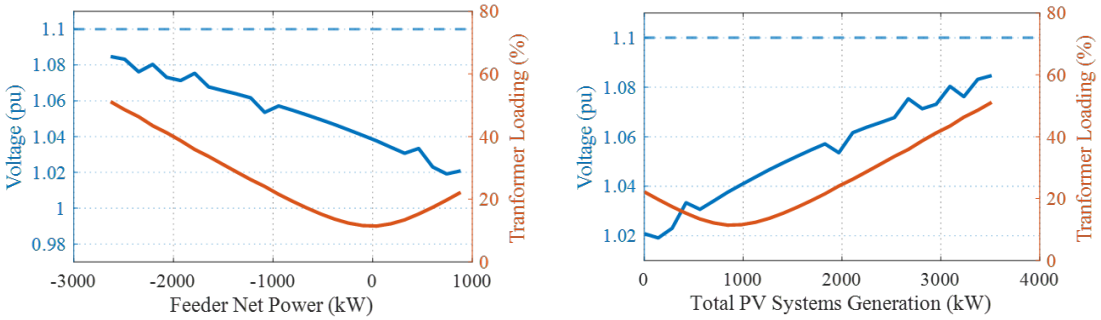

Fig. 4.6.37. Voltage magnitude variation of bus B_LV.T09.01.10 and the occupied capacity of transformer TF-T09 when transformers' tap position is -1 in the Donald network.

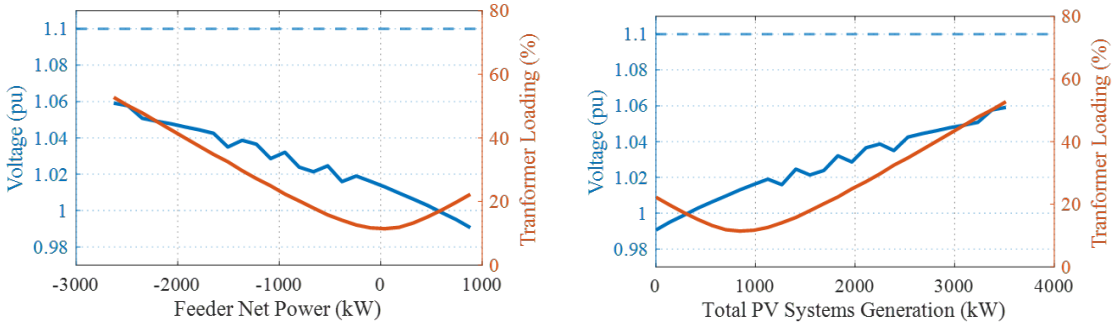

Fig. 4.6.38. Voltage magnitude variation of bus B_LV.T09.01.10 and the occupied capacity of transformer TF-T09 when transformers' tap position is -2 in the Donald network.

Smart inverters, volt/var Control

The same volt/var curve described in Fig. 4.6.8 with the setting of Table 4.6.4 is also used for Donald Network. Moreover, similarly, it is assumed that the inverters are over-sized by 10% in order to provide var control. Two case studies have been carried out utilising *volt/var* control for PV inverters. In the first case, it is considered that all PV inverters are smart (with var control capability) while in the second case, half of them are legacy ones (without var control capability) and half of them are smart. It can be seen in Table 4.6.15 that *volt/var* can improve both P_{Gen} and P_{Net} without decreasing the load hosting capacity of the network. However, there is not any significant difference between the two cases. This is due to the operation of on-load tap changers in upstream transformers, which are changing the voltage profile of nodes in the Donald network. The impact of tap changers operation can be seen clearly when the voltage of bus B_LV.T09.01.10 becomes close to 1.1 pu.

Table 4.6.15. P_{Gen} and P_{Net} when all/half of PV inverters are equipped with volt/var control in the Donald network.

	P_{Gen} (kW)	P_{Net} (kW)
All PV inverters are smart	2934 (10% ↑)	2051 (16% ↑)
Half of PV inverters are smart	2905 (9% ↑)	2022 (14% ↑)

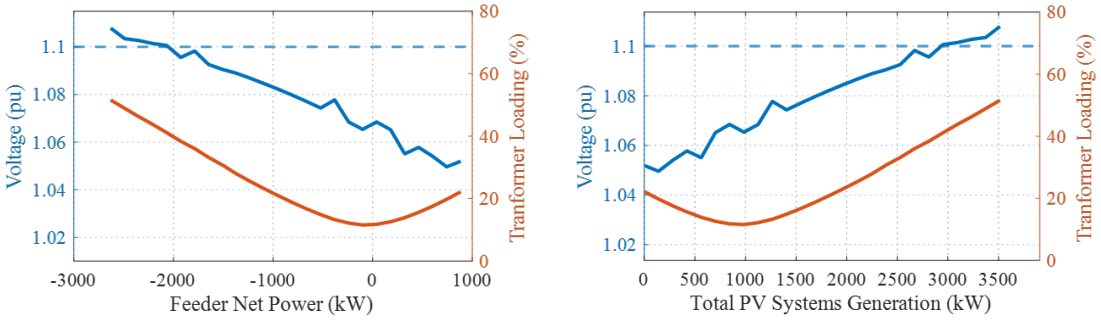

Fig. 4.6.39. Voltage magnitude variation of bus B_LV.T09.01.10 and the occupied capacity of transformer TF-T09 when all PV i inverters are equipped with volt/var control in the Donald network.

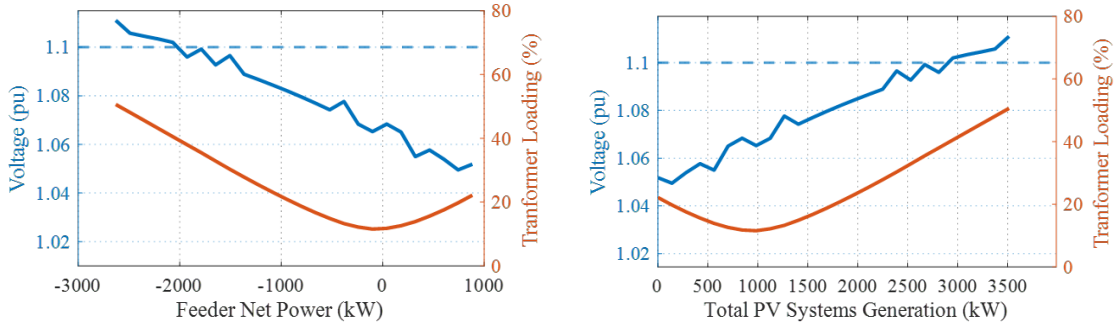

Fig. 4.6.40. Voltage magnitude variation of bus B_LV.T09. 01.1 0 and the occupied capacity of transformer TF-T09 when half of PV inverters are equipped d with volt/var control in the Donald network.

Community Battery

Two locations for the community battery storage are considered, at the head or at the end of the LV feeders. Then, P_{Gen} and P_{Net} have been calculated for the cases in which the battery storages absorb 5, 10, or 15% of the total generated active power of the feeder they are installed on. From Table 4.6.16 and 4.6.17 it is observed that for improving P_{Gen} and P_{Net}, installing community batteries at the end of the feeder is more effective than installing them at the head of the feeders. For example, in 15% absorption ratio, when the batteries are installed at end of the feeder, the overvoltage problem can be resolved in the considered network. While this cannot be achieved when they are installed at the head of the feeders.

❖ **The head of the feeder**

Table 4.6.16. P_{Gen} and P_{Net} when community batteries are installed at the head of the LV feeder in the Donald network.

	Battery storage absorption ratio		
	5%	10%	15%
P_{Gen} (kW)	2796 (5% ↑)	2950 (11% ↑)	3410 (28% ↑)
P_{Net} (kW)	1769 (0%)	1762(-1% ↓)	1999 (13% ↑)

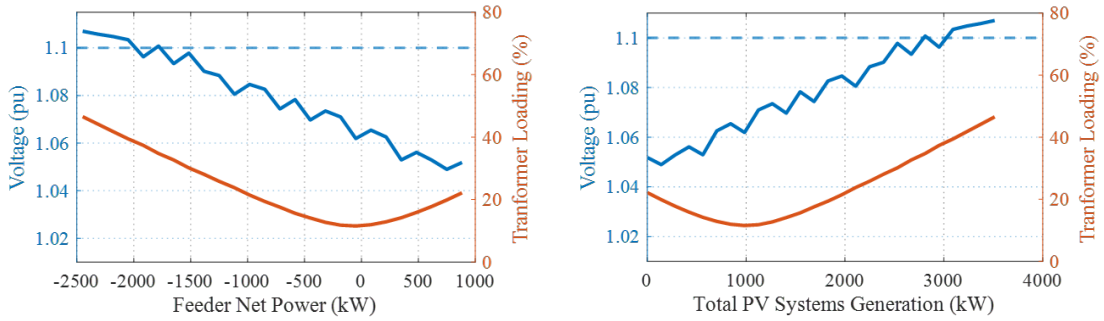

Fig. 4.6.41. Voltage magnitude variation of bus B_LV.T09.01.10 and the occupied capacity of transformer TF-T09 when community batteries absorb 5% of total generated active power of the feeder they are installed at.

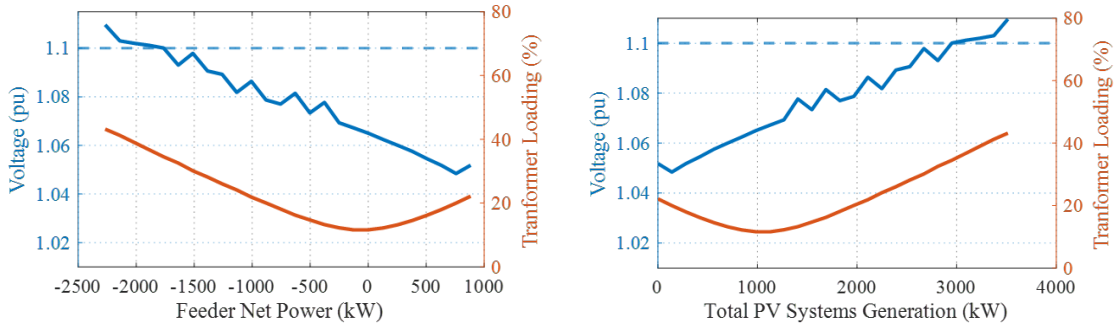

Fig. 4.6.42. Voltage magnitude variation of bus B_LV.T09.01.10 and the occupied capacity of transformer TF-T09 when community batteries absorb 10% of total generated active power of the feeder they are installed at.

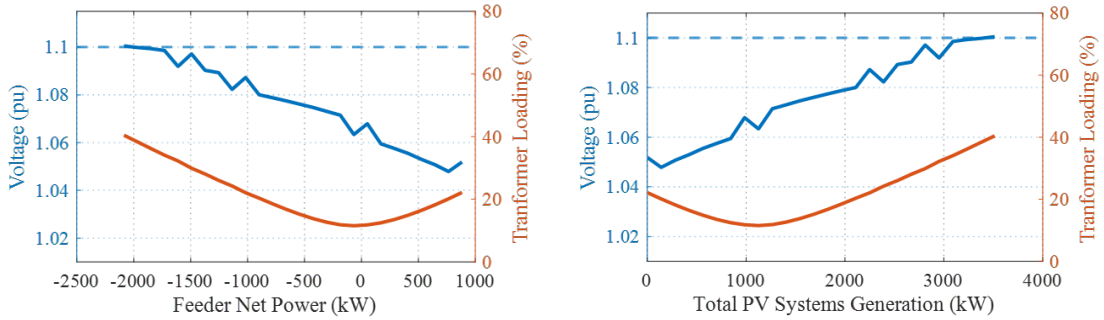

Fig. 4.6.43. Voltage magnitude variation of bus B_LV.T09.01.10 and the occupied capacity of transformer TF-T09 when community batteries absorb 15% of total generated active power of the feeder they are installed at.

❖ End of the feeder

Table 4.6.17. P_{Gen} and P_{Net} when community batteries are installed at the end of the LV feeder in the Donald network.

	Battery storage absorption ratio		
	5%	10%	15%
P_{Gen} (kW)	3090 (16% ↑)	3469 (31% ↑)	3514 (32% ↑)
P_{Net} (kW)	2048 (15% ↑)	2228 (26% ↑)	2086 (18% ↑)

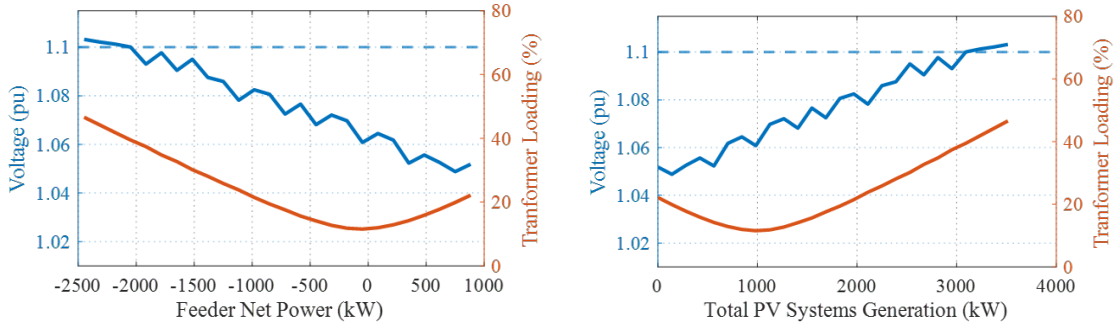

Fig. 4.6.44. Voltage magn itude variation of bus B_LV.T09.01.10 and the occupied capacity of transformer TF-T09 when community batteries absorb 5% of total generated active power of the feeder they are installed at.

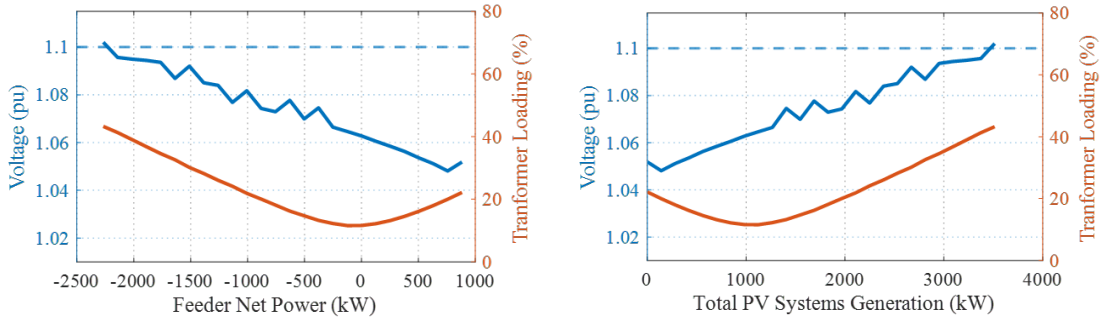

Fig. 4.6.45. Voltage magnitude variation of bus B_LV.T09.01.10 and the occupied capacity of transformer TF-T09 when community batteries absorb 10% of total generated active power of the feeder they are installed at.

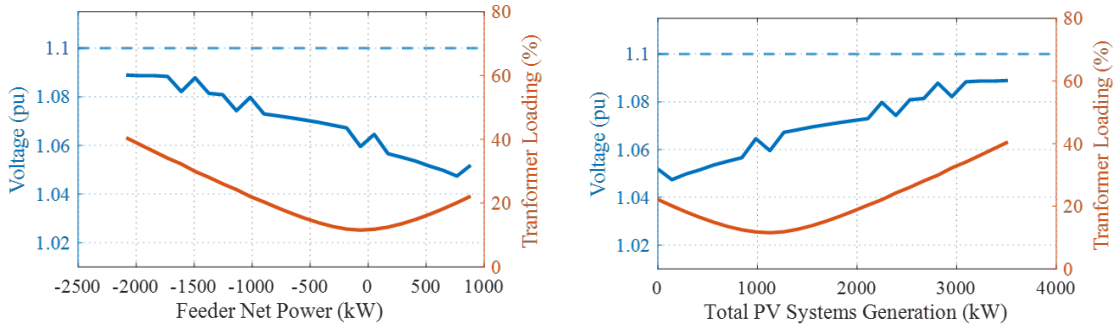

Fig. 4.6.46. Voltage magnitude variation of bus B_LV.T09.01.10 and the occupied capacity of transformer TF-T09 when community batt eries absorb 15% of total generated active power of the feeder they are installed at.

Residential Battery

It is considered that a residential battery storage is installed at each bus of the LV feeders. Then, P_{Gen} and P_{Net} have been calculated for the cases in which each battery storage absorbs 10, 20, 30, 40, and 50% of the generated active power by its local PV system. From Table 4.6.17 it can be seen that by increasing the absorption ratio, P_{Gen} is improving; for a few cases (30-50 %) there is no overvoltage problem. In these cases, PV systems can inject their full capacity without violating voltage limits. P_{Gen}=3514 and after absorbing a portion of it by battery storages, the rest of generated power can be injected to the upstream network.

Table 4.6.17. P_{Gen} and P_{Net} when houses have residential batteries in the Donald network.

	Battery storage absorption ratio				
	10%	20%	30%	40%	50%
P_{Gen} (kW)	3194 (20% ↑)	3322 (25% ↑)	3514 (32% ↑)	3514 (32% ↑)	3514 (32% ↑)
P_{Net} (kW)	1991 (12% ↑)	1773 (0%)	1575 (-11% ↓)	1224 (-31% ↓)	872 (-51% ↓)

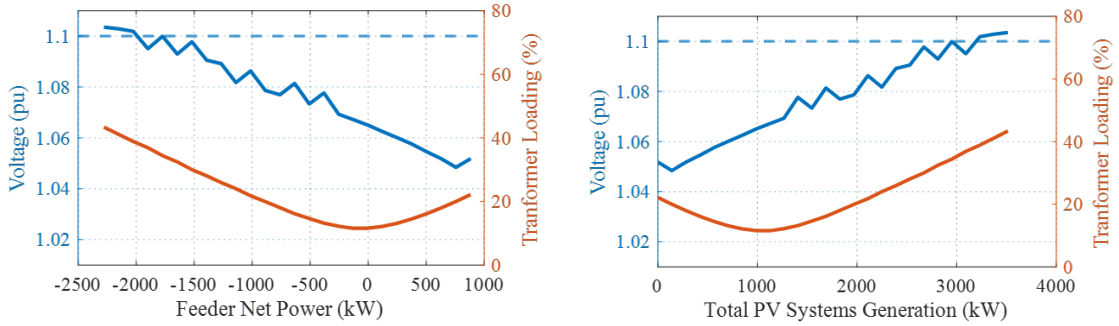

Fig. 4.6.47. Voltage magnitude variation of bus B_ LV.T09.01.10 and the occupied capacity of transformer TF-T09 when residential batteries absorb 10% of their local generated active power.

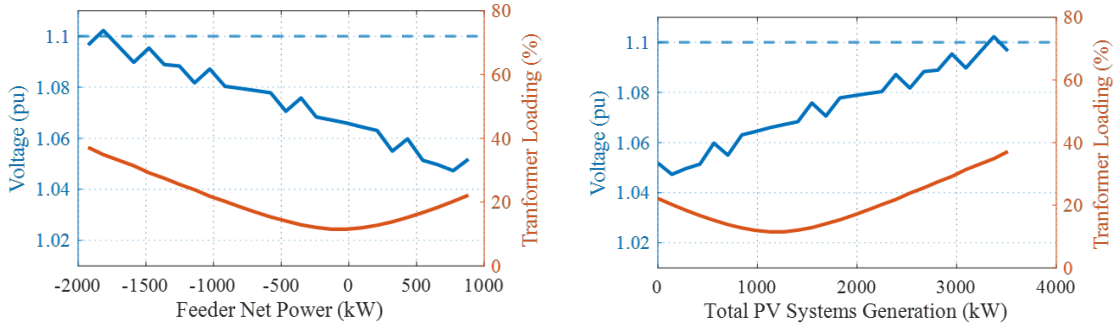

Fig. 4.6.48. Voltage magnitude variation of bus B_LV.T09.01.10 and the occupied capacity of transformer TF-T09 when residential batterie s absorb 20% of their loc al generated active power.

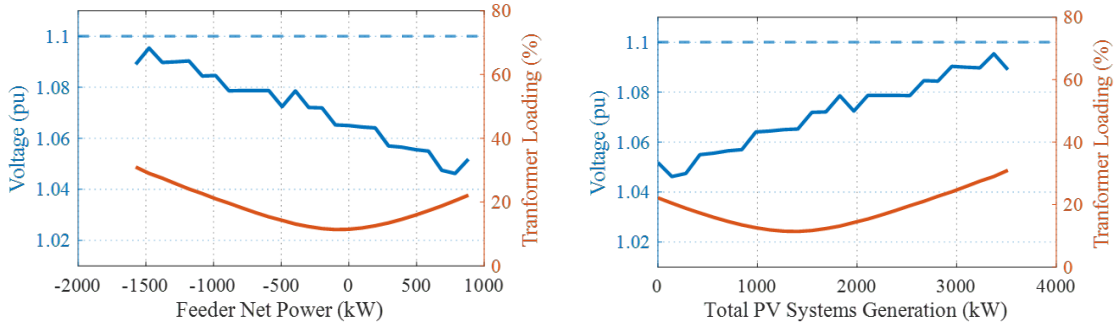

Fig. 4.6.49. Voltage magnitude variation of bus B _LV.T09.01.10 and the occupied capacity of transformer TF-T09 when residential batteries absorb 30% of their local generated active power.

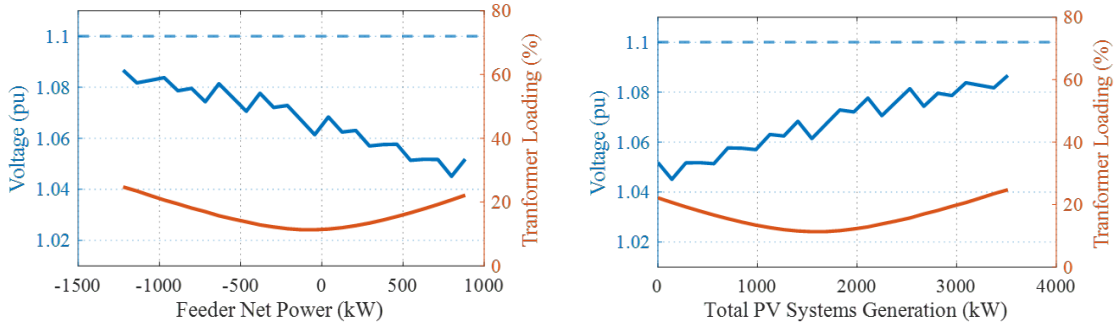

Fig. 4.6.50. Voltage magnitude variation o f bus B_LV.T09.01.10 and the occupied capacity of transformer TF-T09 when residential batteries absorb 40% of their local generated active power.

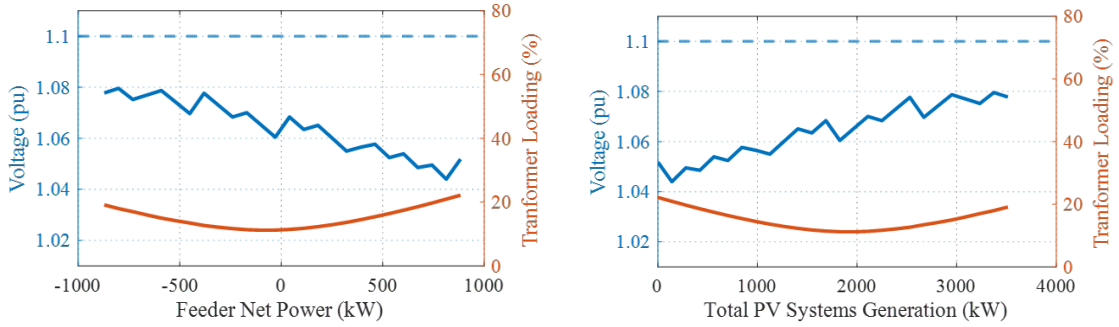

Fig. 4.6.51. Voltage magnitude variation of bus B _LV.T09.01.10 and the occupied capacity of transformer TF-T09 when residential batteries ab sorb 50% of their local generated active power.

4.6.4. Conclusions

Based on the considered simulation studies and with the assumptions used in those studies, the following findings have been observed:

- Changing MV/LV transformers' tap position can be effective, however it may negatively impact the capability of the grid for hosting loads.
- Equipping PV inverter with *volt/var* improves P_{Gen}. However, due to reactive power control, network losses and the occupied capacity of lines and transformers need to be taken into account. For example, for the Tarnagulla network, with the 25% load level and assumed generation, having *volt/var* control for half of PV systems, can improve P_{Gen} by 6%.
- Installing community batteries has been shown to more effective if they are installed at the end of the feeder. As an example, in the Donald network, having a battery at the end of each feeder which is able to absorb 10% to total generated active power by the PV systems on the same feeder can improve P_{Gen} by 31% in 25% load condition.
- Utilising residential batteries can be effective since the surplus generation can be absorbed locally. As an example, in the Tarnagulla network, having residential batteries which are able to absorb 30% their local generated active power can improve P_{Gen} by 42% in 25% load condition.

5. Summary and Conclusions

- The detailed models of the networks of Donald and Tarnagulla with associated distributed energy resources (DERs) have been developed in the simulation platform.
- The customer types and behaviour are identified by applying state-of-the-art machine learning and data analysis techniques on the de-identified smart meter and network data.
- The hosting capacity has been assessed for various operation modes of the microgrids such as grid-connected, stand alone and VPP modes considering both the economic and reliability aspects of the network.
- Various load and generation hosting scenarios are considered to assess the capacity of the MV and LV networks of these towns as well as their supply network.
- The load and generation profiles identified through the data analytics phase of the project are used to perform quasi-dynamic simulation in order to quantify the network impacts associated with the observed customer behaviours.
- The feasibility and effects of advanced and innovative technologies in increasing the hosting capacity of the proposed microgrids are studied.
- From the time series results of net energy balancing, it has been found that the optimally sized microgrid can meet the electric load demand reliably and continuously under different operation scenarios.
- Grid-connected operation of microgrid under load following dispatch strategy provides the most cost-effective design of microgrid. However; if the incoming utility feeder's reliability is somewhat less than the standard requirements, the energy security will be compromised unless a large backup generator or large-capacity storage system is present.
- Grid connected operation of microgrid under virtual power plant (VPP) and load following dispatch strategy provides the ideal design. However, the initial capital cost will be significant and can be recovered within a couple of years.
- VPP operation provides the best energy security. However; if significant forecasting errors are present in the load and generation forecasting, an intelligent energy management solution will be necessary.
- These optimally sized microgrid components are used as the base-case scenario for the microgrid's steady-state and quasi-dynamic operation simulations and are found to be acceptable under distribution voltage limits.

- Standard reliability indices (SAIDI, SAIFI and ENS) have been calculated for grid connected mode and islanded mode – with multiple levels of PV hosting capacity.
- System reliability is increased in islanded mode compared to grid connected mode.
- SAIDI, SAIFI, and ENS are decreased (i.e. system reliability is increased) with the higher PV hosting capacity.
- The MV and LV systems of Donald are capable of supplying the load well above the peak load of the network. They can also host the PV and battery as identified in hosting capacity assessment studies while the Tarnagulla network has been more sensitive to load and generation changes.
- The supply feeders are the main limiting factors in the hosting capacity of load and local generation of both Donald and Tarnagulla
- The voltages across the networks in stand-alone operation modes were more consistent due to the voltage support of the back-up generator.
- The quasi-dynamic simulations supported the findings through time-sweep analysis as the networks did not experienced major over or under voltages in many realistic operational scenarios.
- Minor overvoltage was observed in the LV networks during low load and high PV generation conditions with no batteries which were improved by considering the batteries in the system.
- Changing MV/LV transformers can be effective; however, it may negatively impact the capability of the grids for hosting loads.
- Equipping PV inverter with *volt/var* improves P_{Gen}. However, due to reactive power control, network losses and the occupied capacity of lines and transformers need to be taken into account.
- Installing community batteries has been shown to be more effective if they are installed at the end of the feeder.
- Utilising residential batteries can be effective since the surplus generation can be absorbed locally.